6-21-2021

Porous scaffold and soft hydrogel composite for biomedical applications

Matthew DiCerbo
Rowan University

POROUS SCAFFOLD AND SOFT HYDROGEL COMPOSITE FOR BIOMEDICAL APPLICATIONS

by

Matthew DiCerbo

A Thesis

Submitted to the
Department of Biomedical Engineering
College of Engineering
In partial fulfillment of the requirement
For the degree of
Master of Science in Biomedical Engineering
at
Rowan University
April 30, 2021

Thesis Chair: Sebastián L. Vega. Ph.D.

Committee Members:
Dr. Tae Won Kim, MD.
Dr. Eric Brewer, Ph.D.
Dr. Mary Staehle, Ph.D.
Dr. Vincent Beachley, Ph.D.

Dedications

This dissertation is dedicated to my dearest parents and to the memory of my beloved Uncle, Frank Arthur DiCerbo, who passed away before I completed my graduate studies. Uncle Frank's influence on my life has been tremendous. He was my mentor, support, and a second father to me. Uncle Frank was as "old fashioned" as they come and therefore, I wish to give him the highest form of respect in the dedication of my work. I want to honor his memory by continuing to work hard and by never forgetting that where I go, I could not have done it without the morals he taught, support, and encouragement he provided along the way. Throughout my life, Uncle Frank told me he was proud of me no matter what I did, and he would support all of my decisions. I wish he could still be alive today to share with me the celebration and the success of my graduation. This work is dedicated to you, Uncle.

Acknowledgments

First and foremost, I'd like to thank my research advisor, Dr. Sebastián L. Vega. His guidance, mentorship, and knowledge has helped me accomplish the goals of this work. I'd like to acknowledge a sincere friend of mine, Mehdi, who has helped me through this process when I was unable to make it to Rowan due to work.

Without my Mom and Dad, I would never be in the position I am in today and would not be able to achieve this if I did not have such wonderful parents. Uncle Frank has helped me tremendously throughout my life and this work is dedicated to his memory. I would also like to acknowledge all the rest of my family and friends that were with me during this journey.

Abstract

Matthew DiCerbo
POROUS SCAFFOLD AND SOFT HYDROGEL COMPOSITE FOR BIOMEDICAL APPLICATIONS
2020-2021
Sebastián L. Vega, Ph.D.
Master of Science in Biomedical Engineering

Biophysical signals including stiffness and dimensionality influence a myriad of stem cell behaviors including morphology, mechanosensing, and differentiation. 2D stiff environments cause increased cellular spreading and induce osteogenic differentiation whereas 3D soft environments favor rounder cell morphologies attributed to a chondrogenic phenotype. The goal of this study is to create a composite that integrates these divergent biophysical signals within one system. This composite consists of a stiff and porous polycaprolactone (PCL) backbone that provides mechanical stiffness and a 2D environment. The PCL backbone is then perfused with mesenchymal stem cells (MSCs) and a soft methacrylated gelatin (GelMe) hydrogel to provide an encapsulation technique that exposes cells to a soft 3D environment. Interestingly, MSCs in these composites exhibited differences in morphology and mechanosensing based on pore diameter. MSCs cultured in low pore size (~275 μm) composites were larger and more mechanically active than MSCs in high pore size (~425 μm) composites. Our finite element analysis models suggest that the role of pore size on cellular mechanosensing is linked to local changes in hydrogel stress from PCL-GelMe interactions. This composite is currently being explored for engineering the osteochondral tissue interface which contains a mixed population of osteoblasts and chondrocytes.

Table of Contents

Table of Contents (Continued)

Table of Contents (Continued)

Table of Contents (Continued)

List of Figures

List of Figures (Continued)

List of Tables

Chapter 1

Motivation

Treatment techniques to replace or replenish articular cartilage and the osteochondral interface (OI) are increasing at a rapid scale. However, successful repair of the osteochondral interface and specifically, osteochondral defects require the replacement or regeneration of multiple tissue phenotypes and recreation of a heterogeneous cellular environment[1]. This factor presents a substantial clinical and scientific challenge in replicating these properties.

Figure 1

Synovial Joint Comparison. Comparison of synovial joints as osteoarthritis progresses. A) Synovial joint with no osteoarthritis. B) Synovial joint with mild arthritis. C) Synovial joint with severe osteoarthrosis. [2]

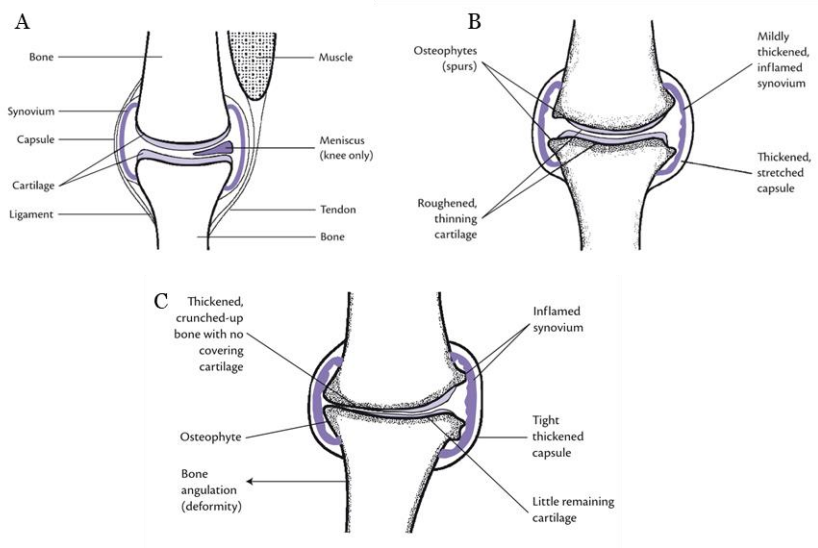

Articular cartilage lesions and defects are an increasing problem in orthopedics and are being encountered consistently and commonly lead to long term consequences. A collection of data shows out of 31,516 knee arthroscopies, chondral lesions were reported in 63% of patients in the study [1], [3]. These lesions are significant and need proper attention because they most likely will lead to degeneration of the joint and osteoarthritis (OA) [4]. Comparison of synovial joints as osteoarthritis progresses is shown in Figure 1. OA is very common among all types of patients especially those with joint injury, obesity, and predisposition. It is estimated from the recent burden of disease that up to 250 million of the world's population has osteoarthritis and the number will continue to increase [5]. Osteoarthritis is defined by musculoskeletal scientists and clinicians to be "chronic condition of the synovial joint that develops over time and is the result of the damaging processes overwhelming the joint's ability to repair itself [5]." OA is an active dynamic process occurring from an imbalance between the repair and destruction of the joint's tissue[6], [7]. The knee joint is the most common site for osteoarthritis to progress as it is subjected to constant loading throughout its lifetime [8].

It has recently been discovered that OA is not solely limited to the articular surface and that its onset may be initiated through activation of the secondary center of ossification which causes thinning of overlying cartilage resulting from thickening of the subchondral bone unit [9], [10]. These findings support OA is a whole joint disease and involves changes to the hyaline cartilage, subchondral bone, ligaments, synovium, and other components of the joint [8]. As osteoarthritis progresses, cartilage composition changes and the cartilage layer lose viscoelastic properties and integrity [11]. Susceptibility to physical forces increases because of compositional changes to the cartilages material

properties and these susceptibilities have a negative downstream effect on patients. A pathological image of an OA joint is shown in Figure 2. Erosions start at the surface of the cartilage and then more deep cartilage fissures are accompanied with expansion of the calcified cartilage zone. Chondrocytes try to repair this problem but essentially make it more complicated by increasing synthetic activity. In return, matrix degradation products and proinflammatory mediators are generated and deregulate chondrocyte function and act on the adjacent synovium to generate inflammatory and proliferative responses. When synoviocytes proliferate, they release proinflammatory products which is associated with tissue hypertrophy and increased vascularity. The bone turnover in the subchondral bone is increased, vascular invasion follows which stems from the subchondral bone into cartilage [5].

Figure 2

Pathological Osteoarthritis. The anatomical and pathological differences between a healthy and arthritic joint. [5]

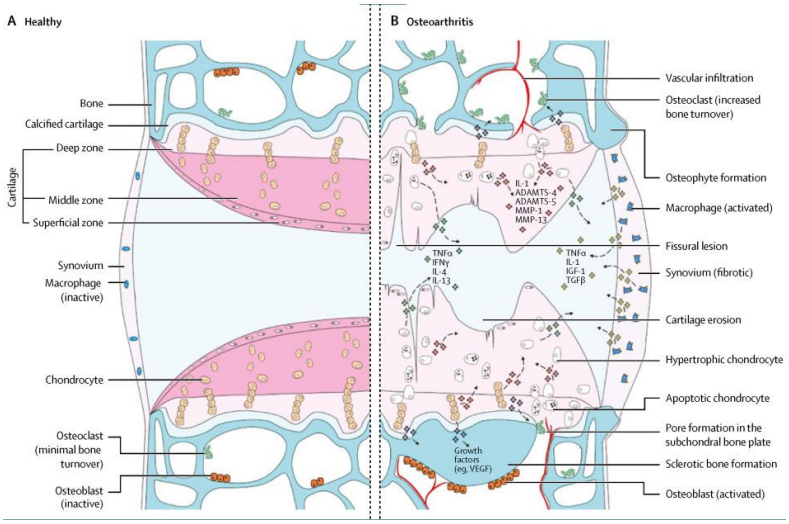

Therefore, it is imperative to examine changes to the subchondral bone along with cartilage to provide explanations of why current treatment procedures are ineffective. One treatment technique in particular, microfracture, may fail because regenerated tissue will overlie a thickened subchondral plate. Essentially, it is not a surface level problem but a chronic problem that roots deep within many tissues of the joint. With this information, it is crucial to not put sole focus on regenerating articular cartilage, but to target the whole osteochondral unit for treatment and prevention of osteoarthritis.

Chapter 2

Background

2.1 Tissue Engineering

Tissue Engineering (TE), an alternative application to tissue grafting and alloplastic repair, is achieved through a multidisciplinary approach of various engineering sectors [12]. The concept of tissue engineering was articulated in detail in 1985 while the first symposium for tissue engineering was held 1988 [13]–[17]. TE and regenerative medicine are gathering much attention and are becoming a focal point in the scientific community of research. This field seeks to restore damaged or diseased tissue and restore and improve their function by developing biomaterials for the task [14], [15], [18]–[20]. An approach to practice TE is incorporating cells and/or bioactive molecules into biodegradable scaffolds to replace the damaged natural tissue [21].

Figure 3

Tissue Engineering. Tissue engineering uses raw Materials in form of cells, biomaterials/scaffolds, and a combination with environmental factors to create engineered tissues [22].

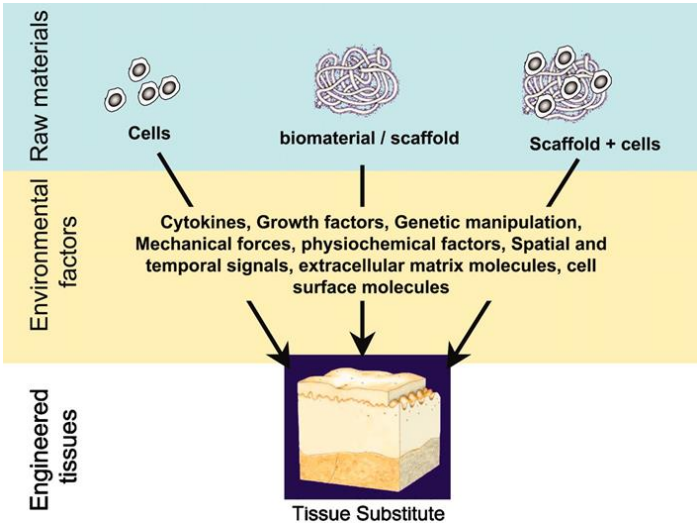

2.2 Musculoskeletal Engineering

One of the many subfields of TE is musculoskeletal tissue engineering (MTE) which concentrates on replacing the damaged tissues related to the musculoskeletal system such as bones, cartilage, muscles, and more [23], [24]. Biomaterial scaffolds are one of the main elements in this field and they are designed to work parallel to cells, environmental factors and signaling molecules which all have a significant effect on the success of the material and engineering aspect [13]. Cartilage and bone have been a main area of interest in musculoskeletal tissue engineering because of the challenges they present. However, cartilage presents a bigger challenge because it is avascular and unlike bone, cartilage

cannot be self-healed. This in conjunction with a life of wear and tear on the joint leads to the degeneration of the cartilage and osteoarthritis.

2.2.1 Mesenchymal Stem Cells

One of the most used cells in the subfield of MTE are mesenchymal stem cells (MSCs) which are multipotent stem cells that can differentiate into several musculoskeletal lineages such as osteoblasts (bone cells), chondrocytes (cartilage cells), and myocytes (muscle cells) [25]. MSCs are the most suitable cells for this work as they are able to be guided into differentiating into resident cells of numerous connective tissues including fat, bone, and cartilage [22]. Figure 4 shows MSC lineage types.

Figure 4

MSC Lineages. [26]

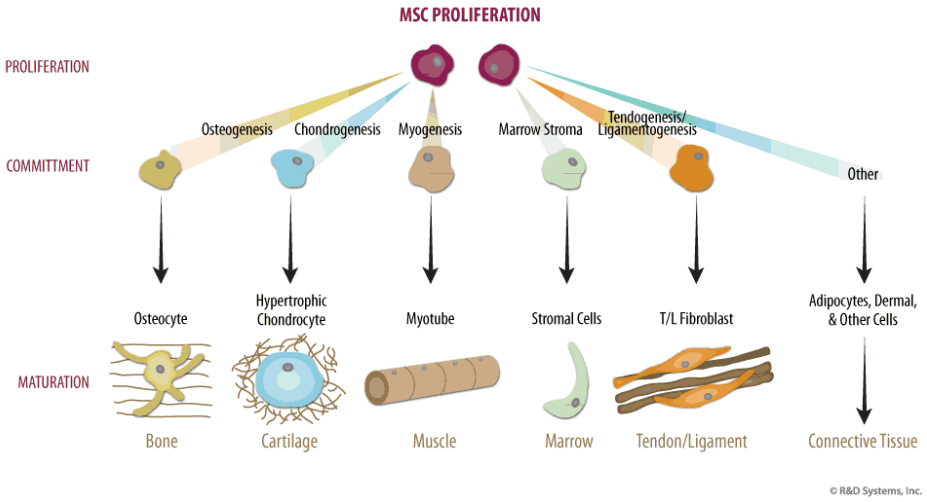

2.2.2 Cell Matrix Interactions

MSC interactions with engineered environments that recapitulate key features of the native extracellular matrix (ECM) has been considered a major aspect of tissue engineering, with the goal of creating biomaterials that act as substitutes for damaged tissues [17], [27]. The ECM is created by cells as they secrete molecules that in return build the surrounding structural and biochemical support. To further understand development of functional tissues through engineering, it is important to research the ECMs chemical and physical properties. To recapitulate and engineer cell environments, the understanding of ECMs gives rise to the design of artificial ECM in structures known as scaffolds [13]

Different tissue types have unique ECM compositions depending on the functional and biological requirements of that tissue. The most abundant fibrous protein within ECM is collagen as it provides the structural support of tissues and attachment of proteoglycans. There are 28 different types of collagens with fibrillar collagen being the most prevalent in the body. However, depending on the tissue function, collagen composition varies throughout tissues. On the other hand, glycosaminoglycans or GAGs are long unbranched polysaccharides and an important ECM component in all tissue types. GAGs function to provide structural support and help maintain healthy tissue by protecting and preserving ECM proteins and cytokines when they attach to proteoglycans, adhesive glycoproteins, and fibrous proteins [28], [29]. This information is crucial to understand because the type of cells, GAGs, proteoglycans, and proteins present determine the characteristics of the tissue [13].

The complexity of ECM environments and the requirements needed to replicate them are case dependent and vary greatly. For instance, this intricacy is observed upon inspection of the articular cartilage environment. Relevant to this work, are the zonal differences of ECM in articular cartilage. It is anisotropic in nature and can be classified as having three architectural zones. In Figure 5 the zones of articular cartilage are shown. These zones are the superficial, middle, and deep zone and have striking differences between their composition with reference to structure, chondrocyte phenotype, and mechanical properties [30]–[32]. Chondrocytes are elongated in the superficial zone due to the highly packed collagen fibers which are parallel to the surface to dissipate tensile strength and have a lower concentration of proteoglycans [31], [33].

Figure 5

Articular Cartilage. The organization of chondrocytes and collagen fibers in articular cartilage [13].

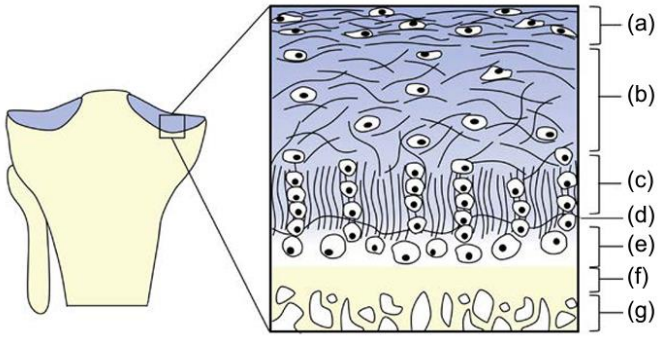

Rounded chondrocytes reside in the middle zone with a random collagen fiber orientation to strengthen the unpredictable compressive force that will be dispersed to this zone [31], [34]. The deep zone contains the necessary shape and morphology of chondrocytes to provide the cartilage with high compressive stress resistance. This natural design constraint results in the chondrocytes to be stacked in columns with radial collagen architecture and high proteoglycan concentration [31], [33].

Figure 6

Cartilage Types. Histological differences between hyaline, fibrocartilage, and elastic cartilage [13].

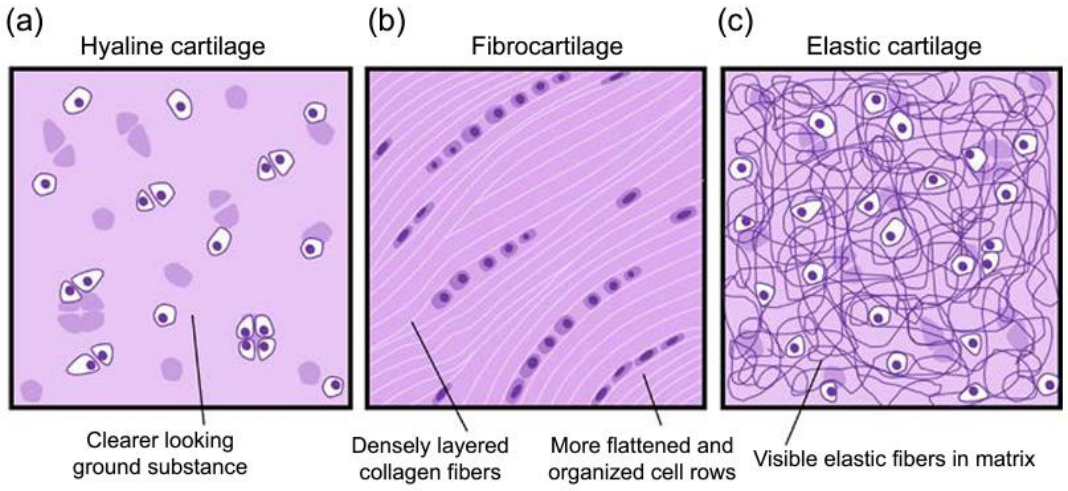

2.3 Mechanobiology

Understanding how cells interact with the environment via mechanics is referenced as mechanobiology. This space focuses on how physical forces and changes in the

mechanical environment change cellular function, differentiation, and morphology. The ECM is a highly dynamic 3D structure where cells interact with a myriad of biophysical and biochemical cues that can direct their cell lineage and function. Mechanical stimulation can dictate cell response through the modification of the cytoskeletal which leads to cell-matrix interaction and provides intracellular biochemical responses [35],[36]. For instance, the stiffness and fiber alignment highly influence the cellular function (i.e. morphology and mechanosensing/mechanotransduction) and differentiation [37]–[39]. Mechanotransduction is the ability of the cells to converse the biophysical cues from the matrix into chemical or biological signals [40]. Mechanosensing is the capacity of a cell to sense mechanical cues (e.g., matrix stiffness) from its environment [41]. Furthermore, work has been done by Chen et al., displaying environmental physical factors can result in cell shape differences.

The lab proved with biopotential media in combination with osteogenic media, when cells were in restricted environments, they were large and spread and eventually differentiated into osteoblasts. They mentioned a Rho, ROCK, tension, signaling pathway and attributed osteogenic lineage with the tension experienced from the restrictive environment [35]. The aforementioned cell properties can be determined by analyzing the localization of the Hippo pathway Yes-associated Protein 1 (YAP), and Transcriptional coactivator with PDZ-binding motif (TAZ) which are considered the primary sensors of the cell's physical nature and will diffuse into the nucleus [27], [39], [40], [42]. Cellular morphology and mechanosensing can be altered by varying dimensionality of a biomaterial [41], [43]. Buxboim et al., showed that cells can sense the effective stiffness of rigid objects that are not in direct cellular contact. The group concluded cells can increasingly respond

to the rigidity of an underling surface and sense the stiffer material [44]. An example of how cell stiffness and traction force influences cell lineage and morphology is shown in Figure 7. Furthermore, Subramoney et al., proved that when MSCs were in an aligned matrix while sensing mechanical stimulation, they differentiated into ligament fibroblast-like cells. However, in an unaligned environment, its attachment morphology changed [38].

Figure 7

Cell Morphology. Morphological cell response to material stiffness [26].

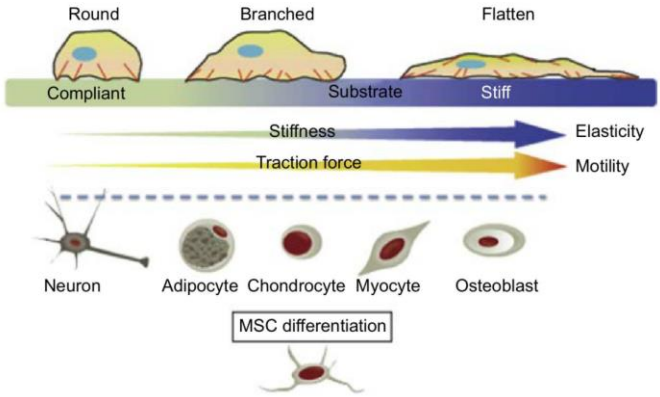

2.4 Knee Joint

The knee is the largest joint in the body. It is a synovial joint where the femur and tibia meet and are connected by ligaments and paired with cartilage to create a cushioned, stable, frictionless interface (Figure 8) [45], [46].

Figure 8

The Knee Joint. Simplistic biological view of the knee joint.

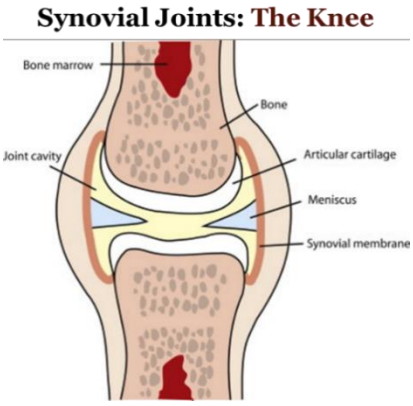

The ligaments that connect the femur to the tibia and provide joint stability include the anterior cruciate ligament (ACL), posterior cruciate ligament (PCL), medial collateral ligament (MCL), lateral collateral ligament (LCL), and antero lateral ligament (ALL). The ACL and PCL primary purpose is to prevent movement of the joint forward or backward and the MCL and LCL provide stability against lateral movement.

Figure 9

The Knee Joint Components. A) Articular cartilage composed of hyaline cartilage lines the condyle of tibia and fibula. B) The stabilizing ligaments of the knee. C) The menisci which act as shock absorbers. [47]

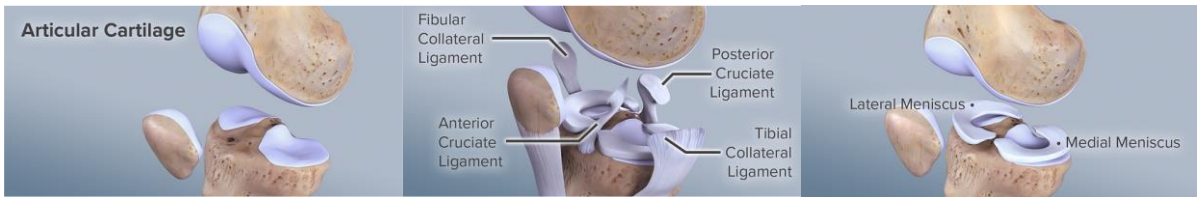

Articular cartilage covers the surfaces of the bones including where the femur meets the tibia and has important functions. It is highly specialized connective tissue found at the epiphyses of synovial joints and 2-4 mm thick referenced in Figure 9[47]. This cartilage's purpose is to protect the underlying subchondral bone and is composed of hyaline cartilage which in combination with synovial fluid, minimizes the frictions between movable joints. This cartilage also acts as a shock absorber and helps redistribute the shear forces and loads of everyday movements evenly throughout joints.

Another major component of the knee joint are the menisci. The menisci reduce shock and absorb the impact distributed to the joint when the bones move or bear weight. They function as the primary cushion, shock absorber, and first layer of defense for articular cartilage integrity [1]. Maintaining the integrity of the articular cartilage is crucial in the preservation of the joint and entire bone cartilage interface.

2.5 The Osteochondral Interface

The interface where bone meets cartilage is referred to as the osteochondral interface comprising of articular cartilage and subchondral bone [48]. Osteochondral tissues are multilayered and heterogenous consisting of a high concentration of osteoblasts in the underlying bone which merges in a gradient like fashion with chondrocytes in the cartilage lining the bone. This unit consists of mineralized and highly vascularized subchondral bone layer, an articular cartilage later that is acellular and avascular, and between bone and cartilage exists a gradient tissue layer with biochemical and physical properties [49]. The osteochondral unit is shown in Figure 10 [50].

Figure 10

Osteochondral Tissue. A) The layers of osteochondral tissue. B) A representation of the osteochondral interface where cartilage and bone meet and there is a gradient of osteoblasts and chondrocytes.

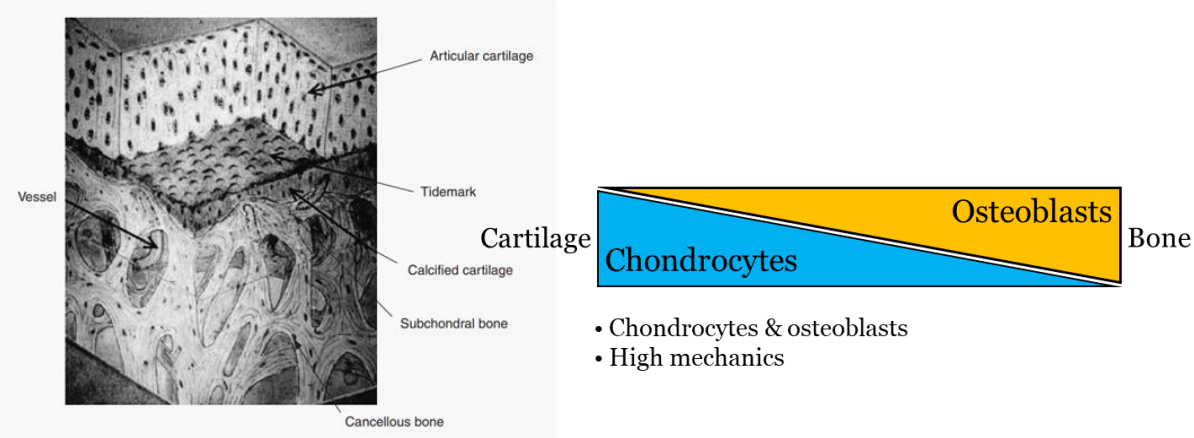

Damage in natural osteochondral tissue i.e., a defect or lesion, can lead to osteoarthritis initiating matrix degradation and implies the need for engineering synthetic osteochondral tissue as a treatment of the disease [50]. Injury to orthopedic tissues is highly prevalent as the demand for primary knee arthroplasties is projected to increase to over 3.4 million procedures by 2030 [51]. These osteochondral injuries/defects produce a significant burden around the world as there are hundreds of thousands of surgical procedures performed annually [52]. It has been cited osteochondral defects can be found in more than 60% of patients undergoing knee arthroplasty [52]. This statistic is a result of different factors including trauma, tumors, infections, and the progressive aging of the world population. For instance, people affected from these misfortunes develop bone and joint diseases which cause them to endure suffering for years to come [13]. Furthermore,

osteoarthritis is on the increase due to the multitude of mentioned factors and is expected to affect two billion people by 2050[53]. Therefore, it is important to continue research in this field and help relieve the burden osteochondral defects will cause on a significant population of the world.

2.6 The Goal of This Work

The main objective of this work is to develop a mechanically stiff environment that recapitulates the gradient tissue zones in the osteochondral interface. The general focus is to observe the morphological differences between MSCs as they are exposed to varying mechanical forces created by a composite biomaterial. The composite will be fabricated using salt leach method to create a porous stiff polycaprolactone backbone. The PCL provides a 2D environment and the force necessary to create a stress gradient of an injected hydrogel. This hydrogel will be synthesized using methacrylate gelatin and UV light for the purpose of a softer 3D environment inducing spread and round morphologies of cells. Biophysical signals including dimensionality and stiffness have been shown to influence cell behavior including mechanosensing, morphology and differentiation. The goal of this study is to create a composite that integrates these divergent biophysical signals within one system. The two separate environments will coexist inside the composite allowing for heterogeneous cell morphologies based on location of the cell in the pore. Through this work it is shown cells in the composite not only exhibit differences in morphology and mechanosensing than cells in gel alone, but they display differences based on pore diameter. The composite is currently being researched for the osteochondral tissue interface to provide an avenue exposing cells to varying biophysical forces like those presented in native tissues.

Chapter 3

Treatment Methods and Fabrication Techniques – A Review

3.1 Introduction

The complex structure and function of articular cartilage is prone to injury, it can be disrupted by everyday activities, and the response varies depending on the severity and depth of injury [4]. Response of superficial injuries can be as trivial as a disruption to the surface level cells or could initiate a cascade toward degeneration of the surface that are not visible. However, cartilage is susceptible to macro disruption when the injuries are more severe and can result in chondral fissures or partial thickness loss. The most severe case of injury occurs when the subchondral bone is immediately affected which can result in full thickness injury and osteochondral fracture [4]. As damage occurs, it results in limited metabolic capacity for repair of chondrocytes and a decrease in proteoglycan concentration. In turn, this causes decreased cartilage stiffness, and increased hydraulic permeability which directly results in increased force transmission to the underlying subchondral bone [54]–[57]. The increase of force causes an increase in stiffness of the bone and transmits the loads of impact back to the damaged cartilage thus, resulting in multifactorial tissue complex involvement and more articular cartilage injury that is caused from stiffening of the subchondral bone [58]. These injuries, responses, articular cartilage's avascular nature, and its inability to properly heal itself are examples of how osteoarthritis is such a prevalent condition and is consistently a problem for orthopedics. To treat these injuries a variety of techniques are used without much regenerative efficacy.

Current scaffolds on the market like the traditional techniques of monolayer scaffolds and injectable hydrogels often fall short of replicating spatial patterning of biochemical cues in native osteochondral tissue. This evokes the question; what type of treatment is there for these lesions to prevent osteoarthritis? Below are mentioned some of the current treatments for lesions and chondral defects.

3.2 Cartilage Techniques

3.2.1 Arthroscopic Lavage and Debridement

Debridement is usually the first level of chondral injury treatment [4]. This is done to reduce mechanical symptoms and inflammation however, there is no standalone evidence this technique helps restore cartilage or has long term benefits other than immediate pain relief [59]. This technique combined with lavage has shown benefits but only in patients with a specific history minimum cartilage damage [60].

3.2.2 Microfracture

Microfracture is a common technique used to stimulate the production of cartilage. Microfracture is a reproducible, atraumatic method that consists of creating 1-2 mm diameter holes in underlying cancellous bone releasing blood and to recruit bone marrow MSCs to restore the cartilage within a carefully prepared lesion (Figure 11) [4], [61], [62]. However, the main caveat of this method is that it generates a cartilage that resembles fibrocartilage which is mechanically inferior to hyaline cartilage [63], [64]. A study showed deterioration is present in the joint within 18-24 months post microfracture surgery and deterioration is greater when trying to treat a large defect [64]The results can be even less effective due to poor patient compliance as the procedure requires patients to be non-

weight bearing for at least 6 weeks [61]. This method is considered the gold standard for cartilage repair even with reports the fill of the chondral defect is rarely over 75% [65].

Figure 11

Microfracture. [66]

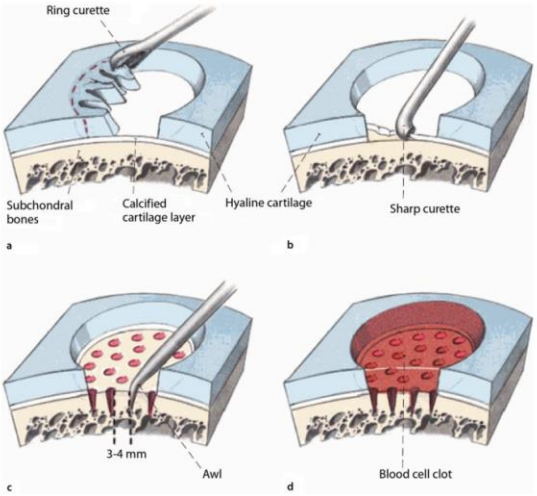

3.2.3 Osteochondral Autograft

Osteochondral autographs involve the transfer of intact hyaline cartilage and subchondral bone otherwise called a bone plug, and they heal to the surround recipient tissue [62], [67], [68]. The osteochondral autograph is removed from non-weight bearing areas of the knee and is transferred to the chondral defect to produce chondrocytes and maintain the extracellular matrix with load bearing capacity (Figure 12) [69]. As with all techniques, it has benefits and contraindications. This procedure is limited by donor tissue

available in the knee and has certain ideal indications. Symptomatic distal femoral condyle articular cartilage lesions with intact menisci and tibial cartilage with proper mechanical alignment in a non-degenerative joint is the ideal indication of this technique [61]. The drawbacks and limitations of autograph transfer include ideal lesion size of 1 to 2 cm in diameter, risk of donor site morbidity, fibrous tissue formation, intensive transfer procedure, and limited graph volume [67], [70].

Figure 12

Osteochondral Autograph. [13]

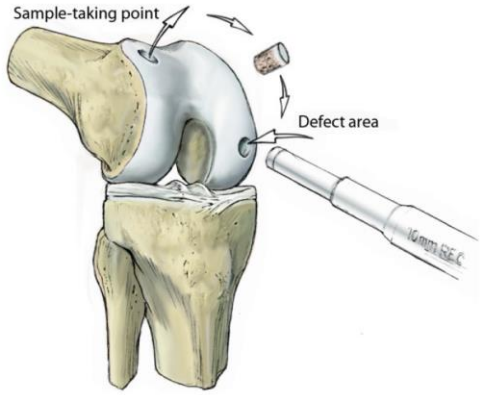

3.2.4 Osteochondral Allograft

This technique is employed when larger constructs are necessary and harvested from cadavers [4]. It allows for bigger lesion treatment and with no concern for donor site morbidity [61]. Osteochondral allograft has different limitations than autograft methods mentioned previously as it is not suitable in lesions caused by diffuse disease processes

like osteoarthritis, graft ability, cell viability, immunogenicity, and disease transmission risks [61]. However, if avascular necrosis is localized and the rest of the bone is healthy, this procedure may be explored and with a higher positive outcome chance with lower age [4].

Figure 13

Osteochondral Allograft. [71]

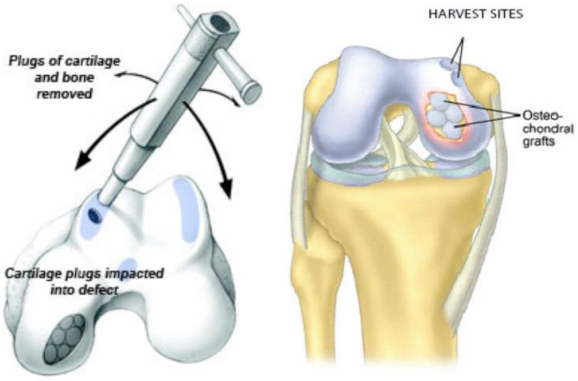

3.2.5 Autologous Chondrocyte Implantation (ACI)

Autologous chondrocyte implantation is a cartilage regeneration technique that includes a two-step surgical process. The process includes surgery that harvests hyaline cartilage from a low weight bearing region of the knee followed by in vitro expansion of chondrocytes and then a second surgery to implant the expanded cells into the defect location shown in Figure 14 [4], [13]. ACI is ideal when first line treatments fail and when osteochondral defects measure 2 to 10 cm^2, are unipolar, and well contained [61]. The

contraindications include are similar with those mentioned before. Bipolar lesions, malalignment, ligament instability, and meniscus deficiency are also obstacles that hinder ACI outcome [61]. ACI has shown more positive results than microfracture when defects are larger but there is not significant data to validate better results when the defects are small[72]–[74]. Also, the two-step surgical process is difficult for patients as the entire process has a recovery time of 6-12 months [75]. ACI has shown fibrocartilage formation in conjunction with hyaline cartilage which may be attributed to the 2-D culture in vitro on tissue plates and without mechanical stimulation. Meanwhile, the 3D structure of in vivo tissues coupled with mechanical loading induces the correct tissue formation without phenotype drift [13], [76].

Figure 14

ACI. Two step surgical process of ACI and MACI [13].

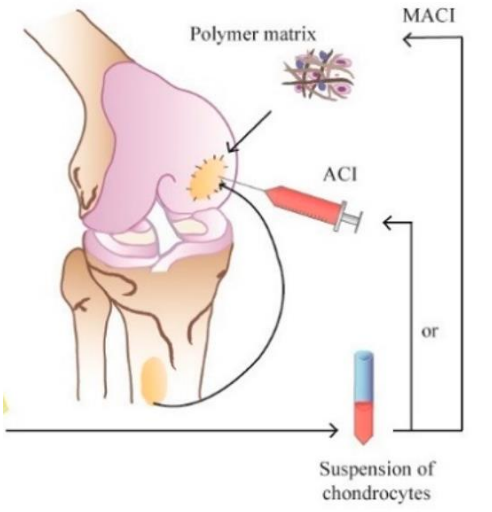

3.2.6 Matrix-Assisted Chondrocyte Implantation (MACI)

Matrix-assisted chondrocyte implantation (MACI) is the second generation of ACI. MACI has an almost identical process to ACI which is depicted in Figure 15. However, the expanded chondrocytes are seeded onto a collagen membrane scaffold before the reimplantation not injected back into the debrided site at random. MACI uses the matrix to help defect filling by localizing the implanted cells at the location of defect and has been shown to have less incidence of hypertrophy when compared with ACI [13], [77]. Also, grafting techniques are recommended for defects of more than 8 to 10 mm in depth as this method does not provide subchondral bone development [61].

Figure 15

MACI. Matrix-assisted chondrocyte implantation schematic [13].

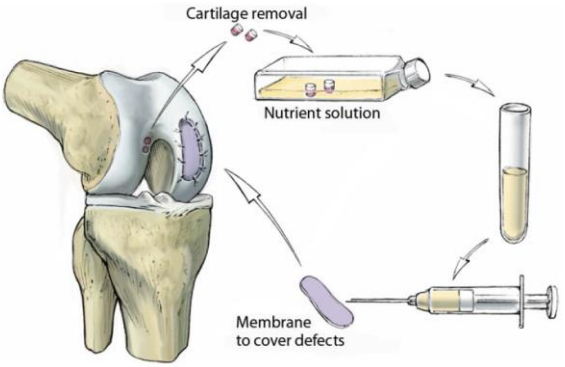

3.2.7 Treatments Overview

Articular cartilage is complex and highly specialized and therefore is difficult to reproduce [4]. Recent advancements in MTE have allowed properly selected patients options for cartilage and osteochondral repair. The problem lies in the techniques used to replace the articular cartilage. MACI is the only FDA approved treatment for articular cartilage defects using a biomaterial scaffold and yet it neglects the underlying issue of the entire osteochondral interface which may only mask the problem of further degeneration of the joint along with fibrocartilage formation. The challenge remains to make a treatment option for osteochondral repair of those patients who do not fit the selectiveness or fit as candidates of the above techniques. A summary of the surgical techniques to try and fix osteochondral defects and lesions is shown in Figure 16.

Figure 16

Treatment Overview. Overlapping treatment options from palliative, to reparative, to partial restorative [4].

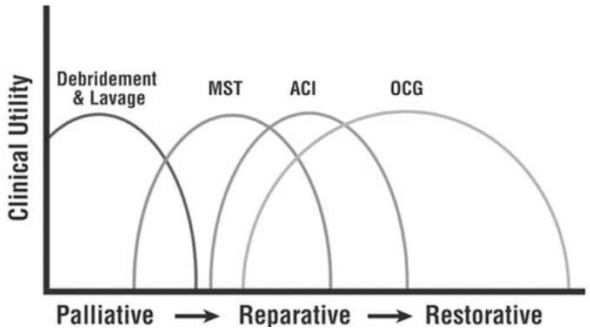

3.3 Scaffolds for Tissue Engineering

3.3.1 Introduction

Fabrication and design of biomaterials are major areas of research and important for the growth and development of tissue engineering and regenerative medicine. Kumar et al., defines scaffolds to be three dimensional porous solid biomaterials that are designed for multiple functions [78]. Generally, scaffolds serve the purpose of structural support and templates for tissue engineering and are composed of natural or synthetic polymers or even a combination of engineered and natural materials (Figure 17). There have been many scaffolds created and used for tissue engineering purposes in the past. Four general purposes for scaffolds include: (1) promote cell and biomaterial interactions, ECM deposition, and cellular adhesion, (2) allow passage of nutrients, regulatory factors, and proliferation and differentiation, (3) appropriate biodegradability, and (4) be bioinert and biocompatible.

Figure 17

Biomaterial Classification. [13]

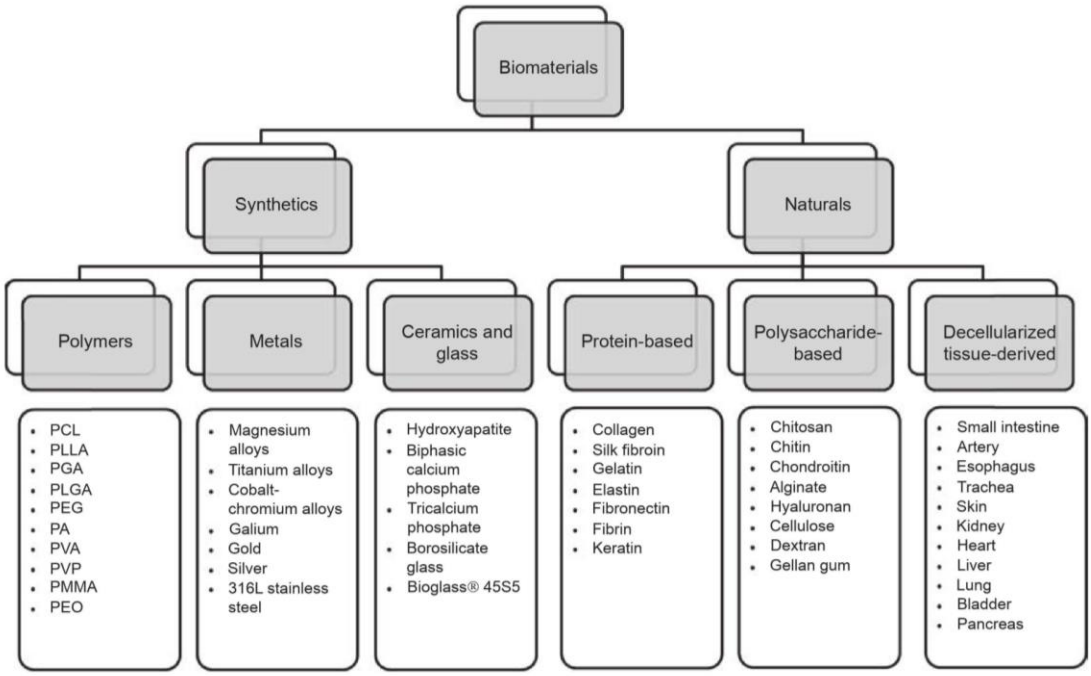

Figure 5.2 Schematic representation of biomaterial classification and examples.

3.3.2 Biomaterials

Depending on the intended use of the scaffold the materials can be synthetic or biologic, degradable or nondegradable [79]. These scaffolds can have two major origins in which they are classified including biological scaffolds that are derived from human or animal tissues, and synthetic scaffolds which are fabricated from polymers, metals, ceramics, and glass [80]. Scaffolds are fabricated and designed for different applications. For example, bone tissue engineering requires a mechanically superior scaffold than one designed for cartilage engineering and may require 2D dimensionality while cartilage

requires 3D dimensionality. Synthetic bioresorbable polymers for bone and cartilage tissue engineering include PCL, PLLA, poly(glycolic acid) (PGA), and polyvinyl alcohol (PVA) provide mechanic stability and can be formulated as either hydrogels, solids, or fibrous constructs. The two major categories are enticing for researchers for their different roles.

3.3.2.1 Synthetic Materials. A synthetic scaffold can be hard, stiff, but lack the biophysical and biochemical ques present in the native ECM. However, synthetic scaffolds may provide optimal characteristics such as rate of degradation, porosity, microstructure, strength, availability, and reproducibility. Porous premade scaffolds can be fabricated using synthetic materials. To improve bioactivity of the scaffold as coatings or surface modifications polysaccharides (chitosan, alginate, agarose), protein-based materials (collagen, gelatin, and fibrin), and glycosaminoglycans (hyaluronic acid and chondroitin sulfate), can be included in the fabrication process of the hard polymers [81], [82]. Therefore, PLA, PGA, and PCL are interesting materials due to their high elastic performance and strength for bone soft tissue scaffolds.

3.3.2.2 Natural Materials. Biological scaffolds that are decellularized may lack the mechanical toughness required to withstand the loads necessary for success, but they can generate less of an immune response and allow for appropriate ECM production. Scaffolds can be made from decellularized ECM from allogenic or xenogeneic tissues (biological), cell encapsulation in self-assembled hydrogel, or other natural materials [83].

As natural biomaterials lack mechanical stability, it is necessary to explore the spectrum of synthetic biomaterials. Synthetic scaffolds have great appeal to this work as the goal of this thesis was to create a construct with comparable mechanical stability as the

osteochondral interface. Synthetic biomaterials allow for development of stronger scaffolds with shape and architecture of native tissue. Synthetics offer high reproducibility and mechanics, but they present poor bioactivity in terms of hydrophilicity and cellular interaction cites when compared against natural materials [84]. One of the most used materials in scaffold fabrication and extremely relevant to this work is polycaprolactone (PCL) which has been used for tissue engineering applications since the 1930s [84]. Other common materials include poly(L-lactic acid) PLLA and poly (lactic-co-glycotic) acid (PLGA).

3.3.3 Scaffold Fabrication Techniques

As previously mentioned, scaffolds for tissue engineering are common and increasing in practice for the regeneration of all tissue types. Materials of biological and nonbiological origin have been used as early as the Neolithic period and sutures may have been used long before that[85]. A timeline of biomaterial applications in the history of recorded time is shown below in Figure 18. In this era of time, there are constraints and design criteria when recreating the OI which encourages a successful scaffold. The elementary first step is to use a biocompatible biomaterial that does not elicit any response from the host. Biodegradability is next as it is crucial to allow cells the opportunity to produce their own ECM. Another important consideration is one must know the mechanical environment of the tissue the scaffold is mimicking as it must perform the mechanical function of the native tissue. In this case, there is a very stiff environment, the underlying bone, and a softer environment, articular cartilage. Scaffold architecture, design of biological interface, and what the purpose the scaffold serves are other concerns that must be reflected in design [13]. The development of biomaterials and fabrication methods

has fostered novel techniques and increasing complex environments for regeneration and repair of tissues. Fabrication methods for porous, hydrogels, decellularized, and bioprinted scaffolds are described in detail below.

Figure 18

Timeline of Biomaterials. View of how biomaterials progressed as technological advancements have been made [13].

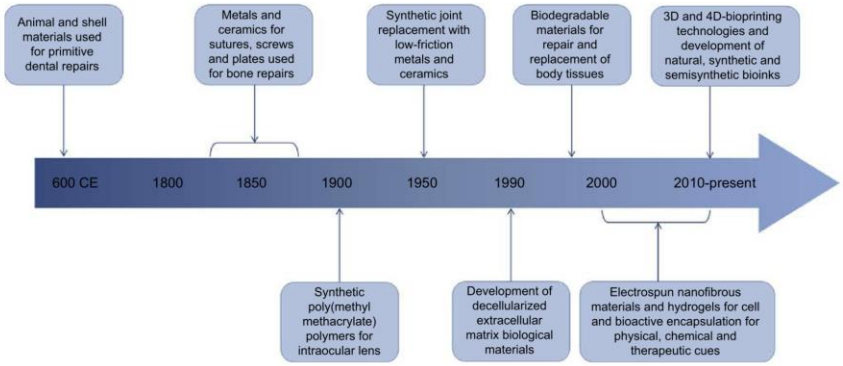

3.3.3.1 Porous Scaffolds. Porous scaffolds provide an environment suitable for injection of cells and are an avenue of treatment with regards to disorders and diseases. These scaffolds can be composed of natural or synthetic materials or can be a combination of the two materials which creates a composite [86]. These porous biomaterials can be fabricated using techniques mentioned by Chan et. al like 3D printing, salt leach method, and stereolithography [83]. The next few subsections will provide techniques on how to create scaffolds and their pros and cons. For example, scaffolds can be produced using

methods of electrospinning, but this technique creates a lack of compressive strength [87], [88].

3.3.3.1.1 Solvent Casting and Porogen Leaching (SCPL). Solvent casting and porogen leaching (SCPL) includes a simple, reproducible technique that requires two main steps. First, the solid is dissolved in a solvent mixed with an insoluble porogen which is typically NaCl, sugar, or other particles followed by casting the mixture and evaporating the solvent to produce a solid consisting of polymer and porogen [13]. The porogen is leached out of the construct by submerging it in an aqueous solution to yield an interconnected pore network throughout the solid (Figure 19). A benefit of this technique is its simplicity and tunability in terms of pore size, shape, and uniformity within the structure.

Figure 19

Solvent Casting. Schematic depicting the steps in sequential detail of the fabrication process for solvent casting and porogen casting [13].

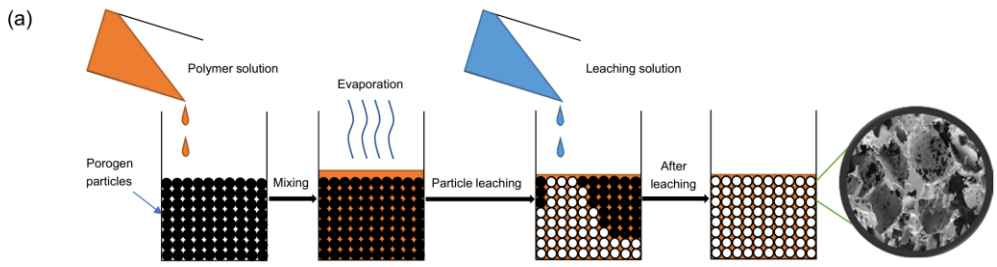

3.3.3.1.2 Phase Separation. Phase separation is a technique that can be used to create scaffolds. However, as pore size usually is less than 200 µm the application for tissue engineering is limited. In this process a homogeneous polymer solution separates into polymer rich and polymer poor phases when it becomes thermodynamically unstable by cooling the solution below the solvents freezing point to initiate crystal nucleation and drives phase separation. After completely frozen the solid material is sublimed which removes the solvent and leaving the polymer rich regions forming scaffold walls and the polymer poor regions yield the pores.

3.3.3.1.3 Gas Foaming. Gas foaming technique relies on a blowing agent which generates gas bubbles in a solid polymeric sample, leading to pores. This technique is advantageous as it does not rely on use of porogens and solvents however, controlling pore size, uniformity and reproducibility remains challenging.

3.3.3.1.4 Sintering. The sintering technique bonds together polymer and ceramics into a porous scaffold. This process includes heating a bed of particles above the base material transition temperature but below its melting point to encourage diffusion of molecules on the surface of the beads toward the contact point of the particles to fuse them together and produce a porous structure. These scaffolds usually have lower porosity and smaller pores than scaffolds produced by other methods [89].

3.3.3.1.5 Electrospinning. Electrospinning (ES) is the most widely studied fabrication process in the field of TE [90]. Electrostatic principle is the governing theory in which the electrospinning process works. The depiction below (Figure 20) shows an overview of the process. It relies on an electric field generated between a polymer solution

and a collector which draws the solution into a fiber. A syringe with a nozzle, a counter electrode, electric field source and a pump compose the necessary elements of the process. To start the process, the solution to be electrospun is loaded into the syringe and is pulsed by the pump. Then the solution is exposed to the difference in electrical voltage between the nozzle and counter electrode which generates a charge on the polymer solution and results in a cone shaped deformation of the drop of polymer solution. As the solution makes its way to the counter electrode, the solvent evaporates and produces a continuous solid filament [91]. Fiber diameter can be controlled by polymer concentration, solvent selection, flowrate, needle dimensions, and voltage differential and distance between the needle and collector.

Figure 20

Electrospinning. A) A forward view of the process where the polymer is projected onto the counter electrode. B) A side view of the electrospinning process [91].

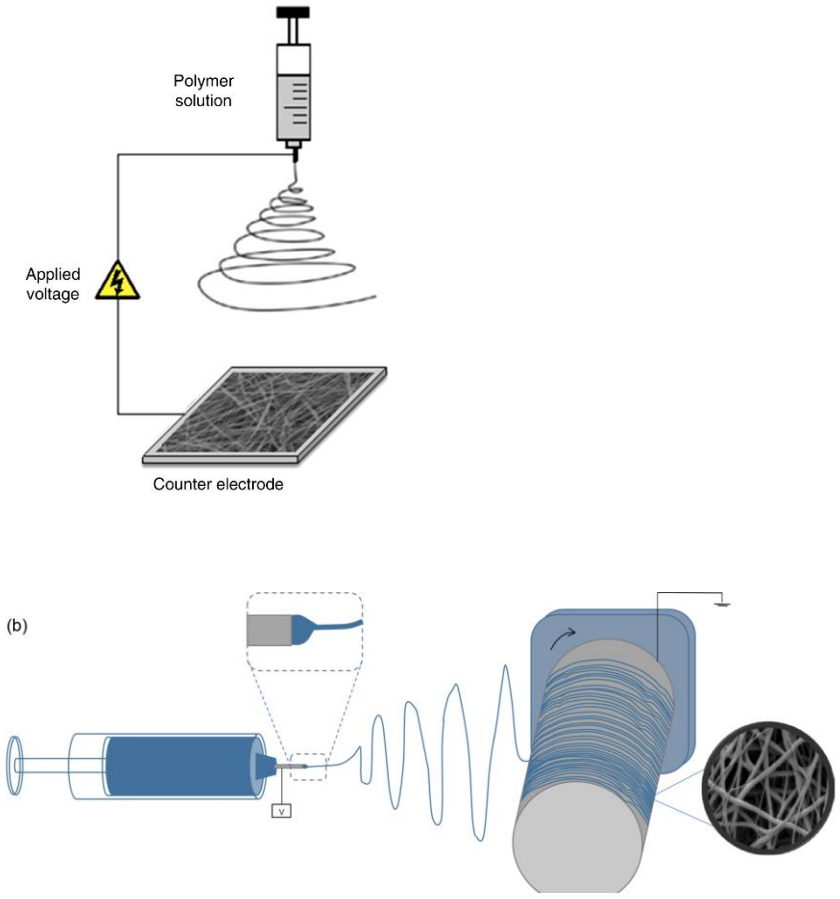

3.3.3.2 Hydrogels. Hydrogels are another class of biomaterials that have been widely explored in 3D as they can mimic the natural extracellular matrix (ECM) including the degradation of the surrounding which allows for remodeling of tissue [92], [93]. They are crosslinked 3-D networks of hydrophilic polymers that can hold and absorb large quantities of water. The benefits of hydrogels are many and their porous and swollen

polymer network allows for nutrients and cell waste to diffuse through the material. These provide a unique way to encapsulate cells within a membrane for specific purposes. Hydrogels are formed by covalent or ionic cross-linking of water-soluble polymers and are one of the best candidates for encapsulation [83]. A GelMe hydrogel fabrication process is shown in Figure 21. Although this approach has weaknesses like poor mechanical properties, it has appealing characteristics as it is minimally invasive, useful for a defect with abnormal shape, and degradable by the cell. The stiffness can be tuned by changing the wt % of the macromer. They can be synthesized from natural biopolymers, synthetic polymers, or a combination of them and the most common used materials include, collagen, elastin, fibrin, hyaluronan, chondroitin sulfate, gelatin, and many others. Hydrogels provide benefits as they have low cytotoxicity and can modulate cell responses like attachment, proliferation, and differentiation.

Figure 21

GelMe Hydrogel Fabrication. [83]

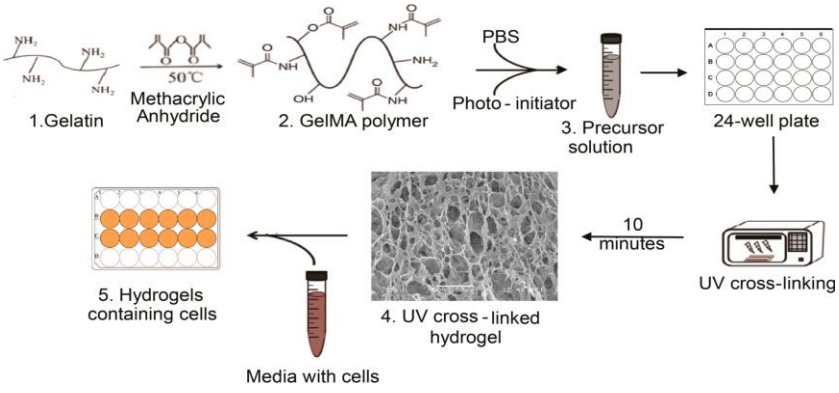

3.3.3.3 Tissue/Organ Decellularization. Decellularized ECM scaffolds for cell seeding have gained popularity in designing scaffolds for tissue engineering applications. The advantages of using these scaffolds include they are biocompatible and have almost minimum to no immune response from the host and the resultant ECM is designed to provide cells in a 3D environment [94]. To create the immuno-friendly scaffold with just natural ECM remaining, detergents or enzymes must be used [94], [95]. To decellularize tissue there are physical, chemical, and or enzymatic protocols. Physical protocols include disrupting the cell membrane and using sonication, freezing, or mechanical force use. To remove via chemically, detergents, acids, bases, chelating agents, hypotonic and hypertonic solutions or of enzymes can be used to remove cellular debris. However, decellularized ECM scaffolds for cell seeding usually lack mechanical properties necessary to create a construct strong enough to bear mechanical loading equivalent to joint tissue.

3.3.3.4 Tissue Bioprinting. There are a few different approaches when considering bioprinting and tissue bioprinting is a rapidly emerging fabrication method for scaffolds in musculoskeletal tissue engineering. A generalized sequential process for tissue bioprinting is shown in Figure 22. The following subsections will give a brief overview of some 3D printing techniques.

Figure 22

General Bioprinting Process. [13]

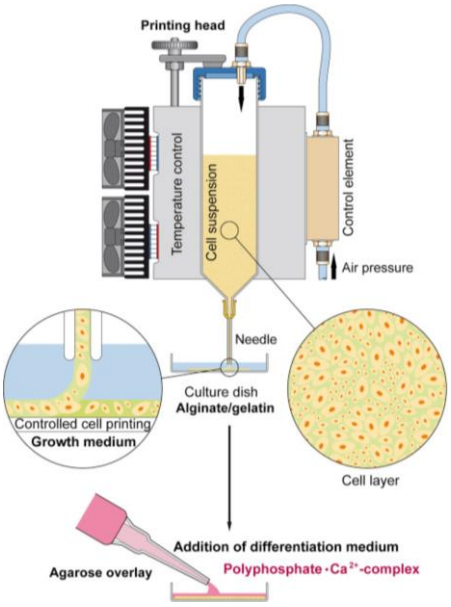

3.3.3.4.1 Powder-bed 3-D Printing. There is powder-bed 3-D printing which relies on the selective spatial delivery of a binder onto a powder bed by an inkjet printer. This process uses sequential application of powder layers intersperse by addition of the binder and a drying step to create 3D structures. The structure is supported as it is built by the uncoated lose powder bed. This is followed by removing the loose powder and sintering the powder particles together providing mechanical integrity to the structure. The powder properties control the resolution of this technique as well as the printer technology. This process can allow for generation of scaffold gradients in the z-axis via changes of the powder bed [96]. However, a limitation of this technique is it suffers from construct

shrinkage and deformation during the sintering step, and it is difficult to make pores smaller than 600 μm because of the strayed loose powder [97].

3.3.3.4.2 Selective Laser Sintering (SLS). Selective laser sintering (SLS) is a similar process to powder-bed 3-D printing however, the powder particles are sintered directly in the powder bed rather than bound with a binder and sintered later.

3.3.3.4.3 Fused Deposition Modeling. Fused deposition modeling (FDM) is an example of melt extrusion-based technique. A computer aided design (CAD) model dictates spatial coordinates whereby a polymer extruded by a heating nozzle by which it is melted [13]. This process can become very intricated as multiple extrusion nozzles can be used to apply the polymer that acts as temporary support while creating compositional gradients in three axes.

3.3.3.4.4 Stereolithography. Stereolithography (SLA) creates a 3D structure and uses computer-controlled laser beam or ultraviolet light to polymerize a photocurable liquid monomer film in a spatially selective manner (Figure 23). The uncured polymer is removed to reveal the intended structure and can be further polymerized to increase the bonding and mechanics of the scaffold. As the base material typically is introduced as liquid, SLA is not easily amenable to changes in the construct composition across its depth. It allows the fabrication of parts from a computer aided design file. The external and internal pore geometry can be devised using 3d computer drawing software, mathematical equations, or from scanning data like MRI [13]. The structure can be fabricated by uploading the data to the SLA apparatus which makes the biomedical fabrication of this method enticing.

Figure 23

Stereolithography Process Overview. [13]

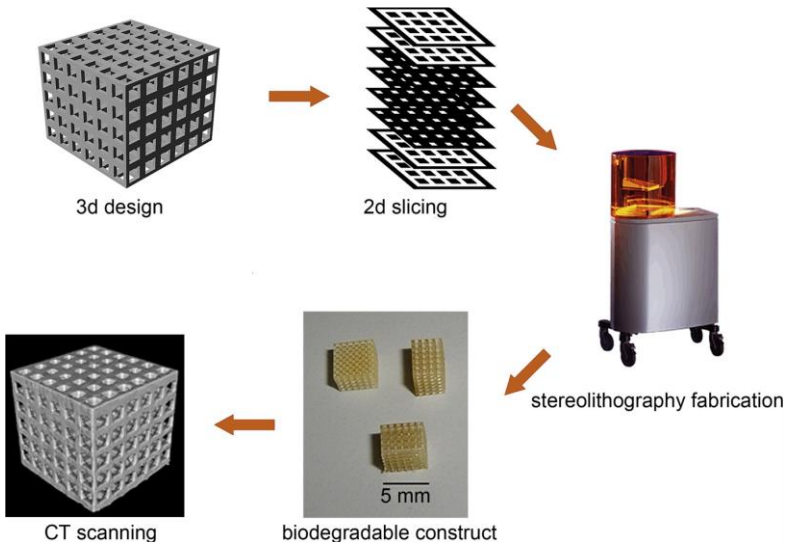

3.4 Conclusions

We proposed the formation of a composite biomaterial made of a 2D rigid material (PCL) and a 3D elastic one (GelMe hydrogel). It is hypothesized this mixture may cause heterogeneity in the cellular environment with varying dimensionality and stress. Additionally, we hypothesized that the PCL scaffold will cause mechanical stimulation and stress loading on the cell-encapsulated hydrogel due to the large differences in Young's modulus leading to a stress gradient within the hydrogel pore region of the composite and that the cell can sense this gradient which will impact cellular morphology [44]. The cell remodeling phases and MSC morphology changes to different compressive loading will be

explored. This composite will be crucial in TE application since it can replace damaged interfaces such as osteochondral interface (OI), located between bone and cartilage due to the mechanical adaptation of MSC to the different environment [48][50].

The synthetic OI will be crucial in preventing osteoarthritis specifically in the knee joint between femur and tibia which could eventually reduce the large increase of demand for primary knee arthroplasty[51] [45], [46], [98]. Even though the effect of dimensionality and remodeling on cellular behavior has been widely studied, to this date, there have been no engineered materials combining the effects of dimensionality and remodeling properties to investigate cell-material interactions. This combined scaffold could be useful for creating tissue substitutes such as an osteochondral interface located in the knee.

Chapter 4

Studying Bulk Compression vs. Cellular Remodeling

4.1 Introduction to Environmental Factors

Dimensionality and mechanical stimulation are important factors that can influence MSC mechanical behavior. Depending on the dimensionality of the substrate, cells can vary in their response to the matrix stiffness. MSCs cultured in 2D rigid material are large, spread, and YAP localized in the nucleus [43], [99]–[101]. Meanwhile, in 2D, MSCs can only differentiate into osteoblasts if seeded in 2D rigid materials and exposed to the bone morphogenetic protein 2 (BMP2) [102][102]. Polycaprolactone (PCL) porous scaffold can be fabricated to encompass stiff characteristics and qualities that are used in TE. As PCL can be fabricated to be very stiff, degrade over time, and biocompatible, it can mechanically mimic the properties of bone [103]–[107].

It is also important to note articular chondrocytes have shown dramatic morphology changes as they have demonstrated spreading when cultured on 2D monolayers from the smooth elliptical shapes of chondrocytes found in normal articular cartilage [108]. On the other hand, MSCs have an alternate mechanical response when encapsulated in soft 3D biomaterials such as hydrogels. MSCs encapsulated in the 3D elastic hydrogel can be smaller, have their YAP/TAZ localized in the cytoplasm, and be round in morphology which encourages MSC chondrogenesis [104]. It has been discovered by Mcbeath et al., cell spreading regulates stem cell differentiation. Environments that favor a spread shape help MSCs differentiate into osteoblasts and environments that favor a round shape help

MSCs differentiate into chondrocytes (Figure 24) [26]. Therefore, an objective of this work was to engineer an environment that allowed a co-population of spread and round MSCs.

Figure 24

Environmental Morphology Differences. [108] *Cell's cytoskeleton stained red on a stiff substrate with spread morphology help cells differentiate into osteoblasts. Cells stained in magenta encapsulated in a 3D environment and with round morphology will help cells differentiate into chondrocytes.*

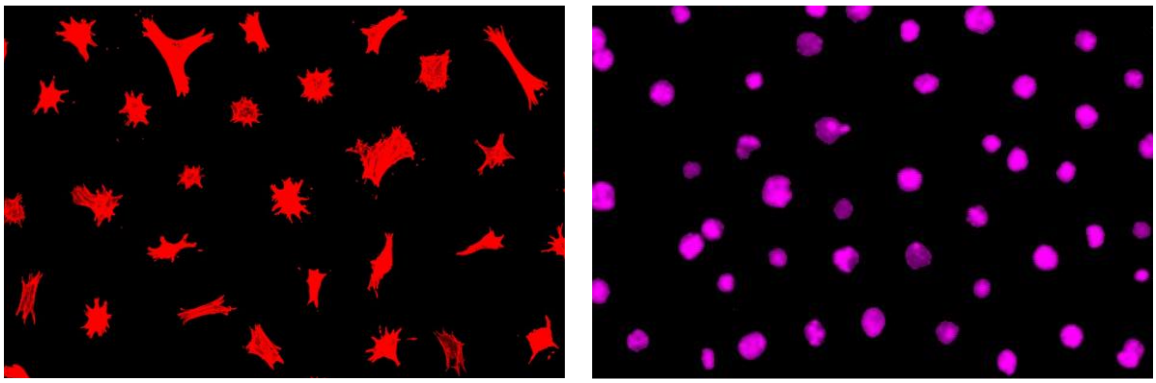

4.1.1 Cellular Remodeling

Cellular remodeling plays a crucial role in cellular behavior because it can lead to differentiation, morphological changes, migration, and proliferation [93], [109], [110]. A result of this finding emphasizes the importance to synthesize a hydrogel that can degrade over time [110]–[112]. During the remodeling phase, cells exhibit normal spreading while having YAP/TAZ localized in the nucleus [113]. A degradable hydrogel can either be

formed by incorporating protease-degradable crosslinker such as Hyaluronic Acid modified with norbornene or by means of incorporating a biodegradable backbone such as Gelatin [114]–[116]. Methacrylated gelatin (GelMe) hydrogel contains a gelatin backbone and degrades at the presence of matrix metalloproteinases (MMP). MMP is secreted by cells during the remodel process leading into the localization of YAP/TAZ in the nucleus [36], [117].

4.2 Methods

4.2.1 GelMe Macromer Synthesis

Methacrylated gelatin was synthesized using the technique described previously [118]–[120]. Gelatin was mixed in PBS at 10% (w-to-v) at a temperature of 50 °C and a speed of 1200 rpm for 20 minutes. Then 1.74 ml of methacrylate anhydride was added dropwise into the GelMe solution and stirred for one hour under the constant nonvarying speed and consistent temperature without exposure to room air. Once completed, the GelMe solution was centrifuged to remove the supernatant and then mixed with prewarmed PBS. GelMe was dialyzed to further purify it for 5 days followed by a lyophilization process to remove any excess water and kept in a -20 °C freezer until needed then analyzed in H NMR.

4.2.2 PDMS Mold

Polydimethylsiloxane (PDMS) mold was synthesized to support the formation of the cylindrical hydrogel. Sylgard 184 (Electron Microscopy Sciences) was mixed with the curing agent at a 3:1 ratio. Next, the mold was desiccated to remove all air bubbles and then was baked in the oven at the temperature of 80 ^{0}C for 1 hour. The mold then dried at

room temperature for 45 minutes. After completely drying and before hydrogel formation, the PDMS mold was punched by an 8 mm biopsy to have an 8 mm opening for the GelMe solution. The mold was cut and adhered to the thiolated coverslip using silicon as a binding agent.

4.2.3 Coverslip Thiolation

Necessary to synthesize gel and ensure a defined location, thiolated coverslips were assembled. Coupling the gel into the coverslip required several steps. First, coverslips were placed in a sodium hydroxide solution (NaOH) for 20 minutes. Next, it was re-submerged in for another 10 minutes in the same solution. After washing the coverslips twice, they were submerged inside of the thiolated solution (83% of toluene, 4% hexylamine, and 13% of silane) for one hour followed by two Toluene washes. Finally, the coverslips must be baked in the oven for one hour at 110 ^{0}C.

4.2.4 H NMR

After synthesizing GelMe macromer, the polymer was analyzed in H NMR to investigate its structure. Peaks represented between 5 and 6 particles per million (ppm) represent the structure of the methacrylate vinyl group and the one represented after 7 ppm represents the aromatic side of gelatin.

4.2.5 Mechanical Testing of GelMe Hydrogels

The Young's Modulus of GelMe was calculated. 5 wt% of GelMe mixed with PBS, 2mM Arginine-Glycine-Aspartate (RGD), and 0.05wt% I2959 was injected onto a thiolated coverslip adhered with PDMS mold and biopsied in the middle. RGD is included

as it is one of the most effective peptide sequences for stimulating cell adhesion on artificial surfaces [1]. The solution was exposed to UV light under an intensity of 10 mW/cm^2 for 10 minutes. Once the GelMe hydrogel was formed, it was submerged in PBS overnight and then the Young's Modulus was investigated. The hydrogel strain rate was set to 0.1%/min and the Young's Modulus was calculated between 10 and 20% strain for a maximum of 30% strain. The Young's Modulus was calculated between 10 and 20% (n=6). The Young's Modulus was found to be 7.2 kPa which can be considered a stiff biomaterial when comparing to other hydrogels. It is important to understand that the stiffness of the hydrogel can be manipulated by changing the wt% of GelMe macromer in solution.

4.2.6 Cell Culture

Human Mesenchymal Stem Cells (hMSCs) were purchased from Lonza Company. The cells were cultured in Dulbecco's Modified Eagle's Medium with L-glutamine and with sodium pyruvate mixed with 10% of Fetal Bovine Serum (FBS) and 1% of Streptomycin/Penicillin. The cells were passage into P2 before use. Sterile technique was conducted during all experiments involving MSCs. This technique included sterile work surfaces, all live cell culture was conducted in a sterile cell hood, and all sterile tools. Sterility of tools and surfaces was achieved with UV light and Ethanol.

4.2.7 Time Point Experiment

MSCs were thawed at P2 and were cultured until 80% confluency was reached. The cells were passaged then mixed with the GelMe solution with 1,000,000 cells per ml. 100 µl was pipetted of the cell solution in the thiolated coverslip which resided using silicon as adhesive on the thiolated coverslip. The total solution then was exposed to UV light for 10

min under the intensity of 10 mW/cm^2. Each hydrogel was analyzed at different time points 1, 3, 5 & 7 days for volume, sphericity, and nuclear YAP to study remodeling and mechanical activity.

4.2.8 Compressive Simulation

To further investigate the impact of the compressive device on cell encapsulated in GelMe hydrogel. A computational simulation was used using the FEBio program. A cylindrical model was created mimicking the form of the hydrogel with 8 mm diameter and 1.6 mm. The density of the GelMe was chosen to be 1.02 g/cm^3. The Young's Modulus of the model directly mimicked 7 kPa modulus of the hydrogel and a poison ratio of 0.49 showing an elastic type of material. The bottom of the model was chosen to be fixed in x,y, and z since the GelMe hydrogel was attached to the bottom of a 24 well. Two pressures were used representing the force applied by the compressive device on the model. 1230 Pa was chosen to represent 25% of the compressed height of the model and 2370 Pa represented 50% of the compressed height of the model. These pressures were chosen by trial-and-error method. Figure 25 shows the FEBio image of the model.

Figure 25

FEBio Representation of the Hydrogel.

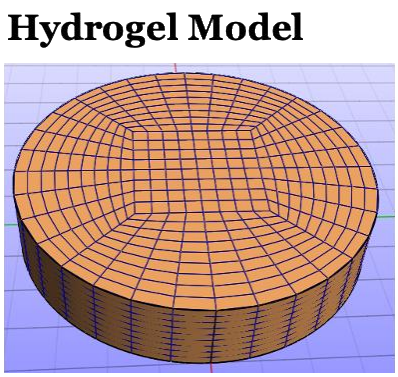

4.2.9 Compression Device Fabrication

The compression device was designed using a sheet, nuts, and bolts of high molecular weight plastic (HMWP) shown in Figure 26. The device encompassed the 24 well plate and was configured using the schematic of the well plate dish. The construct consisted of a top and bottom layer of HMWP and two 50.8 mm side pieces, fastened together using a binding agent and a hinge joint as well as two eye hooks to ensure locking mechanics were without fault. Twenty-four 12.7 mm diameter holes were drilled through the top layer of the device allowing for manipulation of the nylon screws. The height of the module was 50.8 mm, the nylon screws were 6.35 mm in diameter and 76.4 mm in height.

All practices were conducted using sterile techniques. Cells were mixed in the GelMe solution of 100 µl at 1,000,000 cells per ml and then pipetted in an 8 mm PDMS mold and placed on top of a thiolated coverslip. The gel was polymerized, the mold was

separated from the gel and then the gel was washed and submerged in media. The bolt was then twisted to ensure the appropriate percent deformation of the gel. Using a hex head nylon bolt and a digital caliper, the percent of compression was controlled by bolt rotation where 1/6 of a rotation was equal to 325 μm and the gel height was controlled by the height of the PDMS mold which was 2.209 mm. The goal was to compare 0% compression, 25% compression, and 50% compression at a three-day timepoint. For 25%, 50%, deformation, the gel was compressed by twisting the bolt $9\frac{5}{24}$ and $8\frac{11}{12}$ rotations from the initial contact with the nut thread. The gels incubated under compression for 3 days before being stained. The gels were fixed and stained under compression with Phalloidin, PI, and YAP as mentioned and then imaged under confocal microscopy. The gels were imaged at the edge of the gel in mm (0,0), (0.5,0), (1,0), (7,0) (7.5,0) (8,0) and the inner region (3,0), (4,0), (5,0). The results were quantified using volume, sphericity, and YAP expression to compare with the three-day controlled group under no compression.

Figure 26

Compression Device. Customized compression device and well plate dimensions.

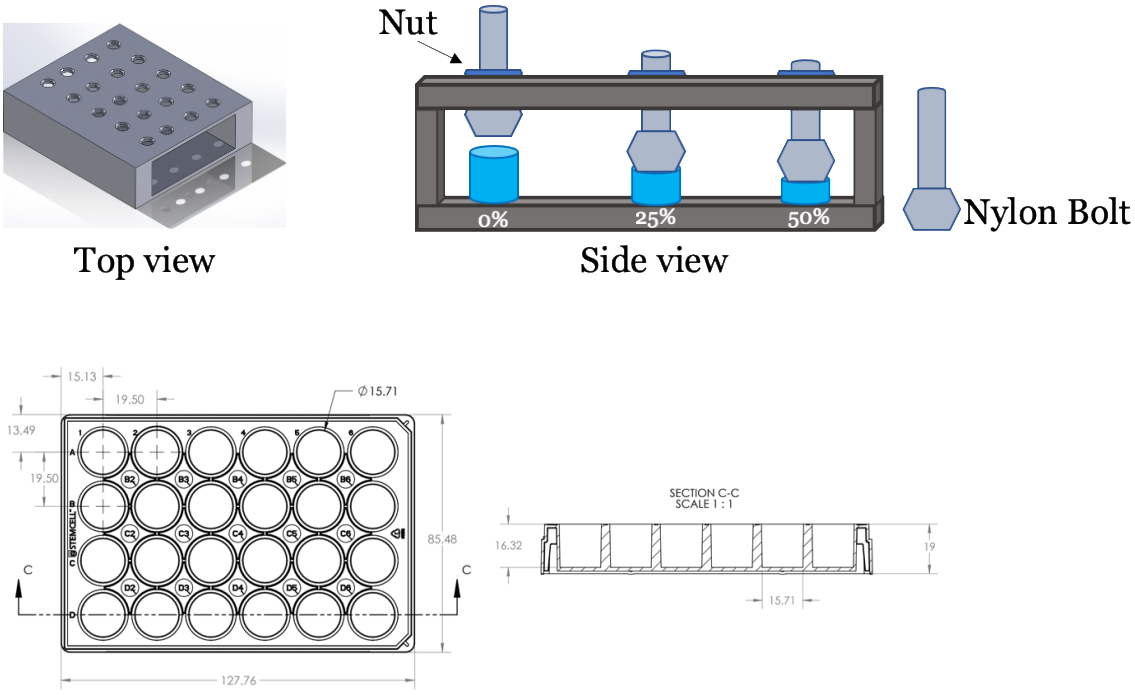

4.3 Results and Discussion

4.3.1 Cell Remodeling in 5 wt% GelMe Hydrogel

As described above, GelMe hydrogel degrades in the presence of cells. As such, there is a need to investigate the degradation rate in function of the remodeling. The study was done on 5 wt% GelMe hydrogels with a Young's Modulus of 7 kPa. A density of 1 million cells/mL were encapsulated in the hydrogel and was tested for different time points: 1, 3, 5, and 7 days. Cells at early time points 1, and 3 days are presented to be small and

more rounded. However, the more the cells spend encapsulated in GelMe hydrogel, the more they begin to degrade their surrounds and spread (Figure 27).

Figure 27

*Timepoint Experiment. A) Bar graph with individual points from cells. B) Histogram data of timepoint experiment. C) Qualification of cell morphology for 1, 3, 5, & 7 days. Cells analyzed > 50 for each experiment and *p<0.05 is significant.*

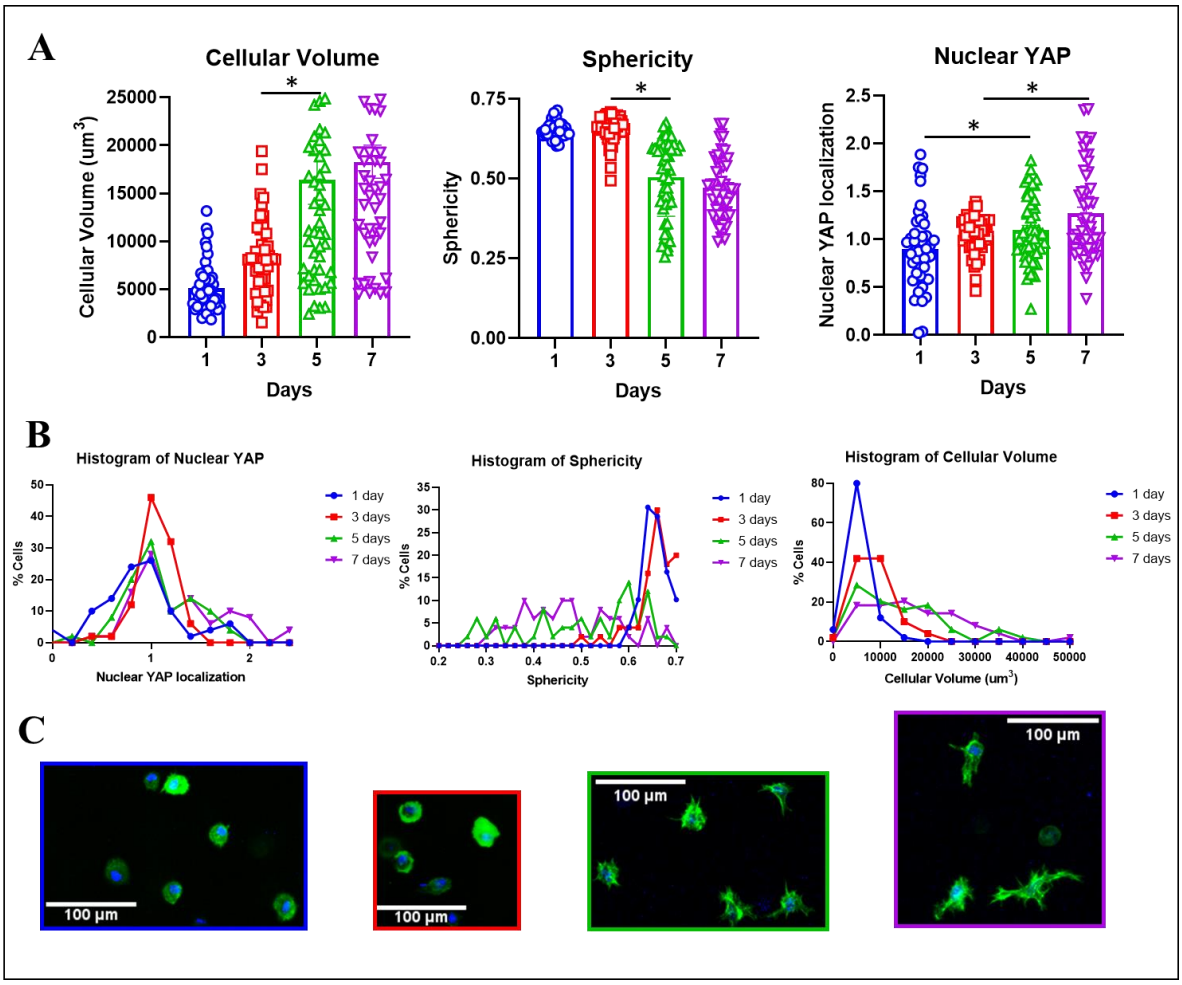

Cell remodeling was observed and the time dependent remodeling behavior of the cells was studied [92], [93], [109]–[111]. When analyzing F-actin, sphericity, and Nuclear YAP of MSCs in GelMe hydrogel for 1 day, 3 days, 5 days, 7 days, it was determined MSCs were remodeling their own tissue by increasing their cellular volume, spreading, and increasing their nuclear YAP expression. Additionally, the cells began to slowly remodel their native environment of the lone GelMe hydrogel. Caliari et al., discovered the same this finding of time varying heterogeneity of cell populations when analyzing their 3D hydrogel [113]. After 3 days of encapsulating MSCs in the hydrogel, the cellular volume increased enough from day 1 by 3000 μm^3 and cellular volume was mostly homogenous for the 3-day time point and cells increased in volume by ~8000 μm^3 from day 3 to day 5 which is considered rapidly faster than 1 to 3 day. Moreover, the cells at 3 days where more spherical and did not exhibit spreading compared to 5 days (0.65 vs. 0.52). The YAP expression shows the cells are sensing their mechanical environment as they spend more time encapsulated in the hydrogel when 1 day is compared to 3 day (0.9 vs 1.04). Observing histogram results, the environment at 3 day was still considered a homogeneous environment with larger results than day 1 (5000 μm^3 more than day 1, 0.1 sphericity unit less than day 1, and about 0.5 Nuclear YAP more).

After 3 days of encapsulating MSCs in GelMe, it was found that the cellular volume increased by about 3000 μm^3 (5120 μm^3 to 8160.56 μm^3), sphericity stayed steady, and the nuclear YAP increased by 15%. Throughout the 4 timepoints cell average volumes are between 5000 μm^3 and 20,000 μm^3, sphericity between 0.45 and 0.7, Nuclear YAP localization between 0.6 and 1.5.

Taking all these into consideration, encapsulating MSCs in 3 days was the optimal time point since it represents the time where the cells were starting to adapt with the environment. Waiting for cells to remodel so much of its own tissue (5 and 7 days) would also be problematic because cellular heterogeneity may be more widely observed. These considerations are imperative when analyzing cells in future experiments. Subsequential studies were conducted to observe if cells can remodel their environment quicker if exposed to mechanical force as they will experience in vivo.

4.3.2 Numerical Prediction of GelMe Hydrogel to Compressive Device

To further understand the change of the homogeneity of the environment, it is crucial to use a computational numerical simulation to understand the gradient of the stress. The testing was to be conducted at 75% gel height and 50% gel height due to compression (25% & 50%). These were chosen to represent the elastic and plastic phases of the gel respectively. When representing the 25% of hydrogel's height, it was found that the stress was about 0.5 kPa in the center and 1 kPa in the edge. As for 50% of hydrogel's length, the stress applied at the center was 1 kPa and 1.5 kPa at the edge (Fig. 28). Therefore, when the loading was applied on the gel causing 25% of strain, most of the impact occurred at the edge leaving the cell cellular volume, sphericity, and nuclear YAP localization about the same when loading was applied. On the other hand, when loading caused 50% of strain, even though the edge was more impacted, the cellular behavior was equally impacted which may be a result of an optimum force applied. Table 1 shows the forces and stress on the hydrogel under compression.

Figure 28

Hydrogel Compression Simulation. FEBio was used to simulate local stress differences within the hydrogel with compression of 25% and 50%.

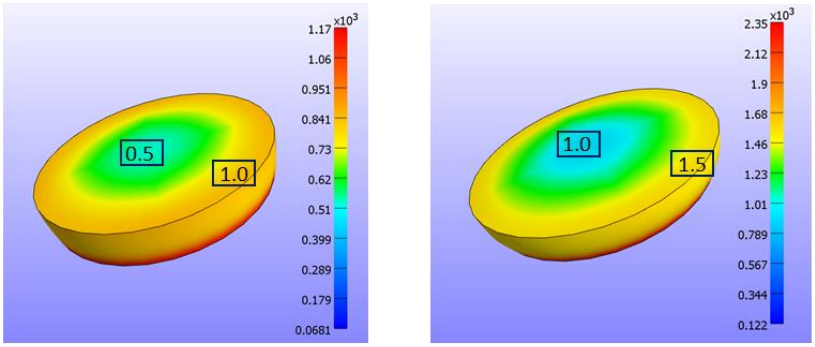

4.3.3 Compressive Device Alters Cellular Morphology

The construct was made to provide insight on how cells can remodel their environments based on stiffness gradients and model cell behavior in contractile and less contractile environments along with the forces that affect their behavior. The simulation described above predicted the forces on the gel under compression, and due to the compression, gels would have a stiffness gradient. Stiffer regions of the gel were quantified to be the edge of the gel or the outer 25% of the diameter of the gel (outer 2 mm) and were hypothesized to have a larger more spread population of cells (Figure 29). Meanwhile, the inner 50% of the diameter of the gel (inner 4 mm) was hypothesized to be softer which

allowed for less mechanotransduction of cells and a more spherical shape signaling less remodeling hydrogel remodeling.

Three different types of hydrogels were tested to investigate the cellular response to mechanical stimulation. All hydrogels contained cells and were exposed to the forces for 3 days due to the lack of extreme remodeling of the hydrogel network and expansion of the cell. It was hypothesized that when exposing cells to an environment with mechanical forces they would degrade their surroundings in a faster time dependent manner than what was shown in the timepoint experiment. The first group was a control with no force applied or 0% compression. The second group was exposed to a compression bolt which deformed the hydrogel to 25% of its original height or 1.65 mm and the third 50% compression was 1.05 mm in height as shown in Fig 29.

Figure 29

Design of Compression Experiment. Experimental design of cell encapsulated hydrogel compression.

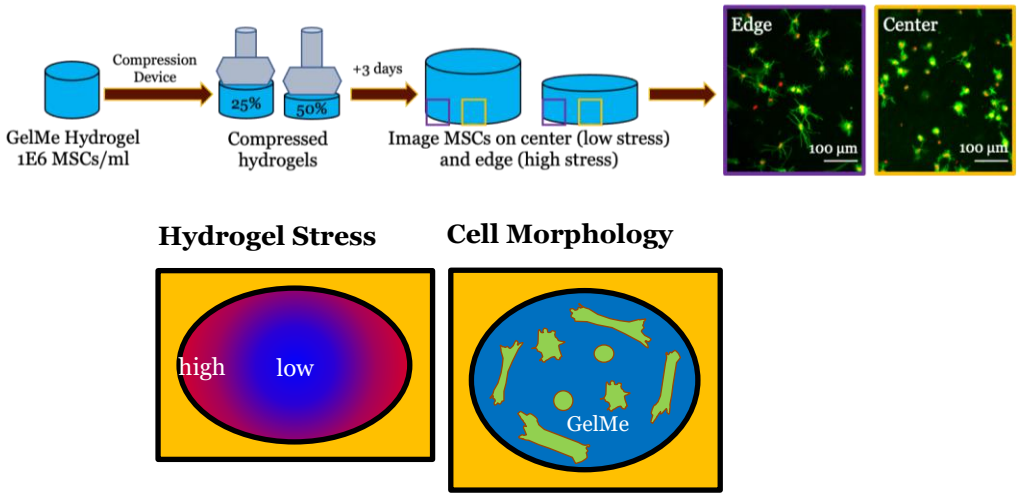

Results demonstrate the cells sensed the mechanical loading from the compressive device as shown in Fig 30. It was found that, at 25% strain, the cellular volume increased by 1.5-fold to 15,138.68 μm^3 when comparing cells at the edge of the hydrogel but no major changes at the center when compared to the control (7198.65 μm^3 vs. 8160.57 μm^3). The sphericity decreased slightly at the edge (0.57) and there were no significant changes in the center (0.619 vs. 0.655). The same trend applied to nuclear YAP as it was greater towards the outer edge of the gel when compared to the center 1.77 vs. 1.37. Therefore, when 25% of the original height of the hydrogel was compressed, the cells responded to the mechanical stimulation and were remodeling the hydrogel quicker than the control. This observation is important when considering how to increase mechanical activity of cells and could potentially lead to further studies which observe differentiation.

Figure 30

*Compression Device Data. Figure 30 a, b, c shows cellular volume, sphericity, and nuclear YAP of 0%, 25% and 50% compression via bar graph and histogram. Cells > 50 *p<0.0001.*

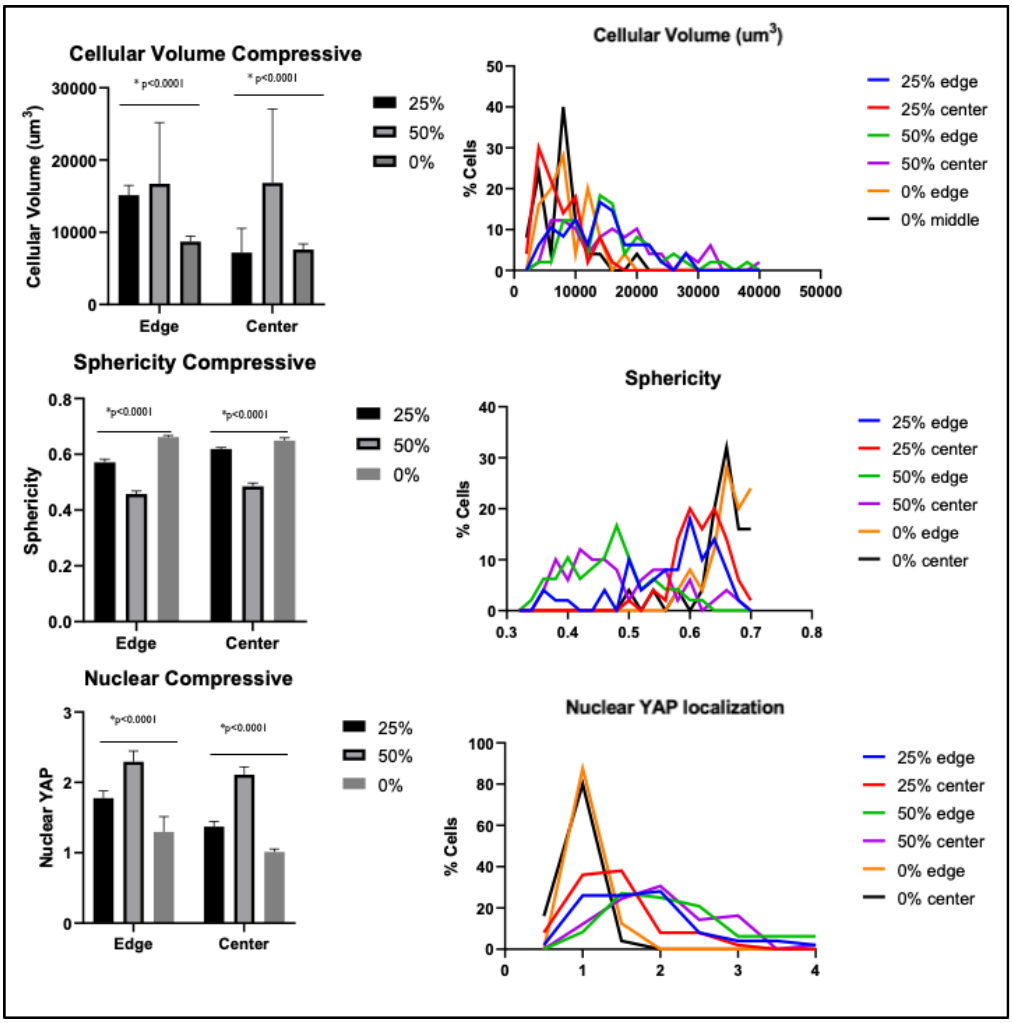

At 50% strain, a major force difference is displayed throughout the entire gel and is larger than the other groups. Fig 30 also showed that the distribution of the cells' morphology (volume, sphericity, and YAP) in the edge and center when the hydrogel was

exposed to 25% and 50% of the strain. When no forces were applied, the cells were encapsulated in a more homogeneous environment compared to the one exposed to the compressive device (cellular volume between 5000 μm^3 and 20000 μm^3, sphericity between 0.5 and 1, and Nuclear Yap between 0.7 and 2).

When there was less stress, the results of the compression and control were comparable across all three markers. However, the more the hydrogel was exposed to mechanical loading, the more stress on the hydrogel creating an environment that varies with stress. Fig 31 shows the morphology of the cells throughout the different stress loads. The cell spreading was almost uniform when the hydrogel was exposed to 50% compression which signified that a constant stress was applied throughout the gel resulting from maximum compression. As for 25%, it was found that the cell is more spread towards the outer diameter of the hydrogel than the center and therefore can sense the gradient stiffness and remodel the hydrogel quicker. These findings make it clear cells can respond to the environment they are in and mechanical forces influence time dependent remodeling.

Figure 31

Compression Morphology. Cellular morphology when exposed to compression.

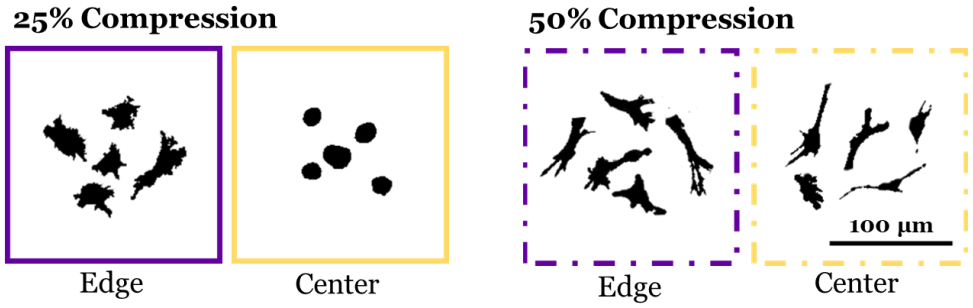

After analyzing the cellular remodeling, it was crucial to investigate the mechanical loading ability of the hydrogel. This was vital to the success of future studies since the PCL scaffold would cause a high stress region of the hydrogel closest to the PCL edge and a low stress region in the center of the pore of the composite. This phenomenon can be attributed to hydrogel swelling as it swells in the pore of the PCL scaffold while submerges in media. As such, using experimental and numerical simulation, 25 and 50% strain of the hydrogel was used to understand the cellular response and demonstrate cells can sense stiffness gradients. It was clear that the cells are resistant to a threshold of stress. When the pressure of 2370 Pa was applied on GelMe and 1.0 kPa of stress was applied on the center, the cellular morphology on the outer diameter was equivalent when there was no pressure applied. However, when the strain was increased two folds, then the cells reacted homogeneously with the loading. The results of the compression experiment can have significant impact on the design of an environment that encourages cell heterogeneity.

Table 1

Computational Model. This table respresents the parameters of stress and stress on the hydrogel during compression via FEBio software.

PARAMETERS	DESCRIPTION
Pressure 25% strain	1230 Pa
Pressure 50% strain	2370 Pa
Condition at the bottom	Fixed x,y and z
Condition at the top	Fixation
Diameter	8 mm
Height	1.6 mm
Density	1.02
Young's Modulus	7 kPa
Poisson's Ratio	0.499

4.4 Conclusions

When exploring cellular distribution to stress, it was found that, even when the stress of 0.5 kPa was applied, the MSC environment was more homogenous than compared to the higher stressed group. Therefore, other than remodeling, a higher loading from the surrounding causes diverse conditions. The supplemental figure further proved the hypothesis (Figure B1). When observing the results of 25% strain at the center versus no stress applied, we could predict that a lower cellular volume and higher sphericity are proportional to lower nuclear YAP localization. Results showed cells were not sensing changes from mechanical loading and confirms the lower limit of detection these cells

sensed to 0.5 kPa in stress. On the other hand, the observable force and proportionality can be confirmed at 50% strain as the cells display mechanotransduction and homogeneity. When analyzing results of the compression experiment, it was clear that, at 25% edge, 50% center, and 50% edge, the environment was under higher stress which caused an increase in cell mechanical adaptation. Also, it was evident that at 0% and 25% center, the environment did not have enough stress to quicken remodeling.

Chapter 5

PCL Scaffold Mechanical Characterization and Fabrication

5.1 Introduction

Scaffold fabrication and biomaterials can be made through various processes as reported in Chapter 3. PCL was chosen for this project due to its biocompatibility, degradation properties, mechanical strength, and its ability to provide cells a 2D environment based on its greater than 100 µm fiber diameter [13], [53]. The most ideal process for this thesis was the Salt Leach Technique or Solvent Casting and Porogen Leaching as this would potentially allow for cell harvesting in the pores of the scaffold. Upon design of the scaffold, a few objectives were taken into consideration throughout the entire fabrication process. The architecture has a key role in cell proliferation, transport, differentiation, vascularization, tissue growth, and mechanics [53] Pore size, distribution, interconnectivity, pore shape, porosity, and fiber diameter all have an impact on the cell in terms of proliferation, differentiation, and phenotype. For a scaffold to provide necessary environmental factors mimicking the OI, it should be highly porous and have full interconnectivity, which will provide the maximum available surface are for cell attachment and allowing transport throughout the scaffold [53].

However, prior to settling on this technique, a version of extruding and electrospinning was brainstormed. In short, the electrospinning process consists of an electric field, an acceleration of a charged jet of polymer solution towards a grounded collector which forms a polymer solution. The solvent evaporates during the ejection and stretching of the jet which allows for a fiber to be formed and collected on the plate. This method was not

pursued after the lack of compressive strength of electro spun fibers. It is hypothesized scaffolds for cartilage tissue engineering should employ a pore size of ~ 200 μm, whereas scaffolds for bone tissue engineering should contain pores larger than 300 μm to enhance vascularization [50]. This hypothesis was the rational for selecting NaCl sizes for the various scaffold types however, it is important to know optimum pore size varies with porosity and type of biomaterial used. Bone specific scaffolds have been created with pores ranging between 20 – 1500 μm and while large pores have a positive result as in, they encourage ECM formation, smaller pores also have benefits in that they enhance cell proliferation and maintenance of phenotype and therefore, suggests a scaffold ranging in pore size may encourage different cell lineages [53].

Before scaffold fabrication was chosen an extruding technique used with the help of the mechanical engineering department was investigated. This technique consisted of melting the polymer (PCL) with NaCl crystals and running it through an extruder. However, this process was inefficient as the salt became embedded deeply in the dissolved PCL and was unable to be leached out. Another caveat of this method was its lack of structure. The extruded PCL was ~2 mm in diameter which left the project with an almost futile solid scaffold. Therefore, both above techniques were abandoned and after discussion with other members of BME and literature review, a salt leaching process was studied.

5.2 Methods

5.2.1 Scaffold Fabrication

The PCL scaffold was synthesized using the salt-leaching technique as described previously [107], [121]–[124] as shown in Fig. 32. PCL scaffolds were created using the

weight-to-weight technique. Scaffolds were created with PCL to DCM weight percentages of 15, 20, 25, 30, 40 and 50%. 30 wt% was the final weight percent chosen for the continuation of research and a sample calculation is as follows. 30% of the mass of PCL was mixed with 70% of the mass of dichloromethane (DCM) (the mass was calculated using the density and the volume). Varying wt% PCL scaffolds were created by changing the amount of PCL dissolved in DCM.

NaCl between 200 µm and 500 µm was sieved using a borrowed salt sieve. PCL concentrations were made with a varying ratio of from 2:1, 3:1, 4:1, 6:1, 8:1, 12:1, and 15:1 salt-to-PCL. 40 wt % was also fabricated at 3:1 and 4:1 NaCl to PCL. The mixture of DCM and PCL was evenly distributed with NaCl, poured into a mold made from a Petri dish, and let DCM evaporate for 24 hours in a fume hood. After DCM evaporation, a biopsy punch (8 mm diameter) was used to create a dry PCL NaCl scaffold. The last step in obtaining porosity was washing the PCL scaffold in DI water for 5 days changing the water twice daily to leach out the NaCl. Figure 32 shows a representation of the process used to create a porous scaffold.

Figure 32

Salt Leaching Technique. Fabrication process of PCL scaffold.

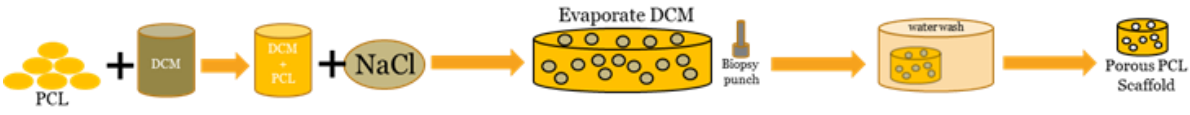

5.2.2 SEM

The porosity of the PCL scaffold was measured using scanning electron microscopy (SEM). After drying the scaffold and spin-coating it, it was exposed under the SEM machine to visualize the porosity. The porosity was quantified by implementing the SEM images into the FIJI software. The pore size was computed by averaging the diameter of the pore diameter in the PCL scaffold. The porosity was determined to choose an optimal PCL scaffold as it is clear to directly affect the mechanics. To further prove porosity was present, the scaffolds were submerged in blue food coloring for porosity verification. The scaffold showed food coloring was present through the entire structure, validating the hypothesis it was porous (Fig 33).

Figure 33

Porous PCL. Image of the porous PCL scaffold cut in half. The blue dye perfused through represents the permeability of the scaffold.

5.2.3 Mechanics

PCL scaffold was dried at room temperature overnight then analyzed for Young's Modulus. The strain rate was set to 0.1%/min and the Young's Modulus was calculated between 10 and 20% strain for a maximum of 30% strain for all tested groups.

5.2.4 Nile Red Fabrication

Nile red was used to fluoresce the PCL. The NaCl scaffold became fluorescent with the incorporation of Nile red to the DCM & PCL mixture. Nile Red was 99% pure and distributed from Acros Organics. 0.1 mg Nile red was dissolved in 20 ml DCM. This was then diluted using the serial dilution method with 1-part Nile red DCM and 10 parts DCM. Scaffold fabrication was then followed as mentioned above with a 30 wt % NaCl. This scaffold is shown in figure 34.

Figure 34

Nile Red PCL. Picture of Nile Red scaffold.

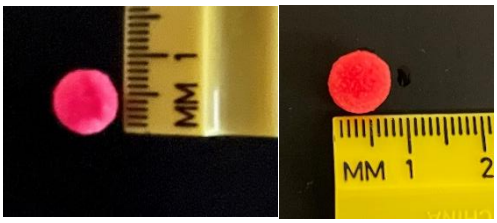

5.2.5 Perfusion

Due to the porosity and mechanical stiffness of the PCL scaffolds, MSCs were perfused through the five-weight percent to observe whether this type of environment could host living cells. To conduct this experiment, 15, 20, 25, 30 and 50 wt% PCL scaffolds of 2:1 NaCl to PCL were sterilized by submerging them in ethanol for 5 minutes followed by washing 3x with sterile PBS. Scaffolds were then submerged in 10% FBS media and left in the incubator for 24 hours to encourage cellular adhesion with a hydrophilic environment.

Cell seeding included passaging as mentioned above followed by perfusion of MSCs through a PCL scaffolds using media. The elementary seeding procedure consisted of resuspending 200k cells in 1 ml of media followed by using a syringe and needle inserted 1 mm inside the scaffold to inject the and perfuse the media through the scaffold at constant speed. This process was repeated 5 times for each scaffold. After 3 days of incubation the cells were fixed and stained with phalloidin and Hoechst according to the procedures mentioned in chapter 4. Later, the scaffolds were imaged to observe cellular adhesion to the PCL.

5.2.6 Customized Perfusion Device

To remove all variables from the cellular seeding method, a customized perfusion device was assembled. Using a syringe pump programmed at 1ml/min, an 8 mm diameter plastic tube, and a syringe loaded with cell infused media, the customized perfusion device was created. To seed each scaffold, the scaffold was fit tightly against the inner diameter walls of the tubes and held in place via friction. The syringe was loaded with 1 ml of cell

infused media and then the needle of the syringe was inserted into the scaffold of 1 mm in depth. The syringe, tube, and scaffold were then placed horizontally as the syringe was placed in the syringe pump. The syringe pump was turned on and media was perfused through the scaffold at 1 ml/min (Fig. 35). Another syringe was attached to the opposite end of the tube and collected the media after the first syringe's load was empty. This process was repeated for a total of 3x. After perfusion of media through the scaffold, the scaffolds were placed in a 24 well plate dish, submerged with the remaining cellular media and incubated for 3 days before staining and imaging.

Figure 35

Customized Perfusion Device. Depiction of customized perfusion device.

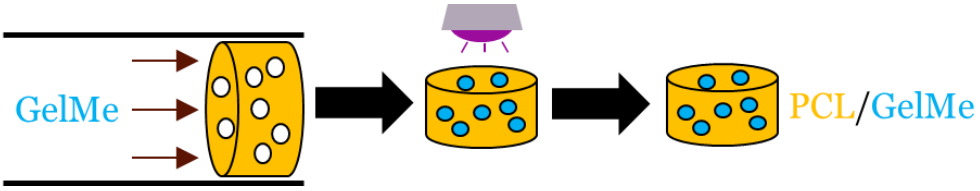

5.3 Results and Discussion

Five different scaffolds were created in the beginning process and the SEM images are shown in the appendix section. The mechanical properties of the PCL scaffold created by the salt leach method were adequate to mimic an osteochondral interface as the young's modulus of cartilage has been reported to range from 0.3 - 4 MPa [125]–[127].

Figure 36

SEM Images of PCL Scaffold. A) represents the porosity of the low, medium, high. B) represents the mechanics of the low, medium, and high porosity scaffold.

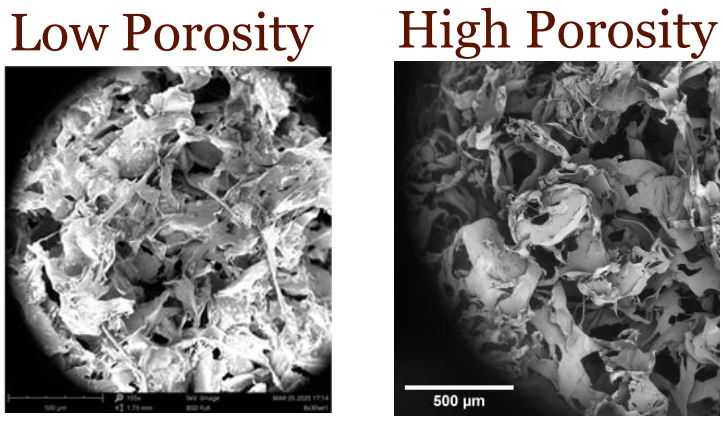

A 30 wt% of PCL scaffold was synthesized with a varying amount of salt (NaCl). The more NaCl was added, the smaller is the Young's Modulus and the larger porosity is. Porosity was shown to have a direct effect on the mechanics of the scaffold. Pictured in the SEM images are the 6:1, 8:1, 10:1, 12:1, & 15:1 NaCl to PCL scaffolds. Appendix C characterizes the data representing early scaffolds. It is clear and apparent pores exist in all images and there are larger pores as the ratio is increased. Low porosity was represented by having porous sides far from each other and an 8:1 NaCl to PCL ratio and pore diameter averaging 283 µm. Medium porosity was defined as 12:1 with pores averaging 319 µm. For reference and ease of terms, 8:1 is represented by the term low porosity, 12:1 is medium porosity, and 15:1 is high porosity. Lastly, a high porosity scaffold was represented by larger pores that were on average 430 µm. The PCL scaffold with low porosity had

Young's Modulus about 500 kPa and decreased as average pore diameter increased (Figure 37).

Figure 37

Characterization of Scaffolds. A) Represents the porosity of the low, medium, and highly porous scaffold. All scaffolds were in the range of 200 – 500 µm in pore size. *B) Represents the Young's Modulus of the scaffolds. As the porosity increases, Young's Modulus decreases. N>5. Ns is no statistical difference, *p <0.05, **p<0.01, ***p<0.001, ****p<0.0001.*

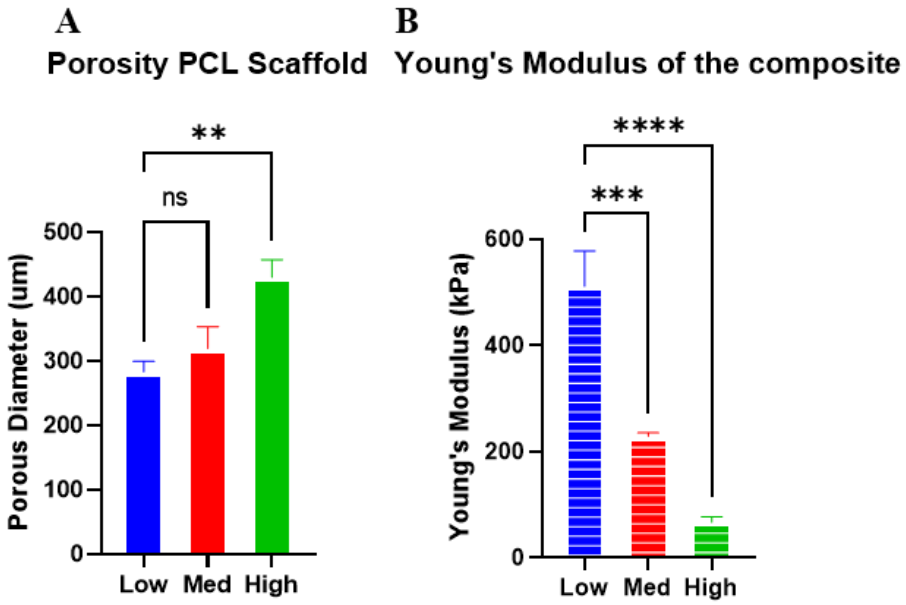

The medium scaffold had a modulus of 228 kPa meanwhile, the high porosity was about 66 kPa. These results demonstrate a clear relationship with average pore diameter

and mechanical stiffness of the scaffold. This small difference in average pore size had a major impact on the stiffness. It is also interesting to note that the mechanics of the dry PCL scaffold were greater for each group when compared to the composite of the respective group. The variances in pore size may be attributed to the salt crystals aggregating together and forming larger pores. These findings may be a result of the hydrophilic properties of PCL and the affect and aqueous environment had on the PCL.

5.4 Conclusions

The mechanical properties of the PCL scaffold were proven to be important in this work. It was found a higher amount of salt decreases the mechanical strength of the scaffold because of the increase in porosity. There was a 200 μm increase of the porous diameter from the highly porous scaffold to the low porous scaffold. Therefore, other than looking into the amount of PCL, controlling the amount of NaCl can completely change the properties of the scaffold. This could be explained as with greater porosity comes smaller PCL components of the scaffold with less structural PCL volume.

Chapter 6

Porous Scaffold and Soft Hydrogel Composite

6.1 Introduction

With the previous experimental results, and the knowledge of a potential stress difference within the pore due to hydrogel swelling and stiffness difference, the hypothesis cells can sense their environment was formed. Also, it could signify that the composite allows for quicker remodeling than cells in GelMe alone which is resulting from the stress gradient. At low porosity, the cells could be larger and more spread due to the force the PCL exerts on the gel in the pore is greater as there is more surface area of PCL. It is believed this would allow for a heterogenous population to exist in the composites with the highly porous scaffold having a more heterogenous population than the low porosity composite. This assumption was concluded when analyzing the pore size which the highly porous composite may have a less force exerted on the cell in the center and less stressful environment overall than the low porous scaffold. This conclusion would be important when examining the biomedical application of the composite because the cellular morphology can indirectly influence MSC differentiation [128].

6.2 Methods

6.2.1 GelMe Coupled with GFP

GelMe was coupled with green fluorescein peptide (GFP) and synthesized to explore the potential of seeding an injectable hydrogel into PCL scaffold then form the hydrogel using photopolymerization technique. To achieve that, GelMe macromer was

coupled with Green Fluorescein Peptide using Michael-Type Addition technique [129], [130].

First, triethanolamine (TEOA) buffer with pH 8 was formed by mixing 0.2 M of TEOA with PBS for 30 minutes. Next, the pH of the solution was adjusted using traditional techniques to achieve a pH of 8. Next, GFP was synthesized using solid-phase peptide synthesis (SPPS). The sequence of the peptide was carboxyfluorescein-glycine-glycine-glycine-cysteine. Glycine was used due to its flexibility and cysteine was used as it contains a thiol group that will couple with GelMe during the Michael-type reaction. The peptide was cleaved with 92.5% of trifluoroacetic acid (TFA) + 2.5% triisopropylsilane + 2.5% 2.2'-(Ethylenedioxy)diethanethiol + 2.5% pure water for 3 hours. Next, the peptide was precipitated twice in cold diethyl ether by centrifuging at high speed for 5 minutes. Next, the peptide was dried overnight, frozen to -80 °C and then lyophilized for 4 days. The peptide was tested in H NMR to show its presence. The GFP was mixed with PBS to create a 10 mM molarity.

The coupling occurred by mixing 5 wt% GelMe with 0.1 mM of GFP in 0.2 M TEOA at a temperature of 40 °C for 1 hour. Next, the coupled macromer was dialyzed for 2 days by changing the water twice daily at a room temperature of 37 °C. Next, the macromer was frozen in -80 °C and lyophilized for 5 days and then tested in H NMR to display the presence of GFP in GelMe.

The GelMe coupled with GFP was mixed with unlabeled GelMe to investigate the right concentration of GFP in GelMe hydrogel. This is done by mixing 5 wt% of labeled and unlabeled GelMe in PBS and 0.05 wt% I2959. The hydrogel was injected into the

PDMS mold biopsied with 8mm diameter and exposed to UV light with an intensity of 10 mW/cm^2 for 10 minutes. The hydrogel was washed twice thoroughly in a room with lower light exposure and then was analyzed in a confocal microscopy room. The images were tested in FIJI using a plot profile to test the average intensity.

Once the concentration was optimized, the labeled and unlabeled GelMe hydrogel was injected into the Nile red PCL scaffold to prove the presence of hydrogel in the scaffold. The coupled and uncoupled GelMe injectable hydrogel was injected in the different porous sides of the PCL scaffold using the customized perfusion device shown in Figure 3A. The composite was exposed to UV light for 10 min for an intensity of 10 mW/cm^2 then was washed thoroughly. The composite biomaterial and Nile red PCL scaffold without hydrogel were tested in confocal microscopy to prove the presence of hydrogel.

6.2.2 Stiffness

The composite scaffold was created by using two biomaterials, PCL and GelMe. This was made by combining the GelMe hydrogel and PCL scaffold (optimal scaffold). This was done by designing a customized perfusion device that included an 8mm diameter plastic connected to a syringe attached to a syringe pump. Using tweezers and surface friction, the scaffold was held perfectly in place in the tube. The syringe was filled with GelMe solution and perfused through the tube injecting the GelMe hydrogel solution into the PCL scaffold through the pores. The scaffold and remaining solution were injected into a well plate and then the mixture was exposed to UV light for 10 min under an intensity of 10 mW/cm^2. The biomaterial went through the same mechanical testing technique. The

strain rate was set to 0.1%/min and the Young's Modulus was calculated between 10 and 20% strain for a maximum of 30% strain.

For the PCL scaffold, MSCs were seeded into PCL using the customized perfusion device shown in Figure 35. The procedure was similar except one million MSCs were passaged and resuspended in 1 mL of the GelMe solution. The syringe was then loaded with the GelMe MSC combination and placed on the syringe pump at a speed of 1 mL/min. The composite was then exposed to UV light, washed in media 3 times, and then incubated for 3 days.

6.2.3 Cell Staining

To analyze the cellular morphology, cells were stained for different biomarkers. First, cells were fixed using 10% formalin for 15 min then 0.1% Triton X was added into the MSC composite occupied well after 3 days of incubation to permeabilize the cell membrane. Then, a composite was submerged in the blocking buffer solution (3% Bovine Serum Albumin mixed in PBS) for 30 minutes. The primary anti-YAP was stained overnight in a dark place due to YAP's light. Several washes later, secondary anti-YAP tagged with fluorescent was added and stayed for 2 hours in low light areas. After several washes later, cells were stained with Phalloidin (1:100) and Propodium Iodide (1:300) to stain for cytoskeleton and nucleus respectively. The cells were detected in the confocal microscope and analyzed in FIJI software.

6.2.4 Fiji

Four metrics were analyzed using FIJI. Cell volume, cell shape index (CSI), aspect ratio, and YAP nuclear localization. For each experiment, 100 cells were analyzed.

Furthermore, binary masks of 3D image stacks of DAPI and Phalloidin were generated using Otsu's intensity-based threshold method. Next, the 3D object's counter function was used to determine the cell volume. The ratio of the largest and smallest side of the cell was used to calculate the aspect ratio. After determining the volume and the surface area, CSI will be calculated as follow:

$$CSI = \frac{\pi^{\frac{1}{3}}(6V)^{\frac{2}{3}}}{A_0}$$

The CSI value will be between 0 and 1. Finally, the Nuclear YAP localization was calculated:

$$Nuclear\ YAP = \frac{\frac{Nuclear\ YAP\ signal}{Volume\ of\ nucleus}}{\frac{Cytosolic\ YAP\ signal}{Volume\ of\ cytosol}}$$

The cytosolic YAP signal was determined by inverting and superimposing nuclei masks with corresponding actin masks which lead masks encompassing the cytosol excluding the nucleus. The Nuclear YAP signal followed the same method by concentration into masks encompassing the nucleus and excluding the cytosol.

6.2.5 Statistical Analysis

All data are presented as $mean \pm standard\ error$. The graphs were created using GraphPad software. The data were imported into a table then the graph was chosen from the top menu depending on the type. The difference between values was calculated using a one-way analysis of variance (ANOVA). Values of $p<0.05$ were considered to be statistically significant. * With p-value was presented on top of the graph. A Histogram of

cell spreading in the function of stiffness to understand whether the cell morphology was high or low.

6.3 Results and Discussion

The peak of the carboxyfluorescein was shown in H NMR between 3 and 4 ppm which was also shown in H NMR of the GelME coupled with GFP confirming the presence of GFP. Fig. S3 represents the MALDI report of the GFP peptide. It was confirmed that the actual molecular weight of the peptide was 650.369 Da compared to the expected one which is 649.62 Da. The % of change of the molecular weight is 0.115% confirming the accuracy of the peptide.

6.3.1 Cell Viability in PCL vs GelMe Gel Alone

GelMe hydrogel and PCL scaffold were synthesized separately, perfused, and analyzed together. This was done as a goal to understand the biomaterial structure before directly apply it to the TE field. First, the cell viability was tested in low, medium and high scaffolds and gels alone. It was confirmed that high porosity decreases the stiffness of the biomaterial and increased the cell viability. The cell viability was tested in PCL mixed with gel and gel alone to test whether the composites were biocompatible. All the biomaterial (scaffolds and gel alone) had very high viability shown in figure 38 (over 87%). Additionally, it seems that the more porosity was increased, the higher cell viability is confirming that the cells preferred a high porous material. The gels had much higher viability than all the scaffolds.

Figure 38

Cell Viability. Cell viability of the composite vs the GelMe alone. N>50 and ns is no statistical difference.

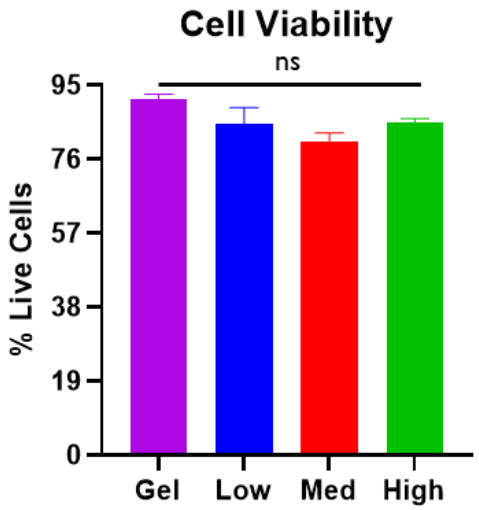

6.3.2 GelMe Coupled with GFP and PCL Scaffold

Labeled GelMe hydrogel was formed to determine the minimum concentration needed to get achieve a fluorescently green hydrogel. The GFP peptide was proven to have a molecular weight of 650 g/mol as shown in MALDI. The peak representing GFP was shown when analyzing GelMe + GFP in H NMR.

A concentration of 0.003 mM of GFP was used by combining 3% of GelMe labeled GFP and unlabeled GFP. The next step was perfusing the labeled GelMe + GFP into PCL with Nile Red as shown in Fig. 35. Supplemental Fig. shows the presence of labeled GelMe

in the middle between the porous sides of red PCL. This confirmed that the mixture was successfully made and injected into the PCL scaffold.

Figure 39

GelMe & GFP. A) Shows nile red pcl with GelMe perfused through the scaffold creating a composite. B) Is a representation of nile red PCL alone. C) Displays the fluorescence of GelMe+GFP compared against no GFP. D) Is a cartoon referencing how the composite was imaged.

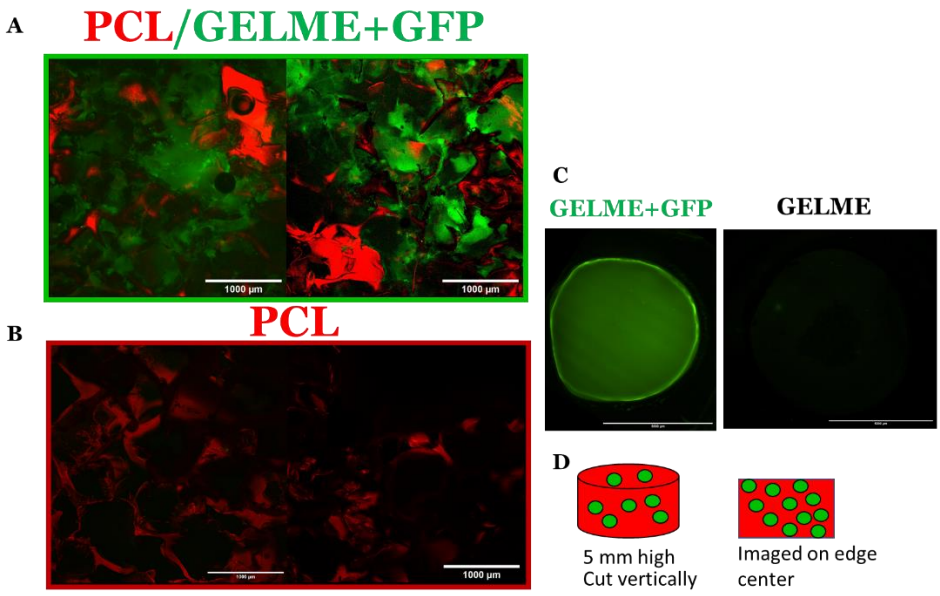

Before analyzing the cell morphology in the composite, it was highly important to investigate whether the GelMe photopolymerized inside of PCL scaffold. This was done by labeling PCL with Nile Red and GelMe with green fluorescence. Observing figure 39

a, red PCL encircles the green hydrogel confirming the presence of GelMe. Therefore, synthesizing composite could be achieved.

Perfusing cells encapsulated in GelMe injectable hydrogel into the PCL scaffold was the next goal confirming whether increased remodeling and heterogeneity existed in the composite. Therefore, a preliminary experiment was conducted to observe this, and the results are shown in supplemental data (Figure D6, E1). Once encapsulation was confirmed, the three varying scaffolds (low, med, high) were investigated and compared to a GelMe alone control gel after 3 days. As previously hypothesized, the amount of porosity had a major impact on the morphology. Cells presented in the low composite had a higher cellular volume, lower sphericity, and YAP more localized to the nucleus compared to the high porosity scaffold and the control. Even cells presented in high porosity composite had higher mechanical activity than the control (Figure 40).

Therefore, the cells presented in the scaffold adapted to the loading applied by the PCL and caused a variant environment compared to the control (Fig. 40 A). Cells tended to be more circular in the middle and more spread towards the edge of the pore as shown in Fig 40C. Supplemental figure confirmed the statement when analyzing this data via histogram (Figure F1). When looking at gels, it was confirmed that lower cellular volume and higher sphericity are proportional to lower nuclear YAP localization. Unfortunately, not the same could be applied for the composite. This means that there was no correlation between Nuclear YAP localization, cellular volume, and sphericity. This could possibly be explained by the mechanical stimulus of the environment inside the pore. Analyzing graphs, it is clear the data is statistically different from the composite groups against the

control. The data shows that the composites were able to create an environment which allows for quicker cell remodeling and more mechanical activity than in a hydrogel alone.

6.3.3 How Porosity Affects Mechanics

Depending on the porosity of the composite and mechanical stiffness MSC behavior varied depending on the scaffold type (Fig. 40). The results display, lower porosity contributes to an increase in the cellular volume (18000 μm^3 vs. 10000 μm^3), a decrease in the sphericity (0.4 vs. 0.6) and higher Nuclear YAP expression (3.5 vs. 3). Even though GelMe hydrogel is a soft hydrogel, its stiffness did not result in comparable remodeling time, cellular volume, sphericity, and nuclear YAP.

Figure 40

*Composite Cell Data. A) Cellular Volume, sphericity, and Nuclear YAP expression. All groups are compared against GelMe hydrogel alone. B) Morpholgy of cells in the various composites presented via silhouettes. C) Image of the pore and cell morphology inside as cells sense the stiff PCL. * P<0.05 signals significant when group is compared against gel alone.*

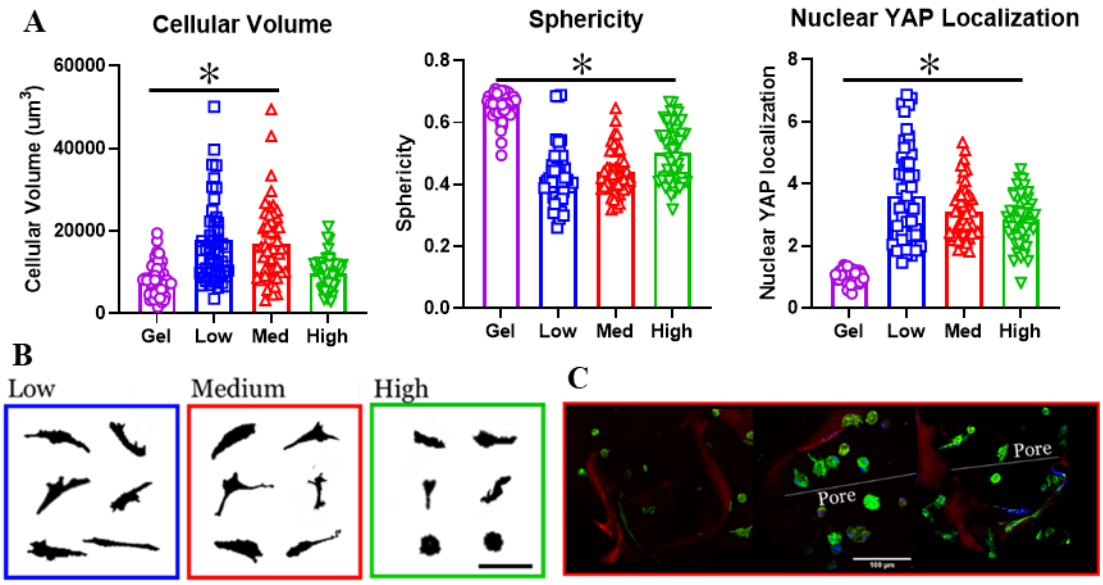

All three groups of composites demonstrated an increase in cellular behavior than the hydrogel alone which may be contributed to the stress of the hydrogel is extremely lower than all three groups. Fig. 40A shows the distribution of the cells when quantifying cellular volume, sphericity, and nuclear YAP. The data shows a heterogeneous population located in the pores of the composite and a potential stress gradient located in the pore shown in Fig 40 A, B & C. It was found that cells in the hydrogel are more homogeneous

compared to the one in PCL which could be explained by the mechanical stress applied by the PCL scaffold onto the hydrogel. Not only can the stress difference within the pore be created from the varying stiffness difference, but the hydrogel swelling properties. The hydrogel is in a more restrictive environment when located in a smaller pore which could be contributing to the stress difference.

6.4 Conclusions

The goal of this study was to observe the differences in cellular morphology resulting from local environmental mechanics and to create a construct that may be used for osteochondral tissue engineering. The environmental mechanics were hypothesized to vary inside a pore of the composite due to the stress gradient proven to exist from during the compression experiment. This was done to understand the effects of harvesting cells in contractile and less contractile phases and to study the variances of cell morphology and the forces that affect it in biomaterials while applying it to TE and recreate the osteochondral interface as cell morphology has been shown to favor osteogenic or chondrogenic differentiation.

Chapter 7

Conclusions and Future Work

7.1 Conclusions

The result on cell morphology by the composite and the compressive device can be widely applied for regenerative medicine. The compressive device confirmed when exposing cells to mechanical load it can alter their morphology and time dependent mechanical response. Furthermore, it showed that a heterogenous population can be created due to mechanical force. This latter has prospect in regenerative medicine since it can be used to create an interface at which soft and hard constructs meet. When tethering an application for the composite a goal is recreation of the osteochondral interface. In turn, this interface may induce differentiation of cells into osteoblasts and chondrocytes. Spread mechanically active cells could represent the beginning of osteogenesis [131], [132]. On the other hand, the rounded cells could represent the beginning of chondrogenesis [133] . Therefore, this composite could one day be considered as a synthetic approach for osteochondral interface engineering. The composite has the appropriate mechanics to recreate the osteochondral interface and has proved to be a suitable environment for harvesting cells.

Our work provides an exploration of a composite with gradient stress that provides an environment created using biomaterials. In this work, PCL and GelMe hydrogel were synthesized and mixed to understand the cell behavior when encapsulated in the pore. The results showed that the hydrogel could be polymerized inside of the scaffold using light and that a gradient of stress was created that cells respond to. Moreover, when cells were

encapsulated in the hydrogel and far from any PCL backbone, they had a rounded, small morphology without sensing mechanical stimulation from the environment. Moreover, when the cells were located close to the edge of the pore, the cells had large and spread morphology and had an increase in mechanosensing. These results have a great potential in TE since they can be implemented for synthesizing any interfaces mimicking the natural one including OI.

7.2 Future Work

Currently, lineage has not been studied. Mechanics of the composite and morphology of cells have. However, future experiments could include further mechanical tuning, observing cell lineage, and in vivo implantation.

7.2.1 Tunable Mechanics

Porosity and mechanics to exactly match the OI may be achieved. The composite is highly tunable, and the mechanics and porosity can be achieved to allow bone vascularization pore sizes greater than 300 μm and cartilage formation with pores smaller than 200 μm. This can be done by coupling a low porous scaffold with a high porous scaffold to allow bone vascularization while inducing cartilage formation by mechanics alone. Also, the weight % can be increased to make the construct stiff and again, these constructs may be layered on top of each other to create a gradient of porosity matching the specific microenvironments. Lastly, the hydrogel stiffness may be manipulated by increasing the wt % of the macromer. The increase will result in cells not as mechanically active as they will be in a more restrictive hydrogel and will not remodel surrounding gel as quickly.

7.2.2 Chondrocytes and Osteoblasts

These studies may be done in the future using chondrocytes and osteoblasts instead of MSCs. Perhaps harvesting chondrocytes from hyaline cartilage from the patient like MACI and harvesting osteoblasts from the patient can yield better results. These results may provide the backbone for expanding application of the composite to all types of joints where bone meets cartilage. Allowing encapsulation of hyaline chondrocytes in our 3D hard/stiff environment may yield greater success in reproducing the native cartilage and is something that would be explored.

7.2.3 Thiol Norbornene Click Chemistry

Click chemistry is a practice used in engineering hydrogels. This process includes modifying a backbone like hyaluronic acid (HA) with tiny elements for specific functions. Essentially, an example of click chemistry is HA functionalized with norbornene groups. The bonding uses a di-thiol crosslinker and forms a hydrogel and extra norbornenes can undergo additional reactions. Norbonene has a few advantages in that it can bind to thiol groups covalently during photopolymerization, it has an orthogonal system which allows for more peptide binding with the thiol groups, and norbornene is biocompatible. The peptide thiol binding is important for addition of biochemical signals to guide differentiation [133], [134].

When using NorHA, the crosslinker would be dithiothreitol (DTT) allowing for cell degradation. NorHA can be more protease degradable when using DTT than GelMe. Click chemistry using NorHA allows for the incorporation of the biological signals to the backbone of NorHA guiding differentiation of cells. For bone, BMP2 can be coupled with

NorHA and Runx2 may be evaluated. NorHA can be coupled with HAV peptide and VEGF encouraging cartilage formation along with evaluation of chondrogenic factors (Fig. 41).

Figure 41

Click Chemistry. A) NorHA is hyaluronic acid modified with norbornene and is a cartoon representation of norbornene added to hyaluronan backbone and binding to each norbornene. B) Biochemical signals coupled to the hydrogel backbone. [133]

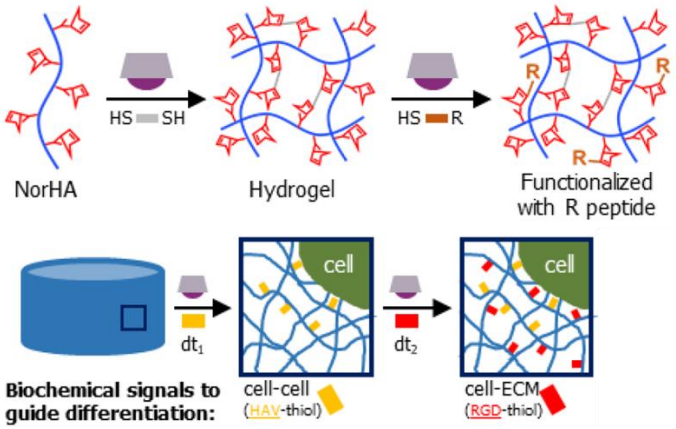

7.2.4 In Vivo

In vivo implantation of the scaffold may be achieved by debriding the damaged cartilage all the way to underlying bone but not denuding the bone. Next, the surgeon must stabilize implant loaded with chondrocytes and osteoblasts onto the bone and affix it to the bone. Another cartilage layer may be added on top of the composite using a collagen scaffold seeded with hyaline chondrocytes similar to MACI. This added step will ensure cartilage formation and the composite loaded with biological signals enhancing

differentiation towards two lineages in combination with another layer of a MACI like scaffold on top of the composite will ensure success of the composite in regeneration of the osteochondral interface.

References

[1] C. A. Baumann, B. B. Hinckel, C. C. Bozynski, and J. Farr, “Articular cartilage: Structure and restoration,” in *Joint Preservation of the Knee: A Clinical Casebook*, Springer International Publishing, 2019, pp. 3–24. doi: 10.1007/978-3-030-01491-9_1.

[2] D. J. Hunter and S. Bierma-Zeinstra, “Osteoarthritis,” *The Lancet*, vol. 393, no. 10182, Apr. 2019, doi: 10.1016/S0140-6736(19)30417-9.

[3] W. W. Curl, J. Krome, E. S. Gordon, J. Rushing, B. P. Smith, and G. G. Poehling, “Cartilage injuries: A review of 31,516 knee arthroscopies,” *Arthroscopy*, vol. 13, no. 4, pp. 456–460, 1997, doi: 10.1016/S0749-8063(97)90124-9.

[4] J. W. Alford and B. J. Cole, “Cartilage restoration, part 1: Basic science, historical perspective, patient evaluation, and treatment options,” *American Journal of Sports Medicine*, vol. 33, no. 2. pp. 295–306, Feb. 2005. doi: 10.1177/0363546504273510.

[5] A. H. Gomoll and J. Farr, “The Osteochondral Unit,” in *Cartilage Restoration*, Springer New York, 2014, pp. 9–15. doi: 10.1007/978-1-4614-0427-9_2.

[6] T. Furukawa, D. Eyre, S. Koide, and M. Gilmcher, “Biochemical studies on repair cartilage resurfacing experimental defects in the rabbit knee,” *J Bone Joint Surg Am*, vol. 62, pp. 79–89, 1980.

[7] R. B. Garretson, L. I. Katolik, N. Verma, P. R. Beck, B. R. Bach, and B. J. Cole, “Contact pressure at osteochondral donor sites in the patellofemoral joint,” *American Journal of Sports Medicine*, vol. 32, no. 4, pp. 967–974, Jun. 2004, doi: 10.1177/0363546503261706.

[8] D. Prieto-Alhambra, A. Judge, M. K. Javaid, C. Cooper, A. Diez-Perez, and N. K. Arden, “Incidence and risk factors for clinically diagnosed knee, hip and hand osteoarthritis: Influences of age, gender and osteoarthritis affecting other joints,” *Annals of the Rheumatic Diseases*, vol. 73, no. 9, pp. 1659–1664, 2014, doi: 10.1136/annrheumdis-2013-203355.

[9] C. G. Armstrong, “An Analysis of the Stresses in a Thin Layer of Articular Cartilage in a Synovial Joint,” *Engineering in Medicine*, vol. 15, no. 2, Apr. 1986, doi: 10.1243/EMED_JOUR_1986_015_018_02.

[10] D. B. Burr and E. L. Radin, “Microfractures and microcracks in subchondral bone: Are they relevant to osteoarthrosis?,” *Rheumatic Disease Clinics of North America*, vol. 29, no. 4. W.B. Saunders, pp. 675–685, 2003. doi: 10.1016/S0889-857X(03)00061-9.

[11] V. Goldberg, “Biologic restoration of articular surfaces.” Caplan, 1999.

[12] S. J. Hollister, “Porous scaffold design for tissue engineering,” *Nature Materials*, vol. 4, pp. 518–524, 2005.

[13] Masami Okamoto, “The role of scaffolds in tissue engineering,” in *Handbook of Tissue Engineering Scaffolds*, vol. one, Masoud Mozafari and et al, Eds. Elsevier Science & Technology, 2019.

[14] F. Sefat, *Cell Engineering of Human Bone*. Scholars’ Press, Lambert Academic Publishing, 2013.

[15] F. Sefat, “Cell Engineering of Human Bone Monolayers and the Effect of Growth Factors and Microcontact Printed ECM Proteins on Wound Healing.,” 2013.

[16] Y. C. Fung, “Centre for Engineering of Living Tissues,” *NSF Proposal*, 1985.

[17] R. G. Wells, “The role of matrix stiffness in regulating cell behavior,” *Hepatology*, vol. 47, no. 4. pp. 1394–1400, Apr. 2008. doi: 10.1002/hep.22193.

[18] Y. Ikada, “Challenges in tissue engineering,” *Journal of the Royal Society Interface*, vol. 3, no. 10. Royal Society, pp. 589–601, Oct. 22, 2006. doi: 10.1098/rsif.2006.0124.

[19] C. T. Laurencin, A. M. A Ambrosio, M. D. Borden, and J. A. Cooper, “Tissue Engineering: Orthopedic Applications,” 1999.

[20] V. Rosa, A. della Bona, B. N. Cavalcanti, and J. E. Nör, “Tissue engineering: From research to dental clinics,” *Dental Materials*, vol. 28, no. 4, Apr. 2012, doi: 10.1016/j.dental.2011.11.025.

[21] S. E. Haynesworth, D. Reuben, and A. I. Caplan, “Cell-based tissue engineering therapies: the influence of whole body physiology.,” *Advanced Drug Delivery Reviews*, vol. 33, pp. 3–14, 1998.

[22] A. Khademhosseini, Y. Du, B. Rajalingam, J. P. Vacanti, and R. S. Langer, “Microscale technologies for tissue engineering,” *Advances in Tissue Engineering*, vol. 103, no. 8, pp. 349–369, 2008, doi: 10.1142/9781848161832_0017.

[23] R. Langer and J. P. Vacanti, “Tissue Engineering,” *Science*, vol. 260, pp. 920–926, 1993.

[24] M. M. Benmassaoud, K. A. Gultian, M. Dicerbo, and S. L. Vega, “Hydrogel screening approaches for bone and cartilage tissue regeneration,” *Annals of The New York Academy of Sciences*, vol. 1460, pp. 25–42, 2019, doi: 10.1111/nyas.14247.

[25] A. I. Caplan, “Adult Mesenchymal Stem Cells for Tissue Engineering Versus Regenerative Medicine,” *Journal of Cellular Physiology*, vol. 213, pp. 341–347, 2007, doi: 10.1002/JCP.

[26] R. Mcbeath, D. M. Pirone, C. M. Nelson, K. Bhadriraju, and C. S. Chen, “Cell Shape, Cytoskeletal Tension, and RhoA Regulate Stem Cell Lineage Commitment several studies have noted that changes in cell shape themselves can alter the differentiation of precommitted mesenchymal lineages. Spiegelman and Ginty (1983),” 2004. [Online]. Available: http://www.developmentalcell.com/cgi/

[27] D. R. Bogdanowicz and H. H. Lu, “Designing the stem cell microenvironment for guided connective tissue regeneration,” *Annals of the New York Academy of Sciences*, vol. 1410, no. 1. Blackwell Publishing Inc., pp. 3–25, 2017. doi: 10.1111/nyas.13553.

[28] K. Gelse, E. Pöschl, and T. Aigner, “Collagens - Structure, function, and biosynthesis,” *Advanced Drug Delivery Reviews*, vol. 55, no. 12, pp. 1531–1546, Nov. 2003, doi: 10.1016/j.addr.2003.08.002.

[29] C. Frantz, K. M. Stewart, and V. M. Weaver, “The extracellular matrix at a glance,” *Journal of Cell Science*, vol. 123, no. 24, Dec. 2010, doi: 10.1242/jcs.023820.

[30] J. A. Buckwalter, H. J. Mankin, and A. J. Grodzinsky, “Articular cartilage and osteoarthritis,” *Instr Course Lect-Am Acad Orthop Surg 54*, pp. 465-undefined, 2005.

[31] S. Camarero-Espinosa, B. Rothen-Rutishauser, E. J. Foster, and C. Weder, “Articular cartilage: From formation to tissue engineering,” *Biomaterials Science*, vol. 4, no. 5. Royal Society of Chemistry, pp. 734–767, May 01, 2016. doi: 10.1039/c6bm00068a.

[32] E. B. Hunziker, T. M. Quinn, and H. J. Häuselmann, “Quantitative structural organization of normal adult human articular cartilage,” *Osteoarthritis and Cartilage*, vol. 10, no. 7, pp. 564–572, 2002, doi: 10.1053/joca.2002.0814.

[33] R. A. Stockwell, “Biology of Cartilage Cells,” *CUP Archive*, vol. 7, 1979.

[34] J. Apostolakos, “The enthesis: a review of the tendon-to-bone insertion,” *Muscles, Ligaments and Tendons Journal*, 2014, doi: 10.11138/mltj/2014.4.3.333.

[35] Y. Chen, L. Ju, M. Rushdi, C. Ge, and C. Zhu, “Receptor-mediated cell mechanosensing,” *Molecular Biology of the Cell*, vol. 28, no. 23, pp. 3134–3155, Nov. 2017, doi: 10.1091/mbc.E17-04-0228.

[36] Y. Ma *et al.*, “3D Spatiotemporal Mechanical Microenvironment : A Hydrogel-Based Platform for Guiding Stem Cell Fate,” *Advanced Materials*, vol. 30, pp. 1–27, 2018, doi: 10.1002/adma.201705911.

[37] A. Freeman and Y. Aharonowitz, “Immobilization of Microbial Cells in Crosslinked , Prepolymerized , Linear Polyacrylamide Gels : Antibiotic Production by Immobilized Streptomyces clavuligerus Cells,” *Biotechnology & Bioengineering*, vol. XXIII, pp. 2747–2759, 1981.

[38] S. D. Subramony *et al.*, “The guidance of stem cell differentiation by substrate alignment and mechanical stimulation,” *Biomaterials*, vol. 34, no. 8, pp. 1942–1953, 2013, doi: 10.1016/j.biomaterials.2012.11.012.

[39] D. E. Ingber, “Cellular mechanotransduction: putting all the pieces together again,” *The FASEB journal*, vol. 20, pp. 811–827, 2006, doi: 10.1096/fj.05-5424rev.

[40] D. E. Ingber, “TENSEGRITY : THE ARCHITECTURAL BASIS OF CELLULAR,” *Annual Review Physiology*, vol. 59, pp. 575–599, 1997.

[41] Y. Chen, L. Ju, M. Rushdi, C. Ge, C. Zhu, and V. M. Weaver, “Receptor-mediated cell mechanosensing,” *Molecular Biology of the Cell*, vol. 28, no. 7, pp. 3134–3155, 2017, doi: 10.1091/mbc.E17-04-0228.

[42] R. G. Wells, “The Role of Matrix Stiffness in Regulating Cell Behavior,” *Hepatology*, vol. 47, no. 4, pp. 1394–1400, 2008, doi: 10.1002/hep.22193.

[43] A. A. Wasik and H. B. Schiller, “Functional proteomics of cellular mechanosensing mechanisms,” *Seminars in Cell and Developmental Biology*, vol. 71, pp. 118–128, 2017, doi: 10.1016/j.semcdb.2017.06.019.

[44] A. Buxboim, K. Rajagopal, A. E. X. Brown, and D. E. Discher, “How deeply cells feel: Methods for thin gels,” *Journal of Physics Condensed Matter*, vol. 22, no. 19, 2010, doi: 10.1088/0953-8984/22/19/194116.

[45] T. A. Blackburn and E. Craig, “Knee Anatomy A Brief Review,” *Physical Therapy*, vol. 60, no. 12, pp. 1556–1560, 1980.

[46] R. Liu-Bryan and R. Terkeltaub, “Emerging regulators of the inflammatory process in osteoarthritis,” *Rheumatology*, vol. 11, pp. 35–44, 2015, doi: 10.1038/nrrheum.2014.162.

[47] Zinovy Meyler, “Knee Anatomy,” 2018.

[48] S. P. Nukavarapu and D. L. Dorcemus, “Osteochondral tissue engineering : Current strategies and challenges,” *Biotechnology Advances*, vol. 31, no. 5, pp. 706–721, 2013, doi: 10.1016/j.biotechadv.2012.11.004.

[49] A. di Luca, C. van Blitterswijk, and L. Moroni, “The osteochondral interface as a gradient tissue: From development to the fabrication of gradient scaffolds for regenerative medicine,” *Birth Defects Research Part C: Embryo Today: Reviews*, vol. 105, no. 1, Mar. 2015, doi: 10.1002/bdrc.21092.

[50] L. A. McMahon, P. J. O’Brien, and P. J. Prendergast, “Biomechanics and mechanobiology in osteochondral tissues,” *Regenerative Medicine*, vol. 3, no. 5. pp. 743–759, 2008. doi: 10.2217/17460751.3.5.743.

[51] S. Kurtz, K. Ong, E. Lau, F. Mowat, and M. Halpern, “Projections of primary and revision hip and knee arthroplasty in the United States from 2005 to 2030,” *Journal of Bone and Joint Surgery - Series A*, vol. 89, no. 4, pp. 780–785, 2007, doi: 10.2106/JBJS.F.00222.

[52] R. D’Ambrosi, V. Ragone, and N. Ursino, “What future in the treatment of osteochondral knee defects?,” *Annals of Translational Medicine*, vol. 6, no. S2, Dec. 2018, doi: 10.21037/atm.2018.11.28.

[53] C. Vyas, G. Poologasundarampillai, J. Hoyland, and P. Bartolo, “3D printing of biocomposites for osteochondral tissue engineering,” in *Biomedical Composites*, Elsevier, 2017, pp. 261–302. doi: 10.1016/b978-0-08-100752-5.00013-5.

[54] L. S. Lohmander, L. Dahlberg, L. Ryd, and D. Heinegård, “Increased levels of proteoglycan fragments in knee joint fluid after injury,” *Arthritis & Rheumatism*, vol. 32, no. 11, Nov. 1989, doi: 10.1002/anr.1780321113.

[55] H. Mankin, “The response of articular cartilage to mechanical injury,” *J Bone Joint Surg Am*, vol. 62, pp. 460–466, 1982.

[56] H. Mankin, V. Mow, and J. Buckwalter, “Form and function of articular cartilage,” *Simon, SR , ed. Orthopaedic Basic Science. Rosemont, Ill: American Academy of Orthopaedic Surgeons*, pp. 1–44, 1994.

[57] V. Mow, L. Setton, and A. Ratcliffe, “Structure-function relationships of articular cartilage and the effects of joint instability and trauma on cartilage function.,” *Cartilage Changes in Osteoarthritis. Indianapolis: University of Indiana Press*, pp. 22–42, 1990.

[58] V. Mow and M. Rosenwasser, “Articular cartilage: biomechanics,” *Woo, SLY , Buckwalter, JA , eds. Injury and Repair of the Musculoskeletal Soft Tissues. Park Ridge, Ill: American Academy of Orthopaedic Surgeons*, pp. 427–463, 1988.

[59] J. B. Moseley *et al.*, “A Controlled Trial of Arthroscopic Surgery for Osteoarthritis of the Knee,” *New England Journal of Medicine*, vol. 347, no. 2, Jul. 2002, doi: 10.1056/NEJMoa013259.

[60] S. F. Harwin, “Arthroscopic Debridement for Osteoarthritis of the Knee: Predictors of Patient Satisfaction.”

[61] J. W. Alford and B. J. Cole, “Cartilage restoration, part 2: Techniques, outcomes, and future directions,” *American Journal of Sports Medicine*, vol. 33, no. 3. SAGE PublicationsSage CA: Los Angeles, CA, pp. 443–460, Mar. 30, 2005. doi: 10.1177/0363546505274578.

[62] F. Sefat, M. Mozafari, and A. Atala, “Introduction to tissue engineering scaffolds,” in *Handbook of Tissue Engineering Scaffolds: Volume One*, vol. one, Masoud Mozafari and et al, Eds. Elsevier, 2019. doi: 10.1016/B978-0-08-102563-5.00001-0.

[63] D. K. Bae, K. H. Yoon, and S. J. Song, “Cartilage Healing After Microfracture in Osteoarthritic Knees,” *Arthroscopy: The Journal of Arthroscopic & Related Surgery*, vol. 22, no. 4, Apr. 2006, doi: 10.1016/j.arthro.2006.01.015.

[64] P. C. Kreuz *et al.*, “Results after microfracture of full-thickness chondral defects in different compartments in the knee,” *Osteoarthritis and Cartilage*, vol. 14, no. 11, pp. 1119–1125, Nov. 2006, doi: 10.1016/j.joca.2006.05.003.

[65] J. Buckwalter, V. Mow, and A. Ratcliffe, “Restoration of injured or degenerated articular cartilage,” *J Am Acad Orthop Surg*, vol. 2, pp. 192–201, 1994.

[66] A. B. Imhoff, K. Beitzel, K. Stamer, and E. Klein, “Cartilage treatment on the knee joint: Surgical procedure/aftercare,” in *Rehabilitation in Orthopedic Surgery: Second Edition*, Springer Berlin Heidelberg, 2016, pp. 171–176. doi: 10.1007/978-3-662-49149-2_12.

[67] Hangody. L, G. Kish, and Z. Karpati, “Autogenous osteochondral graft technique for replacing knee cartilage defects in dogs,” *Orthop Int*, vol. 5, pp. 175–181, 1997.

[68] G. Kish, L. Módis, and L. Hangody, “OSTEOCHONDRAL MOSAICPLASTY FOR THE TREATMENT OF FOCAL CHONDRAL AND OSTEOCHONDRAL LESIONS OF THE KNEE AND TALUS IN THE ATHLETE,” *Clinics in Sports Medicine*, vol. 18, no. 1, Jan. 1999, doi: 10.1016/S0278-5919(05)70129-0.

[69] J. Buckwalter, “Were the Hunter brothers wrong? Can surgical treatment repair articular cartilage?,” *Iowa Orthop J.*, vol. 17, pp. 1–13, 1997.

[70] N. A. Sgaglione, A. Miniaci, S. D. Gillogly, and T. R. Carter, “Update on advanced surgical techniques in the treatment of traumatic focal articular cartilage lesions in the knee,” in *Arthroscopy*, 2002, vol. 18, no. 2 SUPPL. 1, pp. 9–32. doi: 10.1053/jars.2002.31783.

[71] Arun Pal Sing, “Mosaicplasty or Osteochondral Graft Transfer System.” https://boneandspine.com/mosaicplasty-or-osteochondral-graft-transfer-system/

[72] G. Knutsen *et al.*, “A Randomized Trial Comparing Autologous Chondrocyte Implantation with Microfracture,” *The Journal of Bone & Joint Surgery*, vol. 89, no. 10, Oct. 2007, doi: 10.2106/JBJS.G.00003.

[73] D. B. F. Saris *et al.*, “Characterized Chondrocyte Implantation Results in Better Structural Repair when Treating Symptomatic Cartilage Defects of the Knee in a Randomized Controlled Trial versus Microfracture,” *The American Journal of Sports Medicine*, vol. 36, no. 2, Feb. 2008, doi: 10.1177/0363546507311095.

[74] D. van Assche *et al.*, “Autologous chondrocyte implantation versus microfracture for knee cartilage injury: a prospective randomized trial, with 2-year follow-up,” *Knee Surgery, Sports Traumatology, Arthroscopy*, vol. 18, no. 4, Apr. 2010, doi: 10.1007/s00167-009-0955-1.

[75] E. A. Makris, A. H. Gomoll, K. N. Malizos, J. C. Hu, and K. A. Athanasiou, “Repair and tissue engineering techniques for articular cartilage,” *Nature Reviews Rheumatology*, vol. 11, no. 1, Jan. 2015, doi: 10.1038/nrrheum.2014.157.

[76] E. M. Darling and K. A. Athanasiou, “Rapid phenotypic changes in passaged articular chondrocyte subpopulations,” *J Orthop Res 23*, vol. 2, pp. 425–432, 2005.

[77] W. Bartlett *et al.*, “Autologous chondrocyte implantation versus matrix-induced autologous chondrocyte implantation for osteochondral defects of the knee A PROSPECTIVE, RANDOMISED STUDY,” *THE JOURNAL OF BONE AND JOINT SURGERY*, 2005, doi: 10.1302/0301-620X.87B5.

[78] B. Dhandayuthapani, Y. Yoshida, T. Maekawa, and D. S. Kumar, “Polymeric scaffolds in tissue engineering application: A review,” *International Journal of Polymer Science*, vol. 2011. Hindawi Publishing Corporation, 2011. doi: 10.1155/2011/290602.

[79] S. Ramakrishna, J. Mayer, E. Wintermantel, and K. W. Leong, “Biomedical applications of polymer-composite materials: a review.” [Online]. Available: www.elsevier.com/locate/compscitech

[80] R. Kankala *et al.*, “Effect of Icariin on Engineered 3D-Printed Porous Scaffolds for Cartilage Repair,” *Materials*, vol. 11, no. 8, p. 1390, Aug. 2018, doi: 10.3390/ma11081390.

[81] H. E. Jazayeri *et al.*, “A current overview of materials and strategies for potential use in maxillofacial tissue regeneration,” *Materials Science and Engineering C*, vol. 70. Elsevier Ltd, pp. 913–929, Jan. 01, 2017. doi: 10.1016/j.msec.2016.08.055.

[82] A. R. Armiento, M. J. Stoddart, M. Alini, and D. Eglin, “Biomaterials for articular cartilage tissue engineering: Learning from biology,” *Acta Biomaterialia*, vol. 65. Acta Materialia Inc, pp. 1–20, Jan. 01, 2018. doi: 10.1016/j.actbio.2017.11.021.

[83] B. P. Chan and K. W. Leong, “Scaffolding in tissue engineering: general approaches and tissue-specifi c considerations,” *Eur Spine J 17*, vol. 4, pp. 467–479, 2008.

[84] S. Stratton, N. B. Shelke, K. Hoshino, S. Rudraiah, and S. G. Kumbar, “Bioactive polymeric scaffolds for tissue engineering,” *Bioactive Materials*, vol. 1, no. 2. KeAi Communications Co., pp. 93–108, Dec. 01, 2016. doi: 10.1016/j.bioactmat.2016.11.001.

[85] D. Mackenzie, *The History of Sutures*, vol. 17. 1973. doi: 10.1017/S0025727300018469.

[86] A. R. Boccaccini and J. J. Blaker, “Bioactive composite materials for tissue engineering scaffolds,” *Expert Review of Medical Devices*, vol. 2, no. 3, May 2005, doi: 10.1586/17434440.2.3.303.

[87] Q. P. Pham, U. Sharma, and A. G. Mikos, “Electrospinning of Polymeric Nanofibers for Tissue Engineering Applications: A Review,” *Tissue Engineering*, vol. 12, no. 5, May 2006, doi: 10.1089/ten.2006.12.1197.

[88] T. J. Sill and H. A. von Recum, “Electrospinning: Applications in drug delivery and tissue engineering,” *Biomaterials*, vol. 29, no. 13. pp. 1989–2006, May 2008. doi: 10.1016/j.biomaterials.2008.01.011.

[89] L. J. Gibson and M. F. Ashby, *Cellular Solids*. Cambridge University Press, 1997. doi: 10.1017/CBO9781139878326.

[90] D. I. Braghirolli, D. Steffens, and P. Pranke, “Electrospinning for regenerative medicine: A review of the main topics,” *Drug Discovery Today*, vol. 19, no. 6. Elsevier Ltd, pp. 743–753, 2014. doi: 10.1016/j.drudis.2014.03.024.

[91] S. K. Sahoo, S. Parveen, and J. J. Panda, “The present and future of nanotechnology in human health care,” *Nanomedicine: Nanotechnology, Biology, and Medicine*, vol. 3, no. 1, pp. 20–31, Mar. 2007, doi: 10.1016/j.nano.2006.11.008.

[92] C. M. Madl and S. C. Heilshorn, “Engineering Hydrogel Microenvironment to Recapitulate the Stem Cell Niche,” *Annual Review Biomedical Engineering*, vol. 20, pp. 21–47, 2018, doi: 10.1146/annurev-bioeng-062117-120954.Engineering.

[93] C. M. Madl, B. L. LeSavage, R. E. Dewi, K. J. Lampe, and S. C. Heilshorn, “Matrix Remodeling Enhances the Differentiation Capacity of Neural Progenitor Cells in 3D Hydrogels,” *Advanced Science*, vol. 6, no. 4, 2019, doi: 10.1002/advs.201801716.

[94] S. F. Badylak, “Xenogeneic extracellular matrix as a scaffold for tissue reconstruction,” *Transplant Immunology*, vol. 12, no. 3–4, pp. 367–377, 2004, doi: 10.1016/j.trim.2003.12.016.

[95] T. GILBERT, T. SELLARO, and S. BADYLAK, “Decellularization of tissues and organs,” *Biomaterials*, Mar. 2006, doi: 10.1016/j.biomaterials.2006.02.014.

[96] Z. Li *et al.*, “Processing and 3D printing of gradient heterogeneous bio-model based on computer tomography images,” *IEEE Access*, vol. 4, pp. 8814–8822, 2016, doi: 10.1109/ACCESS.2016.2635661.

[97] Y. Shanjani, J. N. Amritha De Croos, R. M. Pilliar, R. A. Kandel, and E. Toyserkani, “Solid freeform fabrication and characterization of porous calcium polyphosphate structures for tissue engineering purposes,” *Journal of Biomedical Materials Research - Part B Applied Biomaterials*, vol. 93, no. 2, pp. 510–519, May 2010, doi: 10.1002/jbm.b.31610.

[98] J. Zhang *et al.*, “Osteochondral Interface Stiffening in Mandibular Condylar Osteoarthritis,” *Journal of Dental Research*, vol. 97, no. 5, pp. 563–570, 2018, doi: 10.1177/0022034517748562.

[99] G. T. K. Boopathy and W. Hong, “Role of Hippo Pathway-YAP / TAZ Signaling in Angiogenesis,” *Frontiers in Cell and Develomental Biology*, vol. 7, pp. 1–12, 2019, doi: 10.3389/fcell.2019.00049.

[100] S. Piccolo, S. Dupont, and M. Cordenonsi, “THE BIOLOGY OF YAP/TAZ: HIPPO SIGNALING AND BEYOND,” *Physiological Review*, vol. 94, pp. 1287–1312, 2014, doi: 10.1152/physrev.00005.2014.

[101] S. Dupont *et al.*, “Role of YAP / TAZ in mechanotransduction,” *Nature*, vol. 474, pp. 179–186, 2011, doi: 10.1038/nature10137.

[102] Q. Wei *et al.*, “BMP-2 Signaling and Mechanotransduction Synergize to Drive Osteogenic Differentiation via YAP/TAZ,” *Advance Science*, vol. 1902931, pp. 1–15, 2020, doi: 10.1002/advs.201902931.

[103] A. D. Doyle and K. M. Yamada, “Mechanosensing via cell-matrix adhesions in 3D microenvironments,” *Experimental Cell Research*, vol. 343, pp. 60–66, 2016, doi: 10.1016/j.yexcr.2015.10.033.

[104] N. J. Hogrebe and K. J. Gooch, “Direct influence of culture dimensionality on human mesenchymal stem cell differentiation at various matrix stiffnesses using a fibrous self-assembling peptide hydrogel,” *Journal of Biomedical Materials Research A*, vol. 104A, no. 9, pp. 2356–2368, 2016, doi: 10.1002/jbm.a.35755.

[105] A. M. Rosales, L. Vega, F. W. Delrio, J. A. Burdick, and K. S. Anseth, “Hydrogels with Reversible Mechanics to Probe Dynamic Cell Microenvironments Angewandte,” *Angewandte Chemie*, vol. 56, pp. 12132–12136, 2017, doi: 10.1002/anie.201705684.

[106] M. Aragona *et al.*, “A Mechanical Checkpoint Controls Multicellular Growth through YAP / TAZ Regulation by Actin-Processing Factors Mechanical Regulation of Cell Proliferation through,” *Cell*, vol. 154, no. 5, pp. 1047–1059, 2013, doi: 10.1016/j.cell.2013.07.042.

[107] B. R. Mintz and J. A. Cooper Jr, “Hybrid hyaluronic acid hydrogel /poly (e - caprolactone) scaffold provides mechanically favorable platform for cartilage tissue engineering studies,” *Journal of Biomedical Materials Research*, vol. 102A, no. 9, pp. 2918–2926, 2014, doi: 10.1002/jbm.a.34957.

[108] A. C. Hall, “The Role of Chondrocyte Morphology and Volume in Controlling Phenotype—Implications for Osteoarthritis, Cartilage Repair, and Cartilage Engineering,” *Current Rheumatology Reports*, vol. 21, no. 8. Current Medicine Group LLC 1, Aug. 01, 2019. doi: 10.1007/s11926-019-0837-6.

[109] C. M. Madl *et al.*, “Maintenance of neural progenitor cell stemness in 3D hydrogels requires matrix remodelling,” *Nature Materials*, vol. 16, pp. 1233–1245, 2017, doi: 10.1038/NMAT5020.

[110] K. M. Schultz, K. A. Kyburz, and K. S. Anseth, “Measuring dynamic cell – material interactions and remodeling during 3D human mesenchymal stem cell migration in hydrogels,” *PNAS*, vol. 112, no. 29, pp. E3757–E3764, 2015, doi: 10.1073/pnas.1511304112.

[111] M. J. Mondrinos *et al.*, “Porogen-based solid freeform fabrication of polycaprolactone – calcium phosphate scaffolds for tissue engineering,” *Biomaterials*, vol. 27, pp. 4399–4408, 2006, doi: 10.1016/j.biomaterials.2006.03.049.

[112] M. S. Kim and G. Kim, “Three-dimensional electrospun polycaprolactone (PCL)/alginate hybrid composite scaffolds,” *Carbohydrate Polymers*, vol. 114, pp. 213–221, 2014, doi: 10.1016/j.carbpol.2014.08.008.

[113] S. R. Caliari, S. L. Vega, M. Kwon, E. M. Soulas, and J. A. Burdick, “Dimensionality and spreading influence MSC YAP/TAZ signaling in hydrogel environments,” *Biomaterials*, vol. 103, pp. 314–323, 2016, doi: 10.1016/j.biomaterials.2016.06.061.

[114] R. J. Wade, E. J. Bassin, C. B. Rodell, and J. A. Burdick, “Protease-degradable electrospun fibrous hydrogels,” *Nature Communications*, vol. 6, no. 6639, pp. 1–10, 2015, doi: 10.1038/ncomms7639.

[115] X. Zhao *et al.*, “Photocrosslinkable Gelatin Hydrogel for Epidermal Tissue Engineering,” *Advanced Health Care Materials*, vol. 5, pp. 108–118, 2016, doi: 10.1002/adhm.201500005.

[116] N. Cheng, W. Lin, T. Ling, and T. Young, “Sustained release of adipose-derived stem cells by thermosensitive chitosan/gelatin hydrogel for therapeutic angiogenesis,” *Acta Biomaterialia*, vol. 51, pp. 258–267, 2017, doi: 10.1016/j.actbio.2017.01.060.

[117] S. Xiao *et al.*, “Gelatin Methacrylate (GelMA) -Based Hydrogels for Cell Transplantation : an Effective Strategy for Tissue Engineering,” *Stem Cell Reviews and Reports*, vol. 15, pp. 664–679, 2019.

[118] A. D. Arya *et al.*, “Gelatin Methacrylate Hydrogels as Biomimetic Three-Dimensional Matrixes for Modeling Breast Cancer Invasion and Chemoresponse in Vitro,” *ACS Applied Materials & Interfaces*, vol. 8, pp. 22005–22017, 2016, doi: 10.1021/acsami.6b06309.

[119] T. Billiet, E. Gevaert, T. De Schryver, M. Cornelissen, and P. Dubruel, “The 3D printing of gelatin methacrylamide cell-laden tissue-engineered constructs with high cell viability,” *Biomaterials*, vol. 35, no. 1, pp. 49–62, 2021, doi: 10.1016/j.biomaterials.2013.09.078.

[120] C. Kuo *et al.*, “Placental basement membrane proteins are required for effective cytotrophoblast invasion in a three-dimensional bioprinted placenta model,” *Journal of Biomedical Materials Research A*, vol. 106A, no. 6, pp. 1476–1487, 2018, doi: 10.1002/jbm.a.36350.

[121] A. Sadiasa, T. H. Nguyen, and B. Lee, “In vitro and in vivo evaluation of porous PCL-PLLA 3D polymer scaffolds fabricated via salt leaching method for bone tissue engineering applications,” *Journal of Biomaterials Science*, vol. 25, no. 2, pp. 150–167, 2013.

[122] S. Taherkhani and F. Moztarzadeh, “Fabrication of a poly (E -caprolactone)/ starch nanocomposite scaffold with a solvent-casting / salt-leaching technique for bone tissue engineering applications,” *Journal of Applied Polymer Science*, vol. 43523, pp. 19–21, 2016, doi: 10.1002/app.43523.

[123] Y. S. Cho, B.-S. Kim, H.-K. You, and Y.-S. Cho, “A novel technique for scaffold fabrication : SLUP (salt leaching using powder),” *Current Applied Physics*, vol. 14, no. 3, pp. 371–377, 2014, doi: 10.1016/j.cap.2013.12.013.

[124] B. A. Aguado *et al.*, “Extracellular matrix mediators of metastatic cell colonization characterized using scaffold mimics of the pre-metastatic niche,” *Acta Biomaterialia*, vol. 33, pp. 13–24, 2016, doi: 10.1016/j.actbio.2016.01.043.

[125] R. K. Korhonen *et al.*, "Comparison of the equilibrium response of articular cartilage in unconfined compression, confined compression and indentation," *Journal of Biomechanics*, vol. 35, no. 7, pp. 903–909, Jul. 2002, doi: 10.1016/S0021-9290(02)00052-0.

[126] N. Kang *et al.*, "Effects of co-culturing BMSCs and auricular chondrocytes on the elastic modulus and hypertrophy of tissue engineered cartilage," *Biomaterials*, vol. 33, no. 18, pp. 4535–4544, Jun. 2012, doi: 10.1016/j.biomaterials.2012.03.019.

[127] E. Hoenig *et al.*, "Mechanical properties of native and tissue-engineered cartilage depend on carrier permeability: A bioreactor study," *Tissue Engineering - Part A*, vol. 19, no. 13–14, pp. 1534–1542, Jul. 2013, doi: 10.1089/ten.tea.2012.0538.

[128] A. J. Engler, S. Sen, H. L. Sweeney, and D. E. Discher, "Matrix Elasticity Directs Stem Cell Lineage Specification," *Cell*, vol. 126, pp. 677–689, 2006, doi: 10.1016/j.cell.2006.06.044.

[129] J. W. Lee and H. S. Yoo, "Michael-Type Addition of Gelatin on Electrospun Nanofibrils for Self-Assembly of Cell Sheets Composed of Human Dermal Fibroblasts," *ACS Omega*, 2019, doi: 10.1021/acsomega.9b02602.

[130] M. Guvendiren and J. A. Burdick, "Stiffening hydrogels to probe short- and long-term cellular responses to dynamic mechanics," *Nature Communications*, vol. 3, 2012, doi: 10.1038/ncomms1792.

[131] S. Ji and M. Guvendiren, "3D Printed Wavy Scaffolds Enhance Mesenchymal Stem Cell Osteogenesis," *micromachines*, vol. 11, no. 31, pp. 1–15, 2020.

[132] S. Shrestha, F. Li, V. X. Truong, J. S. Forsythe, and J. E. Frith, "Interplay of Hydrogel Composition and Geometry on Human Mesenchymal Stem Cell Osteogenesis," *Biomacromolecules*, vol. 21, pp. 5323–5335, 2020, doi: 10.1021/acs.biomac.0c01408.

[133] S. L. Vega *et al.*, "Combinatorial hydrogels with biochemical gradients for screening 3D cellular microenvironments," *Nature Communications*, vol. 9, no. 1, Dec. 2018, doi: 10.1038/s41467-018-03021-5.

[134] A. M. Rosales, S. L. Vega, F. W. DelRio, J. A. Burdick, and K. S. Anseth, "Hydrogels with Reversible Mechanics to Probe Dynamic Cell Microenvironments," *Angewandte Chemie*, vol. 129, no. 40, pp. 12300–12304, Sep. 2017, doi: 10.1002/ange.201705684.

Appendix A

HNMR & MALDI

Figure A1

HNMR of Hydrogel. A) GelMe HNMR. B) GFP HNMR C) GelMe + GFP HNMR

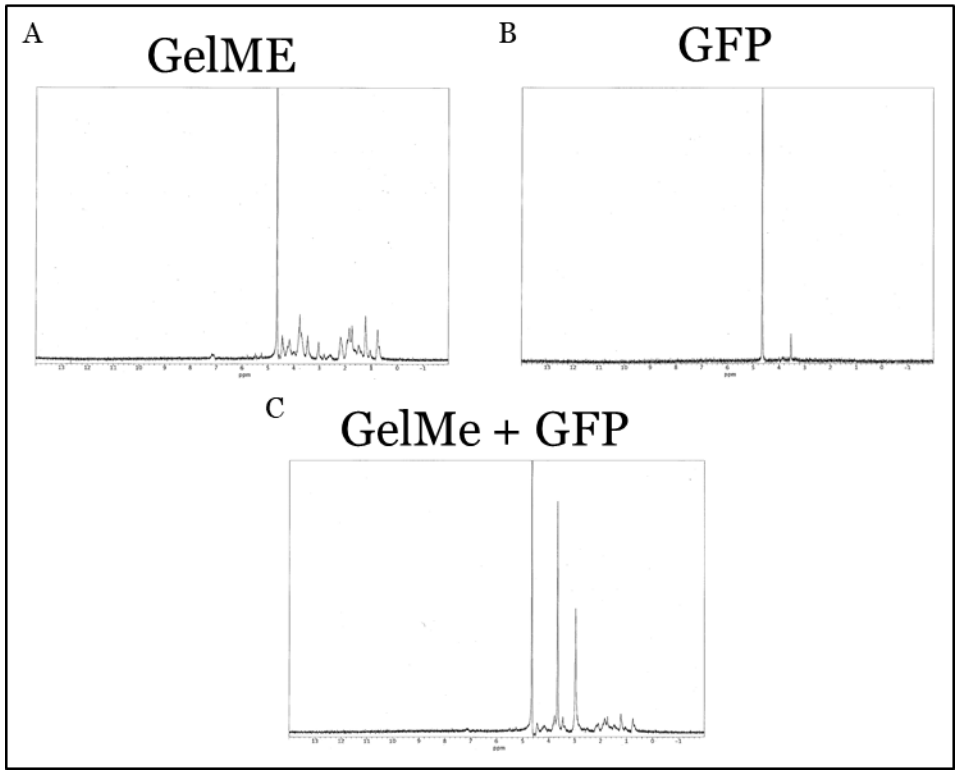

Figure A2

Maldi of GelMe + GFP.

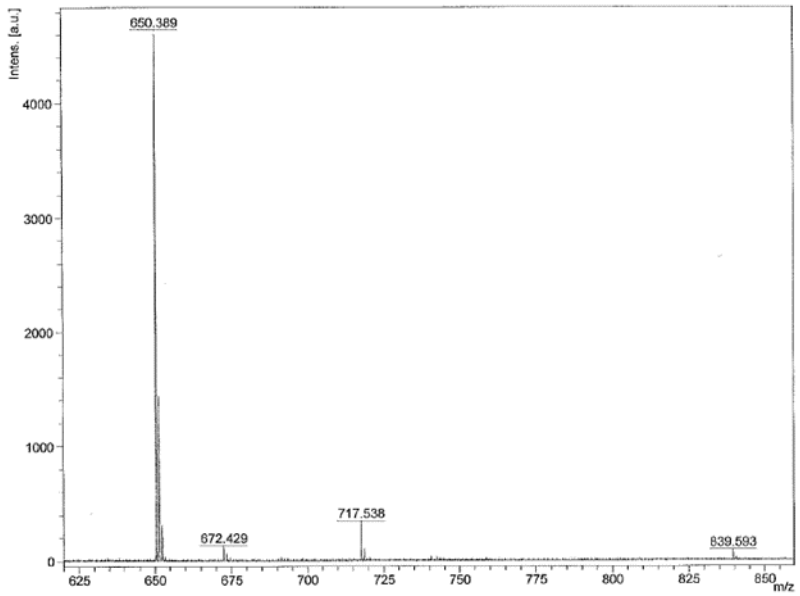

Appendix B

Compression Experiment

Figure B1

Compression Experiments Supplemental Data. A) Shows cell volume sphericity and nuclear YAP of all groups with individual points plotted. B) Shows YAP vs cellular volume and C) displays YAP vs sphericity.

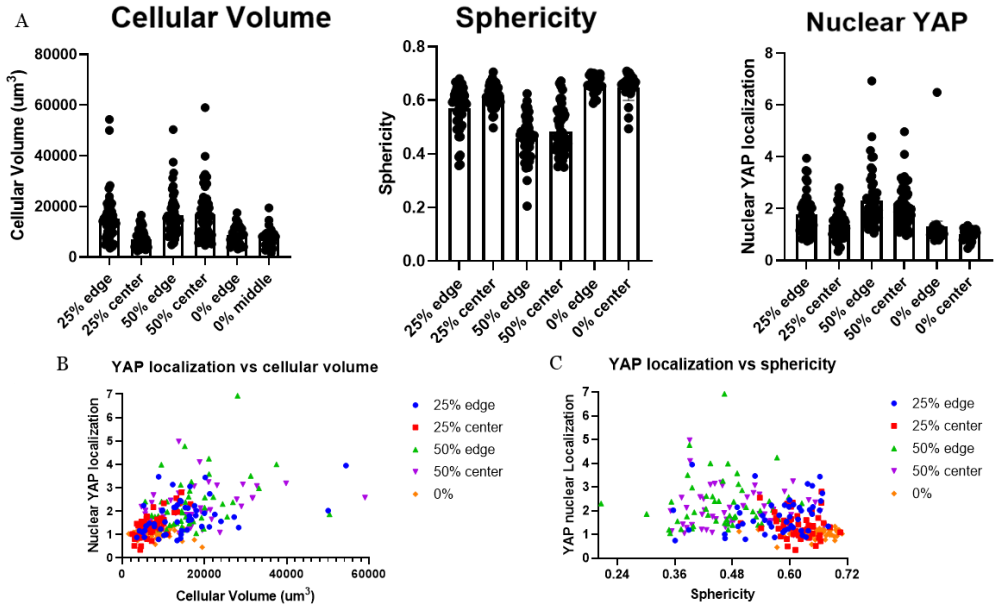

Appendix C

Scaffold Characterization

Figure C1

Different Weight % of PCL Scaffolds Porosity.

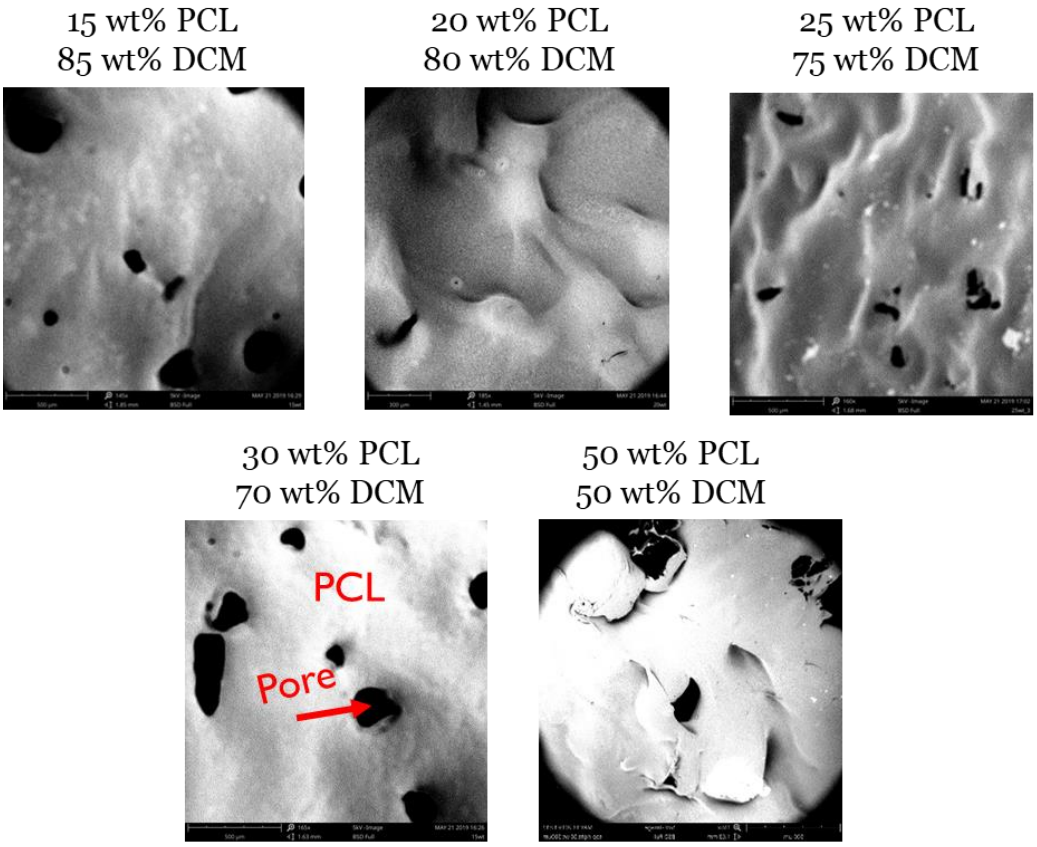

Figure C2

Porosity of PCL Scaffolds

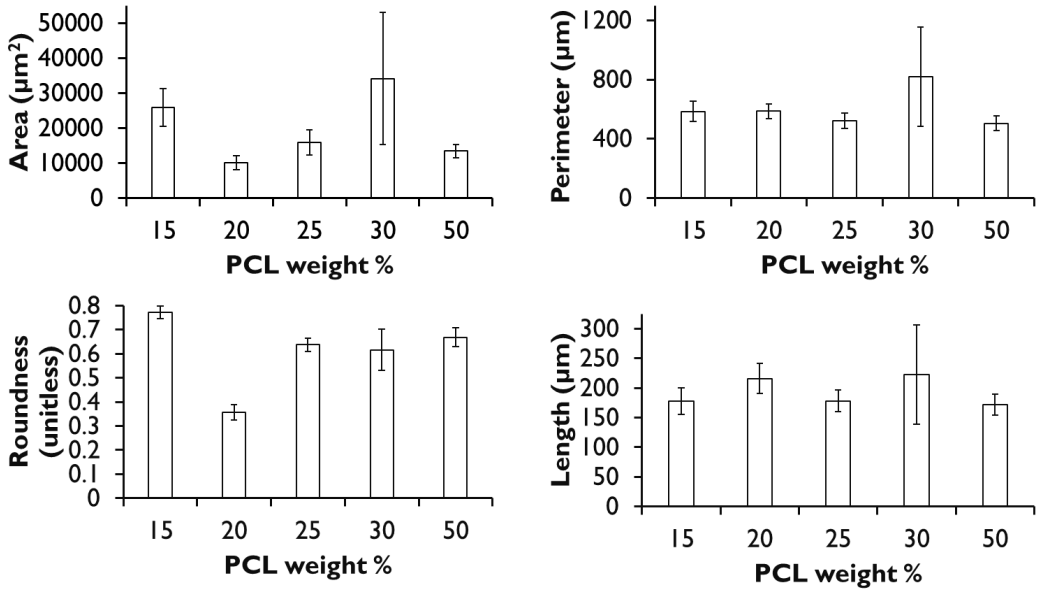

Figure C3

Different Weight % PCL Scaffolds Mechanical Properties.

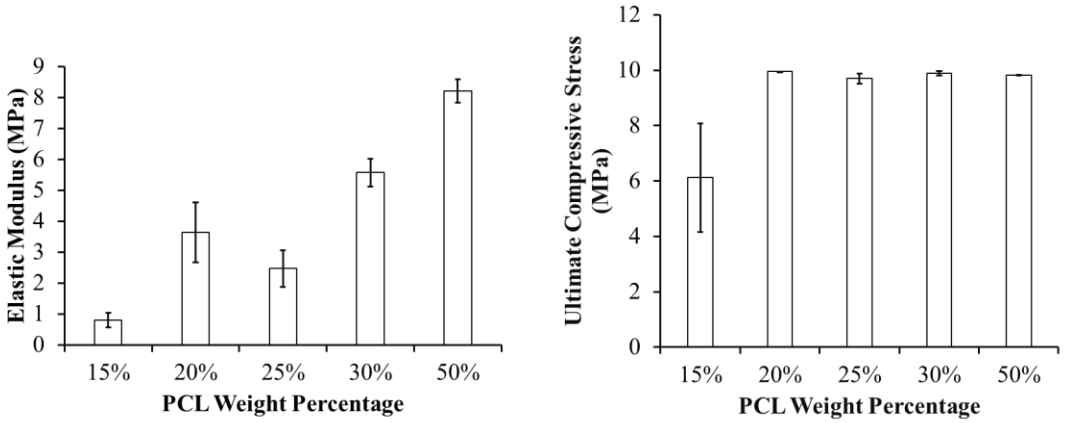

Table C1

Mechanics of Early PCL Scaffolds.

Elastic modulus kPa		Standard Deviation	Ultimate Compressive force MPa		Standard Deviation
15%	798	0.234887438	15%	6.118512843	1.955374499
20%	3638	0.965907863	20%	9.951083239	0.000647102
25%	2463	0.594910148	25%	9.696644221	0.178023484
30%	5571	0.448341055	30%	9.889679273	0.085403443
50%	8215	0.379214296	50%	9.820188246	0.010958538

Figure C4

Direct Comparison of Porosity and Mechanics.

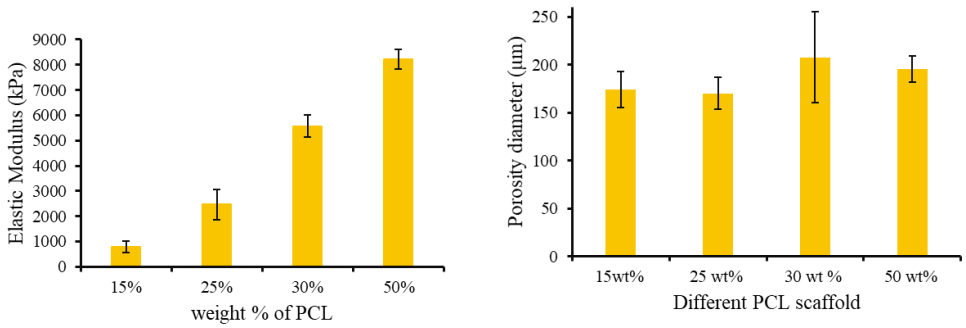

Figure C5

Fluorescent Images with Cells in Early Scaffolds.

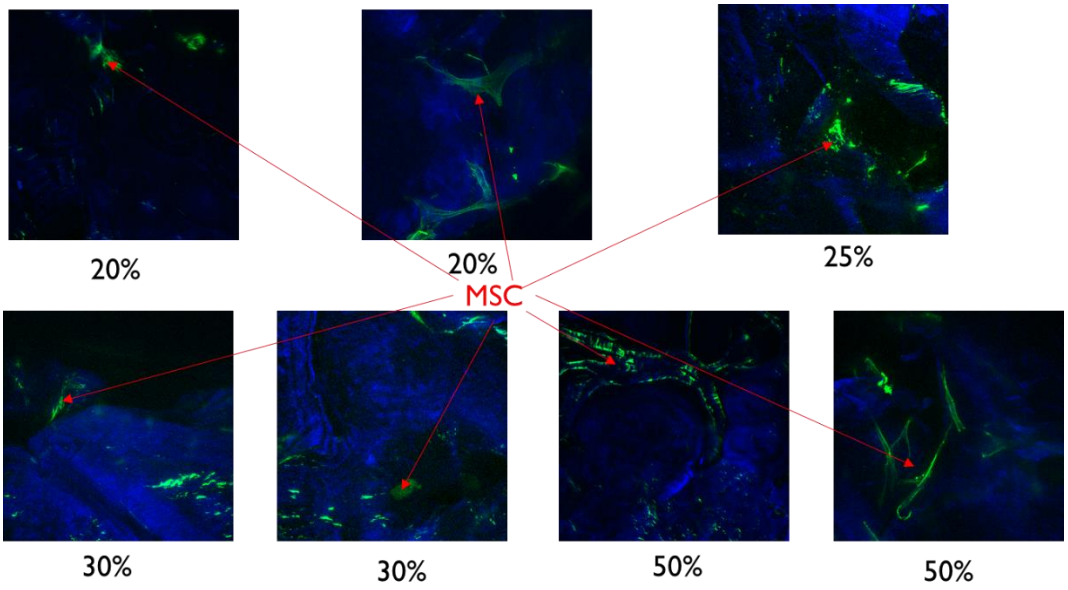

The elastic modulus produced from the scaffolds at a 2:1 NaCl to PCL ratio ranged from 700 kPa to 8215 kPa. The large moduli can be attributed to a lack of porosity and salt content. SEM imaging shows the lack of porosity throughout these scaffolds and results demonstrated, mechanical properties increased as PCL wt % increased meanwhile, porosity remained constant. The values of pore size for 15, 20, 25, 30, 50 wt% for 2:1 NaCl to PCL ratio include 174 mm, 137 mm, 170mm, 207 mm, and 195 mm in diameter on average. The small pore diameter can be attributed to the lack of NaCl crystals in the scaffold as there was only a 2:1 ratio. However, the constant pore size and porosity in conjunction with the increasing wt% of PCL are the main determinants of the increasing mechanical properties. This finding can be explained from the fact as you increase PCL

wt% and keep porosity constant by the amount of salt that is added, mechanics will increase.

However, after analyzing cellular perfusion through the sterilized scaffolds, it was concluded more porosity must be incorporated at the cost of mechanical properties. As it is seen in the figure, after seeding scaffolds with 200k cells and staining their cytoskeleton with PI in direct accordance with the procedure in chapter 4, there was a lack of cellular population in the scaffold environments. The lack of cells could be from a multitude of factors including the elementary seeding method, the lack of cellular concentration, and/or the pore size. After careful evaluation of the factors affecting cellular adhesion in the scaffold, it was concluded a perfusion method needed to be developed to provide consistency in cellular seeding, porosity must increase, and cell concentration will be 500k cells per ml moving forward to the next experiment. The mechanical properties were compromised to increase the porosity in hopes cellular harvesting would be greater in the scaffold. These mechanics resemble the tissues in the OI in terms of mechanics but to increase porosity and encourage cellular proliferation in the scaffold, a more tortuous structure is needed and therefore a compromise to mechanics will be introduced later.

As the mechanical properties of the 30 wt% construct was acceptable for cartilage and perhaps the OI, this wt% was used for all future studies. To further study the effects of porosity and cellular adhesion to the scaffold pores, another study was developed. This experiment included increasing the NaCl:PCL wt% to 3:1 and 4:1. These scaffolds were developed with the idea in mind to explore the effects on porosity for cell adhesion while maintaining mechanical integrity. 40 wt% was also created to compare mechanical properties. 3:1, 4:1 NaCl:PCL for 30 and 40% had an elastic modulus 4111, 4637, 5452,

and 3652 kPa respectively. As these scaffolds were seeded with cells, the cell density was 500k/ml in media and they were seeded with the customized perfusion device shown in the schematic at 1 ml/min and they left to incubate in the incubator for three days. The scaffolds were fixed and stained with PI and Phalloidin and imaged. The images display an increase in cell population in the scaffold due to porosity and perfusion method. Cells show adaptiveness to the PCL by exhibiting spreading and large morphology. This is believed to result from a rigid 2D environment. The high elastic modulus and large fiber diameter > 100 μm results in the cells adopting a morphology favoring osteogenesis.

Table C2

Mechanics with Increased Porosity.

PCL	**Elastic Modulus (kPa)**
3 x30	4111.6
3x40	4637.84
4x30	3813.2
4x40	3851.875

Appendix D

Cell Tracker Experiments

Introduction

Cell tracking experiments were used to provide details on two different cell populations harvested in the composite. Cell tracker red and green was used to stain cells and the results are observed. The lower limits of detection for cell tracker green and red were recorded to ensure the minimum interference with cellular behavior and activity. To stain cells green and red and to find the lower limits of detection the subsequent protocols were followed. Once it was shown that cells can indeed be harvested inside the PCL scaffold and showed spread morphology it was hypothesized that if methacrylate hydrogel was injected into the scaffold after harvesting cells with media only, there could exists a co population of cells and based on morphology favor osteogenesis or chondrogenesis. To track cell lineage and the different populations, it was essential to stain each cell type prior to seeding and encapsulating the cells. To accomplish this task, the lower limits of detection for cell tracker red and green must be found to ensure the least amount of cellular interruption.

Methods

Staining for Cell Tracker Green

To create cell tracker green at 10 mM concentration the below protocol was followed. First cell tracker green was ordered from VWR and 10.78 µl of DMSO was added to cell tracker green. Next cells were thawed followed by passaging them in

accordance with the above procedure. Cells were counted and separated to include 500k cells in a 50 ml conical tube. Next, 5 ml of media with 10% FBS solution was added and centrifuged for 5 minutes at 500 x g. The next step required aspirating the media and resuspending the pellet in 3 ul cell tracker green solution and 5 ml serum free media. The cells needed to be incubated for 30 minutes and perturbed every 10 minutes. It was necessary to centrifuge the cells and wash 3x with 5 ml of media with 2% FBS by repeating centrifuging, aspirating, and resuspending the cell pellet. Lastly, the cell's nucleus was stained by resuspending the stained cells in 0.5 ul Hoechst and 5 ml 10% FBS media and washed 3x with the same procedure as mentioned above. To plate the cells for 10k cells per plate, the 500k stained cells were resuspended in 0.5 ml of media and using a pipette 10 µl of cell solution was seeded on each glass coverslip and incubated. The results of the stained cells are shown below.

Figure D1

Cell Tracker Green and Hoechst-Stained Cells.

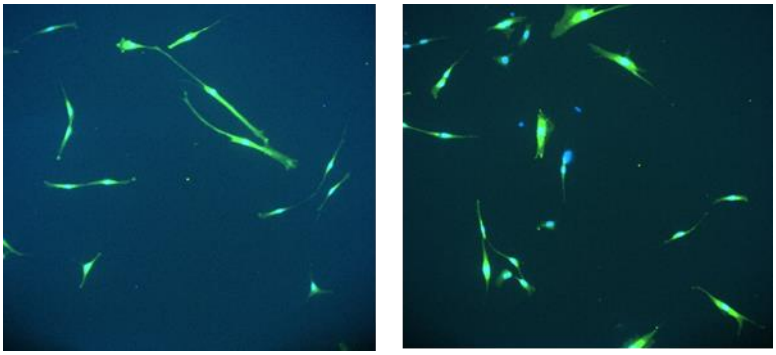

Lower Limit of Detection Cell Tracker Green and Red

To find the lower limit of detection for cell tracker green the procedure for thawing and passaging the cells was identical to the procedure mentioned above. 10.78 µl of DMSO was added to cell tracker green. Next cells were thawed followed by passaging them in accordance with the above procedure. Cells were counted and separated to include 2 million cells in a 50 ml conical tube. Next, 5 ml of media with 10% FBS solution was added and centrifuged for 5 minutes at 500 x g. The next step required serial dilutions. These dilutions consisted of achieving four ratios of cell tracker to media which were labeled A, B, C, D with ratios of 1:2000, 1:4000, 1:8000, 1:16000 respectively. The A solution (1:2000) consisted of 10 ml media with 2% FBS and 5 ul cell tracker green. To make solution B, 5 ml of solution A was diluted with 5 ml 2% FBS media for a ratio of 1:4000. For solution C, 5 ml solution B was diluted with 5 ml 2% FBS media to achieve the ratio of 1:8000. Finally, the lowest limit tested, the concentration of 1:16000 was made from 5 ml of solution C mixed with 5 ml 2% FBS media. To test the fluorescence of each solution, 500k cells were added in 5 ml of each serial dilution. They were incubated for 30 minutes followed by centrifugation with the same properties as above and 3 washes with 5 ml of 10% FBS media. Then, cell pellets of solutions A, B, C, and D were resuspended in 1 ml of 10% FBS media and plated onto glass coverslips within a 24 well plate and incubated for 1 day. The cells were imaged 24 hours later and qualitatively observed in their 2D environment.

Figure D2

Cell Tracker Green at Different Concentrations.

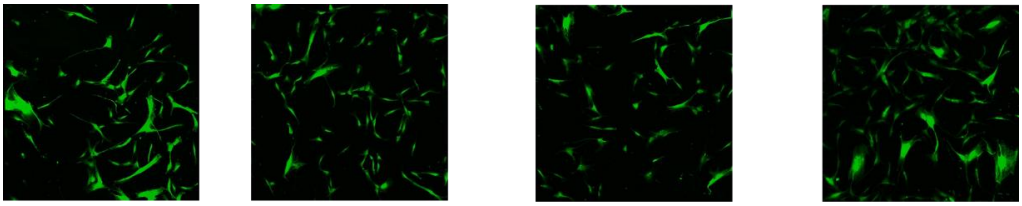

A [1:2000] B [1:4000] C [1:8000] D [1:16000]

To create and find the lower limit of detection for cell tracker red at 10 mM concentration the below protocol was followed. First cell tracker red was ordered from VWR and 7.29 µl of DMSO was added to cell tracker red. Next cells were thawed followed by passaging them in accordance with the above procedure. Cells were counted and separated to include 500k cells in a 50 ml conical tube. Next, 5 ml of media with 10% FBS solution was added and centrifuged for 5 minutes at 500 x g. The next step required serial dilutions. These dilutions consisted of achieving four ratios of cell tracker to media which were labeled A, B, C with ratios of 1:5000, 1:10000, 1:20000 respectively. The A solution (1:5000) consisted of 10 ml media with 2% FBS and 2 ul cell tracker green. To make solution B, 5 ml of solution A was diluted with 5 ml 2% FBS media for a ratio of 1:10000. For solution C, 5 ml solution B was diluted with 5 ml 2% FBS media to achieve the ratio of 1:20000. To test the fluorescence of each solution, 500k cells were added in 5 ml of each serial dilution. They were incubated for 30 minutes followed by centrifugation with the same properties as above and 3 washes with 5 ml of 10% FBS media. Then, cell pellets of solutions A, B, and C were resuspended in 167 µl of 10% FBS media and 10 µl was plated

onto glass coverslips within a 24 well plate and incubated for 1 day. This achieved 10k cells on each coverslip with a 1:1 cell/ml seeding density. The cells were imaged 24 hours later and qualitatively observed in their 2D environment.

Figure D3

Cell Tracker Red at Different Concentrations.

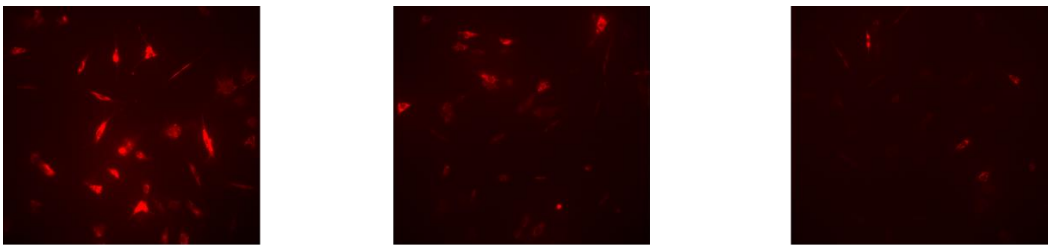

Hoechst Lower Limit of Detection with Cell Tracker Red

A further experiment was conducted to observe the lower limit of detection for Hoechst in these cell tracker studies. These studies were completed using cell tracker red at a dilution factor of 1:5000. The above protocol was followed. Serial dilutions were used to dilute Hoechst to the desired amounts of A, B, and C. The procedure for Hoechst solutions is as follows: Solution A, add 1.5 ul of Hoechst to 10 ml 10% FBS media (1:6,666). Solution B, take 5 ml of solution A and dilute it with 5 ml 10% FBS Media for 1:13,333. For solution C, take 5 ml solution B and dilute with 5 ml 10% FBS Media for 1:26,666. These solutions were plated and imaged after 24 hours of incubation.

Figure D4

Cell Tracker Red and Hoechst at Different Concentrations.

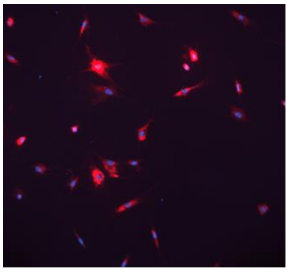

A [1:6,666]

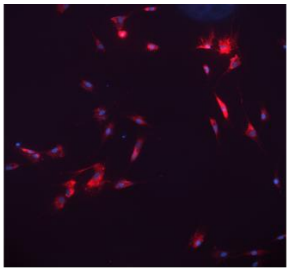

B [1:13,333]

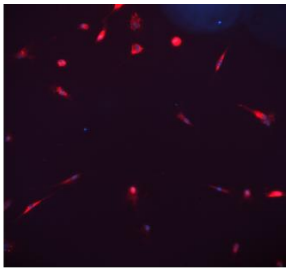

C [1:26666]

Co-population of Cell Tracker Green and Red

Once it was confirmed that cells were able to be seeded and stained with cell tracker green and red it was necessary to test whether green stained cells and red stained cells can exist as a co-population on one glass plate. Therefore, an experiment was conducted to study the ability to stain two populations of cells and observe their color heterogeneity. To stain for cell tracker green, the solution for staining of cell tracker B solution was followed and to stain the cells red, the procedure for cell tracker red solution A was followed. The resuspended solution of pellets for cell tracker green and red were then mixed and plated on a well plate. These plates were imaged 24 hours later after incubation.

Figure D5

Co-population of Cell Tracker Green and Red.

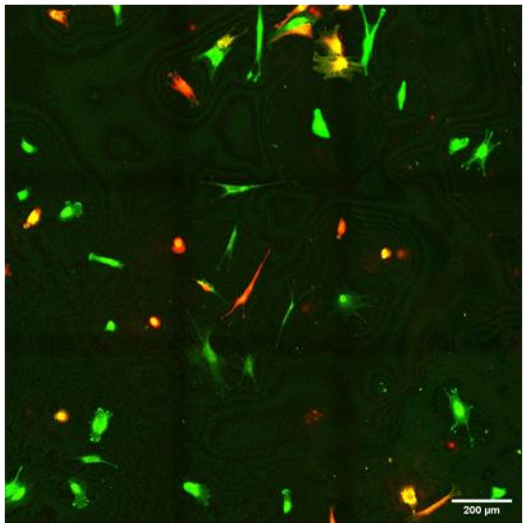

Cell Tracker Perfusion Through PCL

After successfully showing green and red cells can exist simultaneously, it was hypothesized that there could be an observation of two cell populations seeded inside the PCL scaffold based on morphology. Using previous results showing round and spread cells in the scaffold, the objective was to encapsulate red cells in GelMe hydrogel and perfuse that through the scaffold after seeding green MSCs through the scaffold. The goal was to show that green cells would be spread (2D), and red cells would be round as they live in a 3D environment.

First, cell tracker green was used to stain a population of cells 500k cells (1 million cells per ml). Next the group of green cells were perfused through the low porosity PCL

scaffold using the perfusion method described below with 500k cells in media. After 1 day, another group of cells were stained with cell tracker red following the protocol above. 500k cells with cell tracker red were resuspended in 0.5 ml of 5 wt% GelMe solution and then perfused through the scaffold with cell tracker green cells inside. The scaffold was exposed under U V light with an intensity of 10 mW/cm^2 for 10 minutes. The composite was washed 3x with media and incubated for 3 days.

Results and Discussion

Cell tracker green could be observed to stain cells at the lowest concentration recorded which was 1:16000. Cell tracker red could be used at a concentration of 1:5000 before the fluorescents started to become dim and skew qualification. Hoechst staining should not go lower than 1:6,666 for these experiments as the nuclei were not as bright with lower concentrations. Next, it was displayed via confocal microscope green and red stained MSCs could co-populate in one environment without color leaching. This finding was the foundation needed to proceed the following experiment of dual seeding cell populations in the scaffold. MSCs that were stained with cell tracker green and perfused with media were not visible after the group of red MSCs were perfused with GelMe and encapsulated.

Figure D6

Cells Encapsulated in GelMe Labeled with Cell Tracker Red Perfused Through the Scaffold. No visible cells perfused through with cell tracker green.

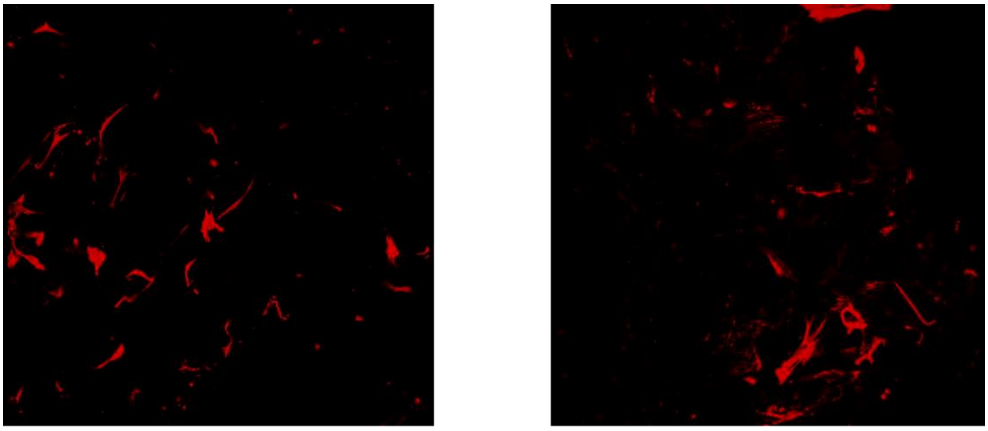

Appendix E

Preliminary Composite Data

Figure E1

Preliminary Composite Data to Show the Composite Can Harvest Cells. C) Shows early co-population evidence of cells.

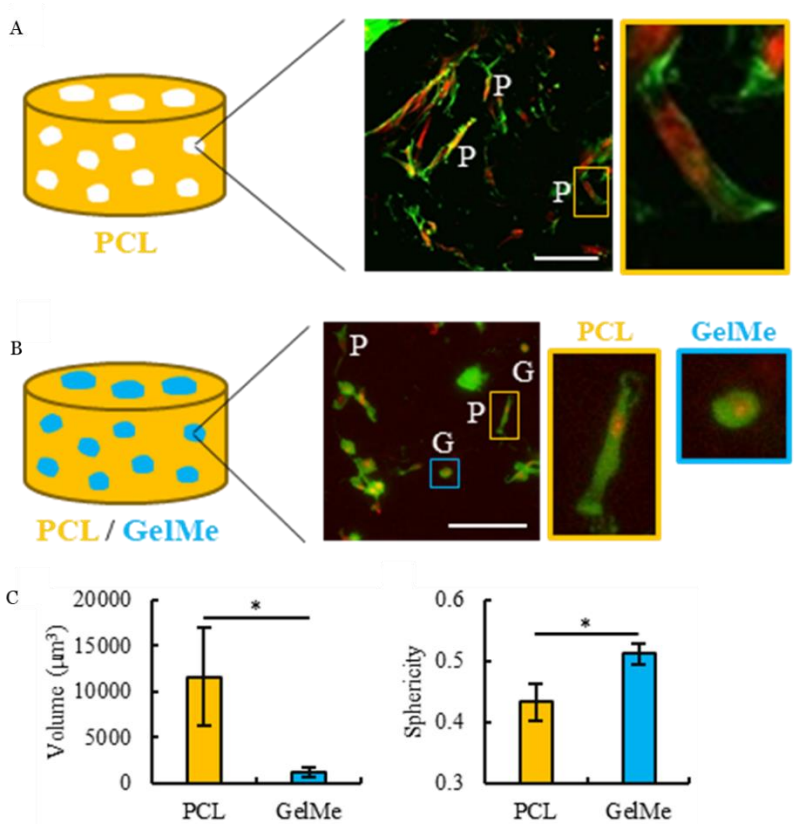

Table E1

Table of Frequency of Round vs Spread Cells in Low and Medium Composite.

	Spread Cells	Round cells	Total	Frequency spread	Frequency round
Low	220	128	348	0.632183908	0.367816092
Medium	141	187	328	0.429878049	0.570121951
gel	69	183	252	0.273809524	0.726190476

Appendix F

Supplemental Composite Data

Figure F1

Composite Histogram Data. A) is histograms of cell volume, sphericity, and nuclear YAP. B) Is YAP localization vs volume and sphericity.

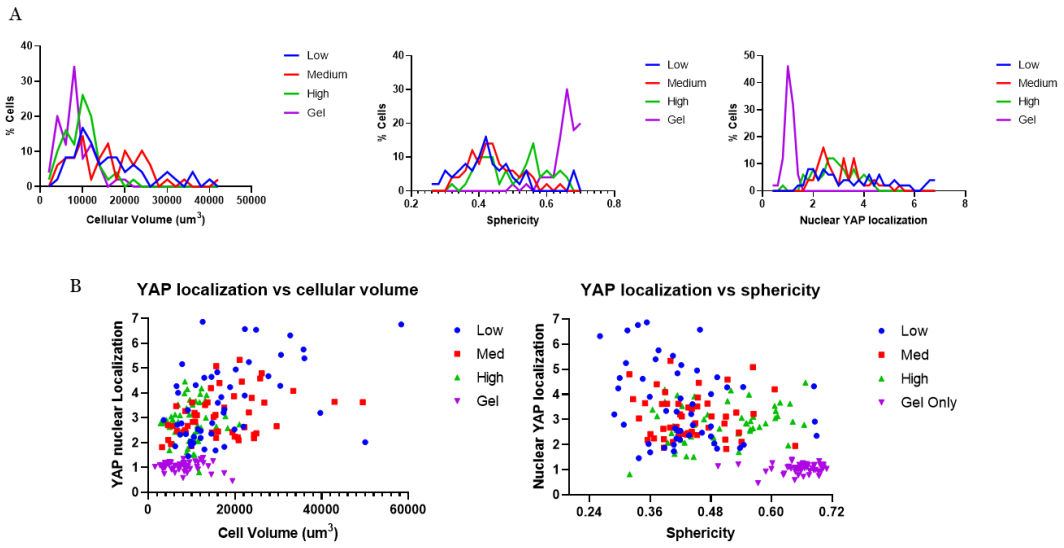

Figure F2

Cell Images in Low, Med, High Composite.

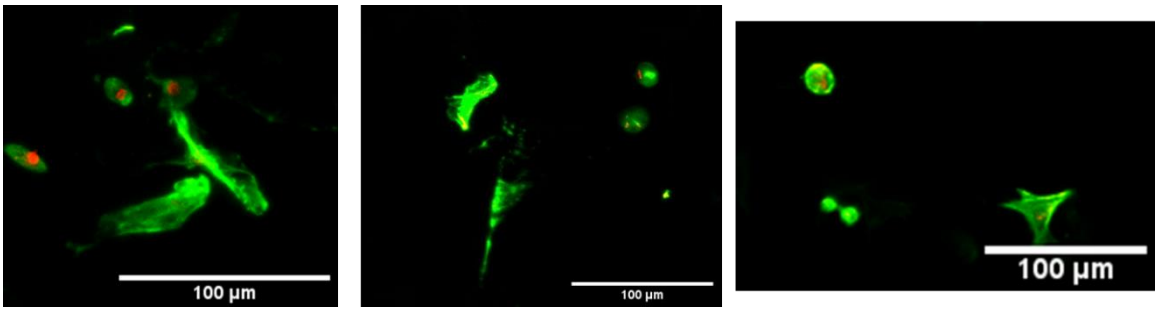

Figure F3

Cell Images in Nile Red. Displays the medium composite exhibiting cellular sensing as cells are close to pore edges.